

---

# **Studies on *E. coli* L-tartrate dehydratase and *M. jannaschii* inosine 5'- monophosphate dehydrogenase**

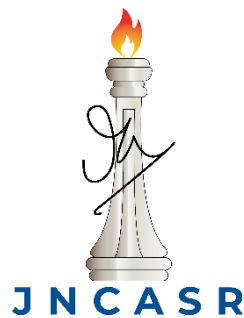
---

A Thesis Submitted for the Award of the Degree of

**Master of Science**

By

**SOURADIP MUKHERJEE**



**Thesis Supervisor: Prof. Hemalatha Balaram**

Molecular Biology and Genetics Unit  
Jawaharlal Nehru Centre for Advanced Scientific Research  
Bengaluru - 560064, India

April 2023

---

**[This page is intentionally left blank]**

---

---

*To my parents and my guru,  
Late Samir Kumar Palit*

---

**[This page is intentionally left blank]**

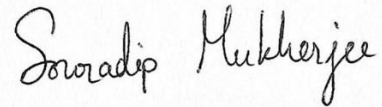
---

---

## DECLARATION

I hereby declare that the matter embodied in this thesis entitled “**Studies on *E. coli* L-tartrate dehydratase and *M. jannaschii* inosine 5'-monophosphate dehydrogenase**” is the result of the research carried out by me at Molecular biology and Genetics Unit, Jawaharlal Nehru Centre for Advanced Scientific Research, Bangalore, India, under the supervision of Prof. Hemalatha Balaram and it has not been submitted elsewhere for the award of any other degree.

In keeping with the general practice of reporting scientific observations, due acknowledgements have been made wherever the work described is based on the findings of other investigators. Any omission which might have occurred by oversight or error in judgement is regretted.



.....  
**Souradip Mukherjee**

**Place: Bangalore, India**

**Date: 27.04.2023**

---

**[This page is intentionally left blank]**

---

---

## CERTIFICATE

I hereby certify that the matter embodied in this thesis entitled “**Studies on *E. coli* L-tartrate dehydratase and *M. jannaschii* inosine 5'-monophosphate dehydrogenase**” has been carried out by **Mr. Souradip Mukherjee** at the Molecular Biology and Genetics Unit, Jawaharlal Nehru Centre for Advanced Scientific Research, Bangalore, India under my supervision and that the results presented in this thesis have not previously formed the basis for the award of any other diploma, degree, or fellowship.



**Prof. Hemalatha Balaram**

(Research Supervisor)

**Place:** Bangalore

**Date:** 27 April, 2023

---

**[This page is intentionally left blank]**

---



---

# Acknowledgements

*“Per aspera ad Astra”*

*-Lucius Annaeus Seneca*

My journey as a master’s student in JNCASR has seen me grow on the path of life, not as a student of science only, but as a human being as well. Being away from home has helped me grow myself and taught me innumerable things. I cherish those who have been with me on this journey and this acknowledgement is to them only.

It is with great pleasure that I express my heartfelt gratitude to my research supervisor Prof. Hemalatha Balaram, without whom this thesis would not be possible. It has truly been an incredible association with her support, guidance, encouragement, and constructive criticism. She has nurtured my scientific interests and inspired me to progress on my journey on the path of science.

Our individual efforts are bound by our own limitations only. The right guide and companion takes us miles beyond. My wholehearted gratitude to Prof. P. Balaram, Prof. Somnath Dutta, Prof. B. Gopal for their guidance and help throughout the course of my masters. I would also like to thank Dr. Rajdeep Das from NCBS and Arnab and Sainath from IISc for their help in conducting my experiments and helping me build the story that is my thesis.

I feel privileged to have gotten the opportunity to work on electron microscopy, a technique I will continue to cherish and work on all my life. A special thanks to Prof. Somnath Dutta, who let us use the electron microscopy facility at MBU, IISc. His course on electron microscopy has helped me learn me a lot and inspired me to further my interest in the field. I would also like to thank Prof. B. Gopal for letting us use the X-ray diffractometer at MBU, IISc.

I would also like to extend my sincere thanks to Prof. Kaustuv Sanyal, Prof. Anuranjan Anand, Prof. Ranga Uday Kumar, Prof. MRS Rao, Prof. Tapas Kundu, Prof. Maneesha Inamdar, Prof. Ravi Manjithaya, Dr. James Chelliah, Dr. Kushagra Bansal, and Prof. Sheeba Vasu for letting students learn and grow not just as researchers but also as good presenters.

I consider myself fortunate to have interacted with some of the best seniors and lab mates in the laboratory. I thank Dr. Asutosh Bellur, Arpitha, Resmi, Anusha, Chitra, Nivedita, Dhanalakshmi ma’am and Bala. I would also like to thank current and past lab members, internship students who have contributed to making the lab more of a home than a workplace. I thank Vaishali, Anirudh, Srujan, Aditi and Akanksha. I would also like to thank my batchmates from Int. PhD 2020 batch of Biological Sciences.

I would like to thank the staff of electron microscopy facility, MBU, IISc, transmission electron microscopy imaging, ICMS, JNCASR, mass spectrometry facility, JNCASR, and X-ray facility at MBU, IISc for extending their support every time we used the facility. My special thanks to Arun, Prathibhan and Babu sir for their kind help.

I would also like to express my gratitude towards the people at the Library, Admin section, Academic section, Hostel office, Security, Housekeeping and Dhanvantari. I sincerely thank JNCASR community for providing a conducive scientific environment.

---

I would like to express my thanks to my friends from JNC: Deepam, Sarbajit, Souvik, Arijit, Koyendrila, Robi, and Soumen. I would also like to thank my friends Sagnik and Anushka for the being the friends they are.

There are a few people without whom I would not have been able to go through this journey of life and for whom words fall short while expressing gratitude. Firstly, I would like to express my heartfelt thanks to my friend, guide and partner-in-crime, Lopamudra, without whose daily encouragement and support this would not have been possible. Next, I would like to express my thanks to my brother, Sarthak, for being the best younger brother ever. Although words may fail to capture my emotions, but my thanks and gratitude to my parents who have made me what I am today, without whom, I would not be penning this down.

---

Synopsis of the thesis titled

**“Studies on *E. coli* L-tartrate dehydratase and *M. jannaschii* inosine 5'-monophosphate dehydrogenase”**

Submitted by

**Souradip Mukherjee**

Molecular Biology & Genetics Unit (MBGU), Jawaharlal Nehru Centre for Advanced Scientific Research, Bangalore, India

Thesis supervisor: Prof. Hemalatha Balaram

---

"Proteins hold the key to the whole subject of the molecular basis of biological reactions."

— Linus Pauling. "Signs of Life."

The thesis presents studies carried out on two enzymes, L-tartrate dehydratase and inosine 5'-monophosphate dehydrogenase. Each chapter has been divided into five sections. The first section introduces the topic to the reader, the second one describes the experimental procedures used. The next three sections consist of results and discussion, a summary of the overall study and future directions.

**L-tartrate dehydratase** (L-TTD) catalyzes the stereospecific conversion of L-tartrate to oxaloacetate. It shares high sequence similarity with class-I fumarate hydratases (FHs) which has often led to misannotation in the databases. Despite this high similarity, the two enzymes catalyze reactions on opposite stereoisomers. Understanding of the enzyme chemistry and catalysis in class-I FH and L-TTD is limited, with biochemical characterizations of the enzymes from only a few organisms e.g., FH from *Pelotomaculum thermopropionicum* (Shimoyama et al., 2007), *Methanocaldococcus jannaschii* (Bellur et al., 2023) and *Pyrococcus furiosus* (van Vugt-Lussenburg et al., 2009), and L-TTD from *Pseudomonas putida* (Kelly & Scopes, 1986), *Escherichia coli* (Reaney et al., 1993), and a L-tartrate fermenting anaerobic bacteria (Schink, 1984). Recent studies on class-I FH (Bellur et al., 2023; Patricia R. Feliciano et al., 2016) have led to a better understanding of the enzyme's biochemical function, whereas L-TTD has limited studies with regard to structure and catalysis. Tight stereospecificity for substrates, a key property of enzymes, is crucial in

---

---

pharmaceutical and chemical industries, because of their potential in synthesizing enantiopure compounds.

A multiple sequence alignment of class-I FH and L-TTD revealed that both enzymes share identical active site residues, despite catalyzing reactions of opposite stereospecificity. To the best of our knowledge, this is the first example of two proteins catalyzing reactions on opposite stereoisomers despite having identical active site residues. The only distinguishing feature between the two proteins was found to be a “KGXGS” motif in class-I FHs present as a “AGGGC” motif in L-TTD. The enzyme-substrate binding in the case of L-TTD could not be explained due to the lack of a structure. Thus, **Chapter 1** discusses how L-TTD shows this unique change in stereospecificity and sheds light on the molecular basis of enantioselectivity in the two classes of enzymes. Sequence alignment shows that other than the “KGXGS”/ “AGGGC” motif, the C-terminal tail is also unique to and conserved in L-TTDs. Gel filtration experiments showed L-TTD to be present as a heterotetramer (dimer of heterodimer). Further studies revealed that the presence of 4Fe-4S cluster bound to the protein. Crystallisation was attempted under various conditions; however, no crystals of good quality were obtained. Due to lack of experimentally determined structure, AlphaFold predicted structures were used for active site analysis. However, no difference was found in the orientation of the active site residues that could explain this changed specificity as compared to class-I FHs. Analysis of the quaternary structure points at a possible role played by the C-terminal tail in reorienting the active site residues, which hints at a possible reorientation mechanism. Moreover, consideration of the “enantiomer superposition model” shows that only a minor reorientation is needed for binding the cognate substrate in the active site.

**Inosine-5'-monophosphate dehydrogenase** (IMPDH) (EC 1.1.1.205) catalyzes the oxidation of inosine 5'-monophosphate (IMP) to xanthosine 5'-monophosphate (XMP) with simultaneous reduction of NAD<sup>+</sup> to NADH, which is the first committed step in the guanine nucleotide biosynthesis pathway. The reaction controls the major branchpoint between adenine and guanine nucleotide biosynthesis and is a rate limiting step in guanosine 5'-monophosphate (GMP) biosynthesis. The enzyme has a core catalytic domain composed of ( $\alpha/\beta$ )<sub>8</sub> barrel and regulatory cystathionine- $\beta$ -synthase (CBS) domain, also known as Bateman domain (Bateman, 1997). It is found to exist as a tetramer or an octamer, which shows polymerization into filaments called cytoophidia in eukaryotes (Anthony et al., 2017; Burrell et al., 2022; M. C. Johnson & Kollman, 2020). The CBS domain allosterically

---

regulates the enzyme, and this mode of regulation differs significantly between prokaryotes and eukaryotes. Prokaryotic IMPDHs have two nucleotide binding sites that only bind ATP, while eukaryotic IMPDHs have an additional non-canonical site that can bind GDP and GTP in addition to ATP. IMPDH is divided into two classes i.e., class-I and class-II, based on their dependence on ATP for catalytic activity. A conformational switch exists in IMPDH wherein bacterial IMPDH requires ATP to achieve full catalytic activity, while eukaryotic IMPDH is inhibited by GDP and GTP (R M Buey & Fernández-Justel, 2017). Although ATP does not cause any change of activity in eukaryotic IMPDHs, human IMPDHs have been shown to form filamentous structures in the presence of ATP (Anthony et al., 2017; M. C. Johnson & Kollman, 2020).

Due to the lack of understanding of archaeal IMPDHs, *Methanocaldococcus jannaschii* IMPDH (MjIMPDH) was studied in the laboratory. Despite high sequence similarity to prokaryotic IMPDHs, it shows behaviour similar to eukaryotic IMPDHs. Moreover, preliminary studies detected the presence of filamentous structures upon addition of Mg-ATP, which were previously reported in IMPDHs of eukaryotic origin only. **Chapter 2** discusses how transmission electron microscopy (TEM) has been used to characterize quaternary organization in IMPDHs. Despite repeated trials, filaments were not observed upon addition of ATP or GTP. Gel filtration chromatography of MjIMPDH shows two peaks on the chromatogram, of which the larger could not be stoichiometrically defined previously and hence assigned as higher order oligomers (Prasoon, 2019). Present studies using TEM show that the early eluting fraction on size-exclusion chromatography correspond octamers in a relaxed and expanded state compared to the later octamer fraction. This study indicates the presence of two different conformational states of MjIMPDH that require further structural characterization using single particle cryo-EM.

---

**[This page is intentionally left blank]**

---

---

# List of Abbreviations

ADP: Adenosine diphosphate  
AMP: Adenosine monophosphate  
ATP: Adenosine triphosphate  
BSA: Bovine serum albumin  
CBS: Cystathionine  $\beta$ -synthase  
CTD: C-terminal domain  
CTPS: Cytidine triphosphate synthetase  
DFT: Density functional theory  
DNA: Deoxyribonucleic acid  
dNTPs: Deoxy nucleoside triphosphates  
DTT: Dithiothreitol  
ESI: Electrospray ionization  
FEP: Free energy perturbation  
Fe-S: Iron-Sulphur  
FH: Fumarate hydratase  
FUM: fumarase  
GDP: Guanosine diphosphate  
GMP: Guanosine 5'-monophosphate  
GMPR: Guanosine 5'-monophosphate reductase  
GTP: Guanosine triphosphate  
HGT: Horizontal gene transfer  
IMP: Inosine 5'-monophosphate  
IMPDH: Inosine-5'-monophosphate dehydrogenase  
IPTG: Isopropyl-thiogalactoside  
kb: kilobases  
kDa: kilodalton  
LC: Liquid chromatography  
Lm: Leishmania major  
Mg: Magnesium

---

Mj: Methanocaldococcus jannaschii  
MM: Michaelis-Menten  
MS: Mass spectrometry  
MSA: Mercaptosuccinic acid  
NAD: Nicotinamide adenine dinucleotide  
NADP: Nicotinamide adenine dinucleotide phosphate  
Ni-NTA: Nickel-nitrilotriacetic acid  
NTD: N-terminal domain  
OD: Optical density  
PAGE: Polyacrylamide gel electrophoresis  
PEG: Polyethylene glycol  
PEI: Polyethyleneimine  
PMSF: Phenylmethyl sulfonyl fluoride  
ppm: parts per million  
QM/MM: Quantum mechanics/Molecular mechanics  
RMSD: Root-mean-square deviation  
RT: Retention time  
SDS: Sodium dodecyl sulphate  
SPA: Single particle analysis  
TB: Terrific broth  
TCA: Tricarboxylic acid  
TEM: Transmission electron microscopy  
TI: Thermodynamic integration  
TPA: Three point attachment  
TTD: Tartrate dehydratase  
XMP: Xanthosine 5'-monophosphate



---

# List of Figures

Figure 1.1. Proposed reaction mechanism for class-I FH.....	11
Figure 1.2. Active site of LmFH with bound L-malate.....	13
Figure 1.3. Mechanism of enzyme catalysis in FH .....	14
Figure 1.4. Multiple sequence alignment of biochemically characterized class I FH and L- TTD enzymes .....	20
Figure 1.5. Standardization of conditions for protein expression.....	21
Figure 1.6. Standardization of L-TTD purification .....	22
Figure 1.7. Attempts at crystallization and structure solution of L-TTD $\alpha\beta$ .....	24
Figure 1.8. Analytical gel filtration to infer oligomeric status of L-TTD.....	25
Figure 1.9. Native mass spectrometry of L-TTD $\alpha\beta$ complex .....	27
Figure 1.10. Assignment of different species of protein complex to the various peaks.....	28
Figure 1.11. Presence of 4Fe-4S cluster in L-TTD $\alpha\beta$ reconstituted complex .....	30
Figure 1.12. MSA binds as an inhibitor and chelates the labile iron atom .....	31
Figure 1.13. Visible circular dichroism spectra of Fe-S reconstituted L-TTD $\alpha\beta$ .....	32
Figure 1.14. Multiple sequence alignment shows the interface residues between $\alpha$ and $\beta$ subunits in class-I FHs and L-TTD .....	33
Figure 1.15. Ni-NTA pull down assay for interface analysis of the interacting subunits in class-I FHs and L-TTD.....	34
Figure 1.16. Comparison of class-I FH structures with AlphaFold predicted structures of L-TTD $\alpha$ and L-TTD $\beta$ subunits .....	35
Figure 1.17. L-TTD $\alpha\beta$ tetramer built from superposition of AlphaFold predicted structures	36
Figure 1.18. L-tartrate, D-tartrate and meso-tartrate docked active site in the structure of L-TTD .....	37
Figure 1.19. The three-point attachment model .....	40
Figure 1.20. Four-point location model for stereoselectivity of a protein .....	40
Figure 1.21. Enantiomer superposition model describing the stereospecificity of L-TTD .....	41
Figure 2.1. Mechanism of IMPDH reaction and cartoon representation of IMPDH .....	53
Figure 2.2. Domain architecture and spatial arrangement of IMPDH .....	54
Figure 2.3. Electron microscopy of uninhibited IMPDH2 filaments.....	57
Figure 2.4. Model of IMPDH2 assembly and the function of filaments in guanine nucleotide regulation.....	58
Figure 2.5. Multiple sequence alignment of IMPDH sequences from various organism .....	63

---

<b>Figure 2.6. Gel filtration profile of MjIMPDH .....</b>	<b>64</b>
<b>Figure 2.7. Negative-staining transmission electron micrographs of IMPDH under various conditions .....</b>	<b>65--66</b>
<b>Figure 2.8. Class averages of (A) stoichiometrically undetermined higher-order oligomer fraction, and (B) octamer fraction .....</b>	<b>69</b>
<b>Figure A.1. Isotopic distribution of peaks of L-TTD<math>\beta</math> at high resolution (120,000) under native condition.....</b>	<b>72</b>
<b>Figure A.2. Replicate of incubation of reconstituted L-TTD in air as shown in Fig. 1.11....</b>	<b>74</b>
<b>Figure A.3. Replicate of incubation of reconstituted L-TTD in air as shown in Fig. 1.11....</b>	<b>74</b>
<b>Figure A.4. Replicate of incubation of reconstituted L-TTD in air in presence of MSA as shown in Fig. 1.12.....</b>	<b>74</b>
<b>Figure A.5. Replicate of incubation of reconstituted L-TTD in air in presence of MSA as shown in Fig. 1.12.....</b>	<b>74</b>

---

## List of Tables

<b>Table 1.1. Oligomeric state of L-TTD<math>\alpha\beta</math>.....</b>	<b>26</b>
<b>Table 2.1. List of conditions screened for negative-staining EM of MjIMPDH .....</b>	<b>67</b>
<b>Table A.1. Mass difference in peaks with no isotopic distribution .....</b>	<b>73</b>

---

**[This page is intentionally left blank]**

---

---

# Contents

Declaration.....	iv
Certificate .....	vii
Acknowledgements .....	viii
Synopsis.....	xi
List of Abbreviations .....	xiv
List of Figures.....	xvii
List of Tables .....	xix
Chapter 1 .....	1
1.1 Introduction.....	3
1.1.1. Substrate specificity and selectivity in enzymes .....	3
1.1.2. Stereospecificity in enzymatic reactions.....	4
1.1.3. Significance of enzyme stereospecificity.....	6
1.1.4. Methodologies for switching stereospecificity .....	7
1.1.5. The curious case of opposite stereospecificity in class-I fumarate hydratase and L-tartrate dehydratase: enzymes with high sequence similarity .....	9
1.1.6. A closer look at catalysis in class-I FHs .....	11
1.1.7. Objectives.....	16
1.2. Experimental procedures .....	17
1.2.1. Sequence analysis by multiple sequence alignment .....	17
1.2.2. Chemicals, strains, and molecular biology reagents .....	17
1.2.3. Protein expression and purification .....	17
1.2.4. Reconstitution of Fe-S cluster .....	18
1.2.5. Enzyme activity .....	18
1.2.6. Analytical gel filtration.....	19
1.2.7. Native mass spectrometry .....	19
1.3. Results and discussion .....	20
1.3.1. Sequence analysis .....	20
1.3.2. Standardization of protein expression and purification.....	22
1.3.3. Crystallisation of L-TTD $\alpha\beta$ .....	24
1.3.4. Oligomeric state of L-TTD $\alpha\beta$ .....	25
1.3.5. Stoichiometric analysis of L-TTD by mass spectrometry.....	27

---

1.3.5. Absorption spectra of L-TTD $\alpha\beta$ .....	29
1.3.6. Circular dichroism spectroscopy of L-TTD .....	31
1.3.7. Specificity of interaction between subunits of class-I FH and L-TTD .....	32
1.3.8. Analysis of L-TTD $\alpha$ and L-TTD $\beta$ structures predicted by AlphaFold.....	34
1.3.8. Substrate stereospecificity in catalysis by L-TTD .....	39
1.4. Summary.....	44
1.5. Future Directions .....	46
1.5.1. Determination of L-TTD structure.....	46
1.5.2. Mutational analysis of the C-terminal tail.....	46
Chapter 2 .....	49
2.1. Introduction.....	51
2.1.1. Regulation of nucleotide biosynthesis and IMPDH .....	51
2.1.2. Structure and catalysis in the enzyme IMPDH .....	52
2.1.3. Modulation of the activity of prokaryotic and eukaryotic IMPDHs by nucleotides...55	
2.1.4. Role of cytoophidia in modulation of IMPDH activity .....	56
2.1.5. Unique regulatory features of an archaeal <i>Methanocaldococcus jannaschii</i> IMPDH.58	
2.1.6. Objectives.....	59
2.2. Experimental procedures .....	60
2.2.1. Chemicals, strains, and molecular biology reagents .....	60
2.2.2. Sequence alignment and phylogenetic tree construction.....	60
2.2.3. Protein expression and purification .....	60
2.2.4. Transmission electron microscopy imaging.....	61
2.2.5. Image Analysis .....	61
2.3. Results & Discussion.....	62
2.3.1. Sequence analysis .....	62
2.3.2. Transmission electron microscopy of IMPDH .....	64
2.3.3. Image processing by reference free 2D classification .....	67
2.4. Summary.....	70
2.5. Future directions .....	71
Appendix I.....	72
Appendix II.....	74
Rights and Permissions.....	75
References.....	78

---

---

**[This page is intentionally left blank]**

---

---

**[This page is intentionally left blank]**

---



---

# Chapter 1

## Towards understanding stereospecificity and substrate selectivity in L-tartrate dehydratase

---

The enzyme L-tartrate dehydratase (L-TTD) is a unique enzyme of the iron-sulfur cluster hydrolyase family with high sequence identity to class-I fumarate hydratase (FH) which leads to misannotation across databases. The two enzymes show complete conservation of the active site residues as well. However, they have been found to catalyze reactions on opposite stereoisomers, making them the first example of two enzymes having identical active site residues while showing substrate specificity for opposite stereoisomers. The key differentiating feature between the two enzymes has been found to be a conserved motif whose sequence is “KGXGS” in class-I FHs and “AGGGC” in L-TTD. In addition, L-TTD has a conserved C-terminal extension that is not found in class-I FHs. From our experiments, we see that L-TTD exists as heterotetramer (dimer of a heterodimer), with an iron-sulfur cluster. Crystallisation was attempted under different conditions; however, no protein crystals were obtained. Due to unavailability of solved structures, analysis of AlphaFold predicted structures was performed. The AlphaFold predicted structures show no major difference in orientation of active site residues from that of class-I FH that could explain the altered preference of substrate stereospecificity in L-TTD. This points towards a possible reorientation mechanism and flexible binding of the substrate which has been discussed at the end of the chapter.

---

---

**[This page is intentionally left blank]**

---

# 1.1 Introduction

## 1.1.1. Substrate specificity and selectivity in enzymes

Enzymes are biological catalysts that accelerate chemical reactions by lowering the activation energy required for the reaction to occur. Enzymes are highly specific for their substrates, meaning that each enzyme catalyzes a specific reaction with a specific substrate or group of substrates. This specificity is due to the unique three-dimensional structure of the enzyme's active site, which binds to the substrate and facilitates the chemical reaction. There are several types of substrate specificities that enzymes can exhibit, including absolute specificity, group specificity, and stereochemical specificity.

Absolute specificity refers to the ability of an enzyme to catalyze the reaction of only one specific substrate. For example, the enzyme lactase is specific to lactose and will only catalyze the hydrolysis of lactose into glucose and galactose (Fernandez et al., 1995). Other examples of enzymes with absolute specificity include urease, which catalyzes the hydrolysis of urea (Fishbein, 1969).

Group specificity refers to the ability of an enzyme to recognize and act on a specific functional group within a substrate. For example, the enzyme chymotrypsin recognizes and cleaves peptide bonds adjacent to aromatic amino acid residues. This means that chymotrypsin can cleave peptide bonds in substrates that contain an aromatic amino acid residue but not in substrates that do not contain this group (Fersht et al., 1973).

Stereochemical specificity refers to the ability of an enzyme to distinguish between stereoisomers of a substrate. Stereoisomers are molecules that have the same molecular formula and connectivity but differ in the spatial arrangement of their atoms. Enzymes that exhibit stereochemical specificity are called stereospecific enzymes. Example of stereospecific enzymes are L- and D-lactate dehydrogenases, which catalyze the conversion of their respective lactic acid enantiomer to pyruvate (Dennis & Kaplan, 1960).

---

In addition to these types of substrate specificity, enzymes can also exhibit kinetic specificity, which refers to the ability of an enzyme to preferentially catalyze one reaction pathway over another, and promiscuous specificity, which refers to the ability of an enzyme to catalyze reactions with multiple substrates, albeit with lower catalytic efficiency (Lizbeth Hedstrom, 2001).

In conclusion, enzymes exhibit a wide range of substrate specificities, allowing them to catalyze specific reactions with high efficiency and selectivity. Understanding the different types of substrate specificity exhibited by enzymes is critical for understanding their function and designing novel enzymatic processes for various applications, such as biotechnology and pharmaceuticals.

### **1.1.2. Stereospecificity in enzymatic reactions**

The concept of chirality was first discovered by Louis Pasteur in 1864, who observed that some organic molecules exist in two mirror-image forms that cannot be superimposed onto each other (Pasteur, 1858). This property arises when a carbon atom with tetrahedral  $sp^3$  hybridization has four distinct substituents, leading to the formation of two enantiomers that are non-superimposable mirror images of each other. The presence of chirality in biological molecules is crucial, as it allows for the formation of highly specific and stable molecular interactions. For instance, proteins are only composed of L-amino acids, demonstrating the importance of homochirality for their structure and function. Enzymes are now extremely selective catalysts that can only catalyze reactions on a single stereoisomer as a result of this. In actuality, a separate enzyme is needed for the anti-enantiomer. This is significant for a number of reasons. Firstly, many pharmaceuticals and natural products appear as stereoisomers, and they can all have various pharmacological properties. Second, in order to guarantee that the right products are produced, enzymes must be able to differentiate between the stereoisomers that can arise as intermediates in biochemical pathways.

Dealing with stereoisomers, which are molecules with the same chemical composition and connectivity but different spatial arrangements, is one of the difficulties enzymes encounter. Different physical, chemical, and biological characteristics of stereoisomers can have a significant impact on how well enzymes engage with them. Molecules that vary in their spatial arrangement despite sharing the same chemical formula and connectivity are known as stereoisomers.

---

Enantiomers and diastereomers are the two major categories of stereoisomers. Enantiomers are mirror images of each other and cannot be superimposed on each other, while diastereomers are stereoisomers that have more than one chiral center. Despite having the same chemical formula, stereoisomers can have very different characteristics. Enantiomers, for instance, have distinct optical properties depending on which way they rotate plane-polarized light. Because they can interact differently with enzymes and other biomolecules, enantiomers can also have distinct biological characteristics.

Enzymes recognize and distinguish between stereoisomers using a variety of complex processes. One process is called steric hindrance, in which the enzyme active site can only hold one specific stereoisomer because of its three-dimensional structure. The enzyme active site interacts more favorably with one stereoisomer than the other owing to variations in charge distribution in an additional mechanism called electrostatic interactions.

Hydrogen bonds, metal coordination, and induced fit are additional processes of enzyme stereoselectivity. While metal coordination entails the binding of a metal ion to a specific stereoisomer, hydrogen bonding happens when the enzyme active site is able to form hydrogen bonds with particular functional groups on the stereoisomer. When an enzyme binds to a particular stereoisomer, the active site goes through a conformational shift, which improves binding and catalysis (Koshland, 1958).

There are several different types of enzymes that are involved in stereoisomerism. When it comes to NAD-dependent dehydrogenases, two different-folded enzymes that have their catalytic sites reversed, catalyze reactions on the L- and D-isomers (Lamzin et al., 1994). When it comes to glycosyl hydrolases, nature has created many kinds of enzymes with utterly unique 3D folds that invert the catalytic base with respect to the substrate, allowing them to recognize and catalyze on anomeric carbons with opposing chiralities (McCarter & Stephen Withers, 1994).

Lipases, however, are a singular exception in that they can catalyze processes involving either enantiomer, though they tend to favor one over the other (Lamzin et al., 1995). The active site's chirality in lipases causes the enzyme to favor one enantiomer while being indifferent to the other. The most frequent way for enzymes to deal with stereoisomers is through the evolution of different

---

enzymes with unique active site architectures that can catalyze reactions on opposing stereoisomers.

An enzyme's stereo-specificity originates from the active site's three-dimensional structure, which allows it to perfectly suit the substrate in alignment with the catalytic residues (Lizbeth Hedstrom, 2001). This guarantees that the enzyme can recognize particular processes and catalyze them with high selectivity and efficiency. In general, studying enzymes and their capacity to deal with stereoisomers is crucial for comprehending their role and developing novel enzymatic procedures for a range of biotechnology and pharmaceutical applications.

### **1.1.3. Significance of enzyme stereospecificity**

Biologically active molecules can exist in different forms called enantiomers, which have distinct physiological properties. It is crucial to create procedures for synthesizing only the desired enantiomer because some of these enantiomers, unfortunately, can have toxic side effects. Currently, over fifty percent of all clinically used small molecule drugs are chiral small molecules (Shen et al., 2016). Enzyme-catalyzed reactions offer a more selective way to make chiral compounds than traditional organic synthesis does (Wombacher et al., 2006). The method of selectively producing one enantiomer over the other is known as chiral synthesis. This is significant because the stereochemistry of a molecule often dictates the biological action of a drug. When compared to pure enantiomers, a mixture of enantiomers known as a racemic mixture may exhibit distinct biological activities. For instance, fluoxetine, an antidepressant, is sold as a combination of enantiomers, but only one of them is actually active, and the other one may have negative adverse effects (Robertson et al., 1988). Thalidomide, a 1960s drug used to treat morning sickness and insomnia, serves as an illustration of the significance of asymmetric synthesis (Wombacher et al., 2006). The S-enantiomer was discovered to be teratogenic and to cause severe birth defects like shortened flipper-like limbs, even though the R-enantiomer was successful as a therapeutic agent.

Asymmetric synthesis, chiral catalysis, and chiral chromatography are just a few techniques that can be used to create chiral compounds. Asymmetric synthesis is the process of selectively adding a chiral core to a molecule during synthesis in order to produce a particular enantiomer. A chiral

---

catalyst is used in chiral catalysis to speed up a chemical process that produces a particular enantiomer. Enantiomers are separated using chiral chromatography based on how they interact with a chiral stationary phase.

For the development of novel pharmaceuticals and the building of more effective industrial processes, it is essential to understand the stereochemistry of enzyme-substrate interactions. Chiral synthesis is important in biochemistry, especially in the research of biological systems and the development of drugs. Enantiopure medicines with greater effectiveness and fewer side effects can be made by selectively producing one enantiomer over the other.

Full control of stereogenic centers in catalyst-controlled reactions remains a challenging task despite recent advancements in asymmetric synthesis (Xu et al., 2019). However, the increasing use of enzymes to make stereospecific products has accelerated the synthesis of chiral molecules, offering intriguing opportunities to develop novel therapeutically effective medications (Mu et al., 2020).

### **1.1.4. Methodologies for switching stereospecificity**

Due to their capacity to promote effective reactions with high yields in an eco-friendly manner, biocatalysts have grown in popularity in the field of chemistry. The importance of stereoselectivity in pharmacology has led researchers to concentrate on figuring out the structural and mechanistic underpinnings of enzyme-mediated events (Chan et al., 2019). The stereoselective characteristics of enzymes have been altered through a variety of techniques, including de novo enzyme engineering, computational rational designing, chemical modification, and in vitro evolution.

One of the earliest techniques for changing the stereospecificity of enzymes was chemical modification, which modifies the enzyme's amino acid residues covalently to change the enzyme's structure and activity. The active region of an enzyme can be modified chemically to add new functional groups or to change the reactivity of a particular amino acid residue. Numerous enzymes, including aspartate aminotransferase and horseradish peroxidase (HRP), have been shown to change their stereospecificity when chemically altered with N-bromosuccinimide (NBS) (Nagashima et al., 1986). As a consequence of NBS treatment, side chains of specific amino acid

---

residues in the enzyme's active site undergo selective bromination. This selective bromination modifies how the enzyme interacts with its substrate and switches the enzyme's stereospecificity.

One approach included creating an enzyme from scratch to catalyze a Diels-Alder reaction, which produced four stereocenters and two carbon-carbon bonds (Siegel et al., 2010). Only two of the 84 predicted enzyme constructs, however, were able to exhibit Diels-Alderase activity in an experimental setting, highlighting the challenges associated with pure de novo design. On the other hand, rational enzyme engineering makes use of contemporary computational techniques and methods to help control the stereospecificity of an enzyme's catalytic properties. These methods provide insights into the atomic interactions between the enzyme and the substrate and can predict the allosteric effects of mutations at sites other than the active site (Chan et al., 2018; Reetz, 2011). Numerous in silico approaches, such as, Poisson-Boltzmann surface area continuum solvation (Genheden & Ryde, 2015), free energy perturbation (Jorgensen & Thomas, 2008), and thermodynamic integration (Ruiter & Oostenbrink, 2016) have been developed to assess relative binding energies. Rational designing frequently requires the conversion of significant polar residues into hydrophobic ones in order to limit the size of the active site pocket and constrain substrate orientation to achieve stereospecificity.

The most effective scientific approach to increase stereoselectivity is directed evolution. This approach includes repeated cycles of protein expression, mutagenesis, and screening for the desired property. The stereospecificity of several enzymes, including esterases and epoxide hydrolases, has been changed through directed evolution. This technique has been used to create enzymes that can catalyze reactions that no enzyme from nature is capable of.

Chemistry is paying increased attention to biocatalysts due to the wide range of applications, including the catalysts' capacity to promote highly efficient, higher-yield reactions that follow an environmentally acceptable approach. Due to the significance of stereoselectivity in pharmacology, research into the structural and molecular underpinnings of the phenomena the enzyme mediates has been extensive. In this field of study, a variety of tools and techniques, including de novo enzyme engineering, computational rational designing, and in vitro evolution, have been utilized to control the stereoselective features of enzymes.

---



In order to achieve stereospecificity, critical polar residues in known enzyme active sites are mutated into hydrophobic ones, which alter the size of the active site pocket and limit substrate orientation. In terms of experiments, directed evolution has the best chance of increasing stereoselectivity. Recursive rounds of mutagenesis are used in this procedure, then protein expression and screening for the required attribute (Li & Reetz, 2016). By using this method, enzymes have evolved to be able to catalyze processes that no other enzymes known to nature can (Hammer et al., 2017).

### **1.1.5. The curious case of opposite stereospecificity in class-I fumarate hydratase and L-tartrate dehydratase: enzymes with high sequence similarity**

Class-I fumarate hydratases (FH, fumarases) bear striking similarity to L-tartrate dehydratase (L-TTD), with both being members of the iron-sulfur cluster hydrolyase family and having high sequence similarity. L-TTD catalyzes the stereospecific conversion of L-tartrate to oxaloacetate. It has been observed only in prokaryotes and remains yet to be identified in archaea and eukaryotes. Studies on L-TTD are limited with the enzyme from *Pseudomonas putida* (Kelly & Scopes, 1986), *Escherichia coli* (Reaney et al., 1993), and an L-tartrate fermenting anaerobic bacteria (Schink, 1984) examined biochemically. To date, no structure of the enzyme has been determined. Class-I FHs on the other hand can be divided into single and two-subunit type enzymes based on the number of genes encoding the functional protein. Two-subunit class-I FHs are found only in archaea and prokaryotes but not in eukaryotes. Recent work has shed some light into the catalytic mechanism of single- and two-subunit class-I FHs (Bellur et al., 2023; Patricia R. Feliciano et al., 2016). From previous literature as well as earlier experiments carried out in the group, it was found out that these two groups of enzymes, L-TTD and class I FH have completely opposite substrate specificity. Class-I FHs use L-malate and D-tartrate as substrates, whereas L-TTD uses L-tartrate and D-malate. Planar and achiral fumarate was discovered to be a substrate for both enzymes, while both classes of enzymes were inhibited by the competitive inhibitor meso-tartrate. L-malate inhibited L-TTD, whereas L-tartrate was found to have no affinity for MjFH (Bellur et al., 2023). However, L-tartrate inhibited *E. coli* class-I FH (Flint, 1994), showing that there are minute differences between single-subunit and two-subunit class-I FHs. Thus, class-I FH and L-TTD function differently in spite of having such a high degree of sequence similarity. This suggests that

---

small variations in the architecture of enzyme active sites must have contributed to the specificity of enzymes in this family of Fe-S cluster hydrolyases.

Both L-TTD and two subunit class-I FHs, exist as tetramers (dimer of two heterodimers). Each heterodimer is composed of two subunits,  $\alpha$  and  $\beta$ . In the case of single subunit class-I FHs, the two subunits are joined by a linker, and the domains are referred to as the N-terminal domain (NTD) and C-terminal domain (CTD). L-TTD and Class-I FH exhibit very high sequence similarity, because of which there are incorrect annotations in RCSB and UniProt databases. The structure of the  $\beta$ -subunit of MjFH (PDB ID: 5DNI) deposited in the RCSB database annotates the protein to be a putative L-TTD  $\beta$ -subunit (Bellur et al., 2023). The structure of the MjFH  $\beta$ -subunit is listed along with the tartrate dehydratase  $\beta$ -subunit in the UniProt database.

Class-I FH catalyzes conversion of D-tartrate to oxaloacetate, while L-TTD catalyzes the reaction to convert L-tartrate to oxaloacetate, showing that the two enzymes have opposite stereospecificity (Kronen et al., 2015; van Vugt-Lussenburg et al., 2009, 2013). Multiple sequence alignment of Class-I FH and L-TTD shows that active site residues are fully conserved. The residues involved in substrate binding and catalysis as deduced in *Leishmania major* FH and *Methanocaldococcus jannaschii* FH are identical in L-TTD. Class-I FHs and L-TTDs are a particularly unique set of stereospecific enzymes with active sites containing identical residues but catalyzing reactions on opposite stereoisomers.

Previous analysis of the sequences of the two enzymes led to the identification of a motif, the sequence of which is specific to class I FH and L-TTD (Fig. 1.4). A highly conserved motif, "KGXGS", present in class-I FH, is replaced by "AGGGC" in L-TTD (Fig. 1.4) (Bellur, 2022). Phylogenetic analysis revealed that two-subunit class-I FHs and L-TTD share a common ancestral origin, suggesting a possible horizontal gene transfer (HGT) event during evolution. Switching the "AGGGC" motif in *E. coli* L-TTD to the "KGXGS" motif in class-I FHs led to complete loss of protein expression highlighting a possible structural role for this motif (Bellur, 2022). However, when residues from L-TTD motif and those neighboring it were used to replace the corresponding residues in MjFH, they failed to develop any ability to bind L-tartrate and only led to decreased enzyme activity on L-malate. This showed that the motif is not solely responsible for the unique stereospecificities.

---

## 1.1.6. A closer look at catalysis in class-I FHs

It still remains unclear how the active site of L-tartrate dehydratase shows a change of stereospecificity compared to class-I FHs. Furthermore, there are sequence misannotations in databases due to a lack of information on the sequence features that distinguish class-I FH and L-TTD. In a small number of organisms, single-subunit class-I FHs have been biochemically characterised (de Pádua et al., 2017; Patrícia R. Feliciano et al., 2012; Jayaraman et al., 2018; Kronen et al., 2015; Shibata et al., 1985; Van Kuijk & Stams, 1996; van Vugt-Lussenburg et al., 2013). So far, three two-subunit Class-I FHs, from *Pyrococcus horikoshii* (van Vugt-Lussenburg et al., 2009), *Pelotomaculum thermopropionicum* (Shimoyama et al., 2007), and *Methanocaldococcus jannaschii* (Bellur et al., 2023) have been biochemically characterized. Aconitase, a well-studied Fe-S cluster hydrolyase, and class-I FHs are two major sources of information on understanding the mechanism of catalysis in L-TTD. (Flint & Allen, 1996). A significant advancement in understanding the molecular mechanism of the L-tartrate dehydratase reaction has been made with the recent reporting of the structures of a substrate and inhibitor-bound class-I FH from *Leishmania major* (LmFH) and apo *Methanocaldococcus jannaschii* FH (MjFH). (Bellur et al., 2023; Patricia R. Feliciano et al., 2016; Patricia R. Feliciano & Drennan, 2019).

### 1.1.6.1. Fe-S cluster hydrolyases

Enzymes classified as hydrolyases [EC 4.2.1.x], facilitate the removal of a water molecule from a carbon-carbon bond, resulting in the conversion of an alcohol to a vinyl group. Within this class, enzymes can be categorized based on whether they contain metal, lack metal, or utilize Fe-S cluster for catalytic activity. Various hydrolyases use Fe-S cluster for catalysis, such as aconitase, homoaconitase, isopropyl malate isomerase, fumarate hydratase, maleate hydratase, mesaconase, tartrate dehydratase, dihydroxy-acid dehydratase, phosphogluconate dehydratase, serine dehydratase, and quinolinate synthase. (Flint & Allen, 1996). Aconitase, fumarate hydratase, serine dehydratase, and quinolinate synthase are the only enzymes of the hydrolyase class that have been thoroughly explored from the context of structure and catalytic mechanism. The majority of our knowledge of the catalysis used by this class of enzymes comes from research on

---

aconitase. The cluster is largely engaged in activating the substrate hydroxyl group by serving as a Lewis acid to make it a better leaving group.

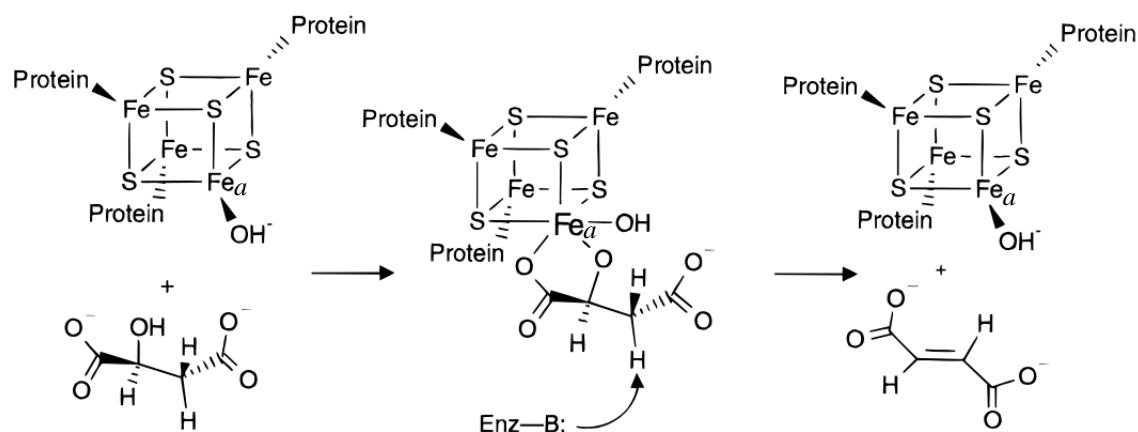


**Figure 1.1. Proposed reaction mechanism for class-I FH.** (Reprinted with permission from Flint, D. H., & Allen, R. M. (1996)) Three cysteine residues hold the Fe-S cluster to the protein. The fourth iron in the cluster is the labile iron,  $Fe_a$ .  $Fe_a$  produces a tetradentate structure with a hydroxyl group in the absence of a substrate. Upon binding the substrate malate, the hydroxyl group on the substrate and its carboxylate group, bind to  $Fe_a$  to create a hexadentate structure. The Fe-S cluster functions as a Lewis acid by pulling the lone pair of electrons on the -OH group of the substrate to facilitate cleavage. The proton from the C3 carbon of malate is abstracted by a catalytic base, resulting in the synthesis of fumarate and the release of a water molecule.

A serine residue works as a catalytic base in aconitase to remove a proton from the substrate, while an ion pair formed by an aspartyl and a histidyl residue eliminates the substrate's hydroxyl group (Zheng et al., 1992). Based on the catalytic mechanism adopted by aconitase, a similar mechanism was proposed to occur in class-I FH as shown in **Fig. 1.1** (Patricia R. Feliciano et al., 2016; Flint & Allen, 1996). Apart from the fact that aconitase is primarily a dehydratase and FH is a hydratase, there are a number of differences between the two that indicate the mechanism may not be quite the same. More research is needed to identify differences in enzymes from the Fe-S cluster hydrolyase class.

---

### 1.1.6.2. *L. major* class-I FH

The crystal structure of the single-subunit type class-I FH from *Leishmania major* has recently been determined. The crystal structures of the enzyme bound to different substrate analogues as well as to the inhibitor thiomalate (mercaptosuccinate, MSA) have subsequently been determined, and the coordinates have been deposited in RCSB (Patricia R. Feliciano et al., 2016). The Fe-S cluster and the substrate are bound at the active site of the *L. major* FH (LmFH) structures, providing crucial information about how active site residues interact with the substrate (**Fig. 1.2**).

With a threonine residue (Thr467) close to the substrate's C3 carbon (3.2 Å) and an aspartate residue (Asp135) close to the C2 hydroxyl group (2.9 Å), a total of 7 residues from the CTD and 5 residues from the NTD are in hydrogen-bonding proximity to the substrate. A 2,000 to 16,000 fold reduction in  $k_{\text{cat}}$  was observed following mutational investigations of the active site residues Thr467 (T467A), Asp135 (D135A), and the three arginine residues, 173, 421, and 471 (R173A, R421A, and R471A) that are at hydrogen-bonding distance with the substrate (Patricia R. Feliciano & Drennan, 2019). The two arginine residues, Arg421 and Arg471, are within hydrogen-bonding distance of Thr467 (2.5 to 3.0 Å), and it has been proposed that either one of them could assist the side chain hydroxyl of Thr467 in the abstraction of the proton from the C3 carbon of the substrate L-malate. It has been proposed that in a base-catalyzed reaction, the three residues function as a catalytic base triad to remove the proton from the substrate. The catalytic acid dyad Asp135 and His334 which are closest to the substrate's C2-OH group (2.64 Å from the carboxyl group of Asp135), are thought to contribute a proton to the hydroxyl group and aid in its removal as a water molecule. It has been proposed that Arg173 is crucial for keeping the substrate in the right position at the active site for effective catalysis. Some of the other residues that are near the substrate and at a hydrogen-bonding distance have not been subjected to mutational studies in LmFH.

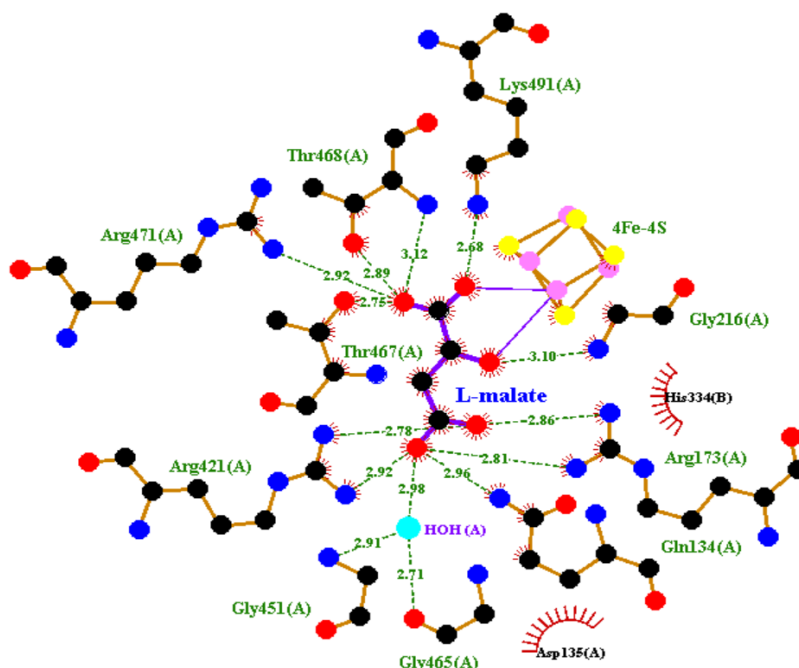


**Figure 1.2.** Active site of LmFH with bound L-malate (5l2r). Active site includes an iron-sulfur cluster, bound L-malate, and substrate binding residues. The residues involved in malate binding and their corresponding distance from the different atoms of malate are shown. Also included is His334 from the neighboring subunit that contacts the side chain carboxyl of Asp135. Image was created using LigPlot+ (Laskowski & Swindells, 2011). Water molecule at the active site is shown in cyan; C, N, O, Fe, and S atoms are shown in black, blue, red, pink, and yellow, respectively. Hydrogen-bonds are shown as green dashed lines with distances highlighted in green.

### 1.1.6.3. *Methanocaldococcus jannaschii* class-I FH

Recently, the structure of a two subunit class-I FH from a hyperthermophilic archaeon *Methanocaldococcus jannaschii* has been determined by our group (Bellur et al., 2023). The apoprotein structure has been determined and it superposes on the LmFH Fe-S cluster and ligand bound structure with RMSD of 3.388 Å. The catalytic mechanism operating in class-I FH has been deciphered through kinetic analysis on site-directed mutants of MjFH and computational studies involving density functional theory (DFT) and QM/MM calculations. Mutation of the catalytic acid and base residues (D62V and T80V) caused only a 37-fold and 196-fold reduction in activity on malate and a 28-fold and 234-fold reduction in activity on fumarate as substrate. This was not a considerable decrease considering that the catalytic rate enhancement in fumarate hydratase is of the order of  $10^{15}$ . This suggested that base-mediated proton abstraction is not the rate-limiting step for the reaction. However, mutation of the residues that form a hydrogen-bonded

network with the substrate caused complete loss of activity. This highlights the importance of binding residues and suggests a critical role for them in transition state stabilization (Bellur et al., 2023).

It has been proposed that charge polarization at the active site due to non-covalent interactions form the basis of catalysis. When the substrate binds to the active site, the surrounding residues polarize it to enable nucleophilic attack and provide electrostatic stabilization for the negative charge on the carbanionic intermediate form of the substrate approaching the transition state. The role of electrostatic stabilization has been long discussed to explain the large gain in entropy observed for binding the altered substrate in transition state rather than in ground state (Bearne & Wolfenden, 1995). Thus, it was proposed that the affinity of the FH active site for binding the transition state is much higher than that for the substrate, which leads to catalysis as shown in **Fig.1.3**.

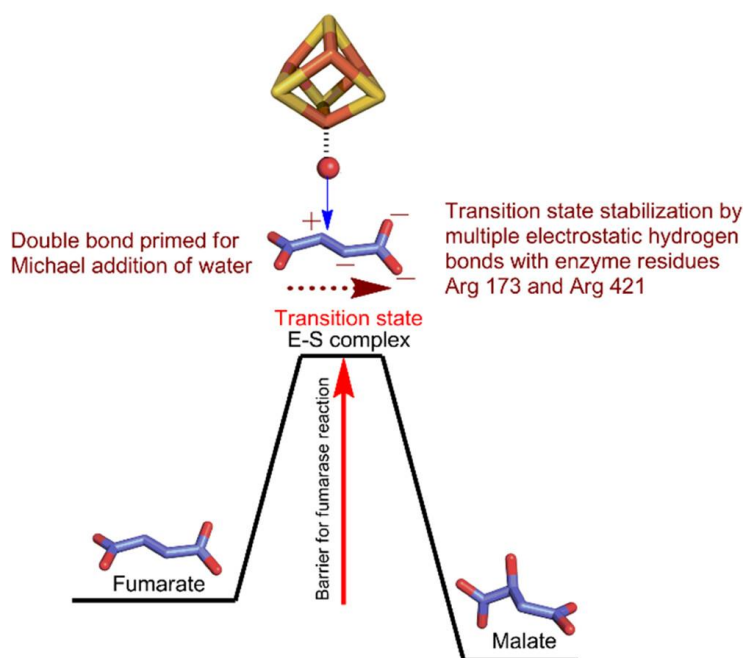


**Figure 1.3. Mechanism of enzyme catalysis in FH.** Reprinted with permission from Bellur, A. et al (2023). *Revisiting the Burden Borne by Fumarase: Enzymatic Hydration of an Olefin. Biochemistry*, 62(2), 476–493. Upon binding to the enzyme's active site, the positively charged residues on both sides of the substrate raise it to its transition state and strongly charge polarize it. A water molecule kept in place by the Fe-S cluster attacks the transition state complex, after which the product is released.

### **1.1.7. Objectives**

L-tartrate dehydratase has not yet been fully biochemically characterised, so the objectives of this study were to: (i) biochemically and structurally characterize the enzyme from *E. coli*; (ii) understand the mechanism underlying the unusual case of stereospecificity; and (iii) understand the specificity-offering residues in the two enzymes that can switch stereospecificity.



## **1.2. Experimental procedures**

### **1.2.1. Sequence analysis by multiple sequence alignment**

Methanocaldococcus jannaschii FH (MjFH), E. coli FH (FumA), and E. coli L-TTD protein sequences were used as queries in the NCBI BLAST-P tool to get the class-I FH and L-TTD protein sequences. Clustal Omega (Goujon et al., 2010) was used for multiple sequence alignment, and ESPRIPT was used to process the result for visualization. (Goujon et al., 2010; Sievers et al., 2011).

### **1.2.2. Chemicals, strains, and molecular biology reagents**

Thermo Fisher Scientific Inc. provided Ni-NTA conjugated agarose beads for use in this experiment. Malic dehydrogenase from pig heart was purchased commercially from Sigma-Aldrich in the United States (product number M2634). E. coli cultures were grown using Himedia media from Mumbai, India.

### **1.2.3. Protein expression and purification**

The L-TTD protein was expressed in BL21(DE3)-RIL E. coli cells that also carried a second plasmid (RIL) that expressed tRNAs for the uncommon codons of arginine, isoleucine, and leucine. This combination allowed for the transformation and overexpression of the L-TTD protein. In the lab, the expression construct pETduet\_LTDD was already available. BL21 (DE3) RIL E coli cells were transformed with the recombinant plasmid pETduet\_LTDD and cultured at 37 °C to an O.D. 600 of >1.0 before being induced with 0.3 mM IPTG and grown for an additional 16 hours at 30 °C to overexpress L-TTD. After being pelleted, the cells were lysed using lysis buffer (50mM Tris HCl, pH 8.0, 5% glycerol, 1mM DTT and 1mM PMSF) using French pressure cell press (Thermo IEC Inc., USA). The lysate was clarified by centrifugation at 30,000 x g for 30 minutes. Without disturbing the pellet, the supernatant was carefully collected, and a 1 mL slurry of Ni-NTA beads (Qiagen) pre-equilibrated with lysis buffer was added. This was done to facilitate the binding of His-tagged protein. After the 3 hours of binding at 4 °C, the beads were washed with 50 mL of lysis buffer to eliminate any remaining unbound proteins, and the Ni-NTA-bound protein was then eluted with various doses of imidazole. Pure protein-containing fractions were

---

pooled and dialyzed in a solution with a pH of 8.0, 50mM Tris HCl, 5% glycerol, and 1mM DTT. Following dialysis and pooling, the fractions were loaded onto a Q-Sepharose anion-exchange column. A linear gradient of NaCl was used to elute the protein in a buffer containing 50 mM Tris HCl, pH 8.0, 5% glycerol, and 1 mM DTT. SDS-PAGE was used to analyze fractions collected at NaCl concentrations greater than 200 mM (U.K.Lammler, 1970), pooled according to purity and dialyzed in dialysis buffer containing 50mM Tris HCl, pH 8.0, 5% glycerol and 1mM DTT. The protein concentration was estimated by the Bradford method with bovine serum albumin (BSA) as the standard (Bradford, 1976).

#### **1.2.4. Reconstitution of Fe-S cluster**

Following standard protocols, purified protein aliquots kept at -80 °C were reconstituted with Fe-S cluster (Beinert et al., 1996; Yano et al., 1996). To completely eliminate any traces of oxygen, the protein solution was incubated for 1 hour in an anaerobic chamber (Coy, USA). The following processes were all carried out inside the chamber under anaerobic conditions. In a nutshell, 10–50 M of protein was used for reconstitution. The reconstitution procedure was initiated by the addition of 50-fold excess DTT to the protein solution followed by constant stirring for 30 min. After that, 10-fold molar excesses of sodium sulphide and ferrous ammonium sulphate were added, and the mixture was agitated for an additional three hours to produce the holoprotein with a completely reconstituted iron-sulfur cluster.

#### **1.2.5. Enzyme activity**

Unless stated otherwise, all procedures for measuring enzyme activity were carried out at 37 °C using a water-circulated cell holder attached to a Hitachi U2010 spectrophotometer. The coupling enzyme porcine malate dehydrogenase (MDH), which was purchased commercially, was used to track activity on tartrate. The reaction was conducted in a final volume of 500 µl using 50 mM Tris-HCl, pH 7.4, 250 µM NADH, 2.5 µg MDH, and various L-tartrate concentrations. The coupling enzyme MDH, which turns oxaloacetate into L-malate by using a molecule of NADH, coupled the conversion of L-tartrate to oxaloacetate to the synthesis of NAD<sup>+</sup>. The addition of 1.6 µg of E. coli L-TTD started the reaction, which was then carefully observed for about a minute at

---

340 nm (molar extinction coefficient( $\epsilon$ ) of NADH is  $6.22 \text{ mM}^{-1}\text{cm}^{-1}$  at 340 nm) to obtain reliable slopes.

### **1.2.6. Analytical gel filtration**

Size-exclusion chromatography was used to examine the co-purified protein's oligomeric state on an analytical Superdex 200 10/300 GL column (10 mm X 300 mm) from GE Health Care Life Sciences, which was connected to an AKTA Basic HPLC system with a UV900 detector. The column was equilibrated with Buffer A (50 mM Tris-HCl pH 8.0, 5% glycerol, 1 mM DTT) and calibrated using molecular weight standards; blue dextran (2000 kDa),  $\beta$ -amylase (200 kDa), alcohol dehydrogenase (150 kDa), bovine serum albumin (66 kDa), and carbonic anhydrase (29 kDa). The empty volume of the column matches the volume of blue dextran that is eluted. The ratio of the elution volume to the void volume of these standards was plotted against their log molecular weight to create a standard curve. 100  $\mu\text{l}$  of pure protein (10 mM) was loaded onto the column, and the elution was measured simultaneously at 280 nm and 220 nm. The flow rate was kept at  $0.5 \text{ ml min}^{-1}$ . By extrapolating the elution volume from the standard curve, the complex's molecular weight was determined.

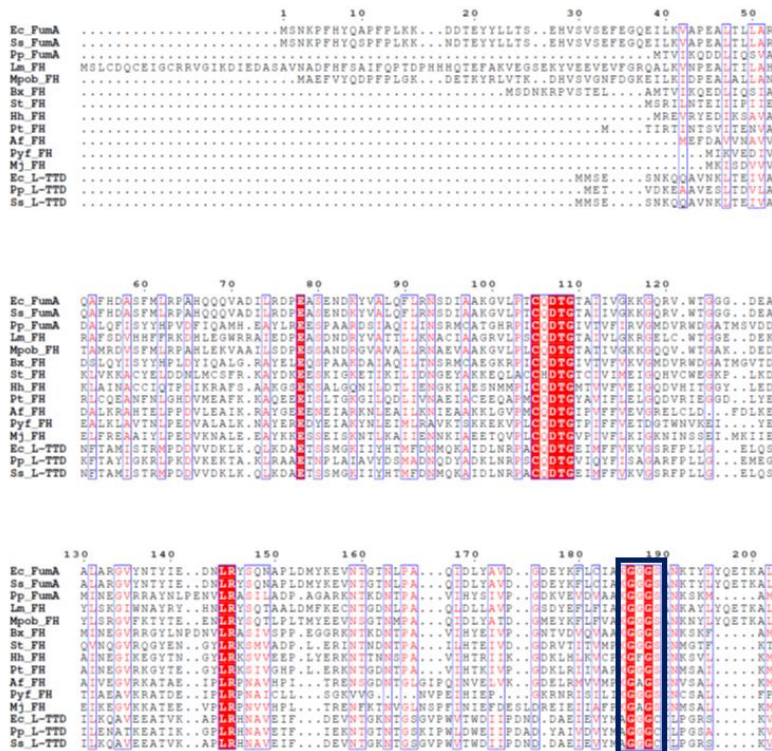
### **1.2.7. Native mass spectrometry**

Native mass spectrometry measurements were performed on an Q Exactive Orbitrap HF mass spectrometer (ThermoFischer) operating in the positive ion mode with HESI-II ion source. 15  $\mu\text{M}$  of freshly purified L-TTD $\alpha\beta$  protein complex (protein sample was not reconstituted with Fe-S cluster), dialyzed against 10 mM ammonium acetate, pH 7.4 was injected using a Hamilton syringe connected to a needle at a flow rate of  $0.5 \mu\text{l min}^{-1}$ . The capillary temperature was set at 250  $^{\circ}\text{C}$  with a capillary voltage of 2500/3000 V. The sheath and auxiliary gas flow rate were maintained at  $20 \text{ l min}^{-1}$  and  $10 \text{ l min}^{-1}$  respectively. Data were recorded in positive ion mode with UV monitoring at 280, 220 and 254 nm.

## 1.3. Results and discussion

### 1.3.1. Sequence analysis

Alignment of class-I FH and L-TTD sequences from organisms in which they have been biochemically characterized was carried out after fusing the  $\alpha$ - and  $\beta$ -subunits of two-subunit FH and L-TTD. The multiple sequence alignment of the single-subunit FH, two-subunit FH and L-TTD reveals good sequence conservation and a domain boundary in single-subunit type FH. Much of the differences seen between these proteins arise from the N-terminus of the N-terminal domain which as an extension in the single-subunit FH that is not seen in two-subunit type protein. The C-terminus stretch of the C-terminal domain also lacks good conservation. Previous analysis had revealed the conservation of the active site residues in L-TTD and class-I FH as well as the presence of the “KGXGS” motif of class-I FH as “AGGFC” motif in L-TTD (Bellur, 2022). Upon further analysis of the multiple sequence alignment, it shows that the C-terminal residues are conserved in L-TTD across multiple organisms and absent in all class-I FHs as shown in **Fig. 1.4**.



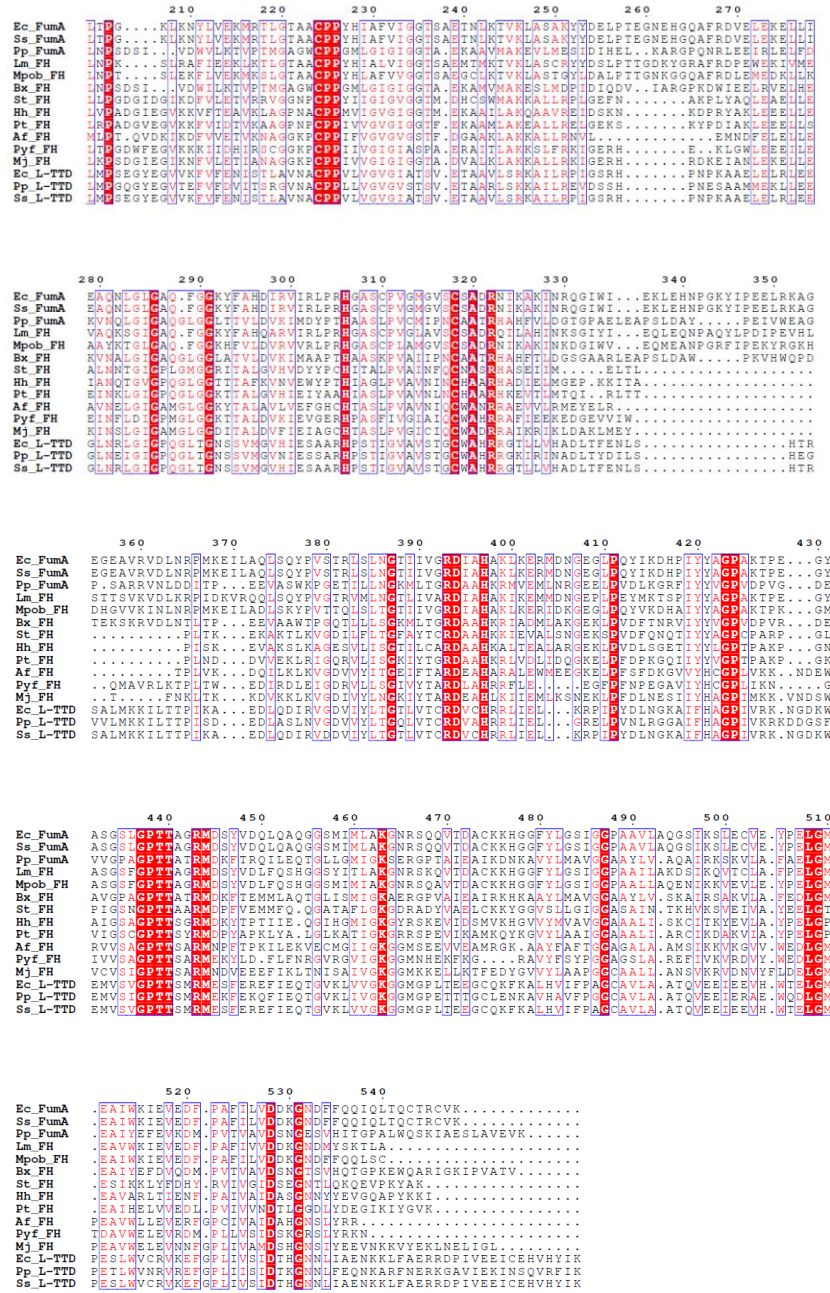


**Figure 1.4. Multiple sequence alignment of biochemically characterized class I FH and L-TTD enzymes.** KGXGS motif present as an AGGGC motif in L-TTD is highlighted in a green box in the alignment. The C-terminal segment in L-TTD has been highlighted with a black underline (extend the line till Leucine of MjFH). Catalytic residues have been marked with a star with the key residues D62, T80 and H257 (in MjFH) marked with an additional green triangle above the star. The abbreviations stated above correspond to the following: FH- fumarate hydratase; FumA- fumarase A; Ec- Escherichia coli; Ss- Shigella sonnei; Pp- Pseudomonas putida; Lm- Leishmania major; Mpob- Syntrophic propionate-oxidizing bacteria; Bx- Burkholderia xenovorans; St- Salmonella typhimurium; Hh- Helicobacter hepaticus; Pt- Pelotomacrum thermopropionicum; Af- Archaeoglobus fulgidus; Pyf- Pyrococcus furiosus; Mj- Methanocaldococcus jannaschii.

### 1.3.2. Standardization of protein expression and purification

Previous attempts at structure determination of the L-TTD, were met with failures due to difficulties in obtaining reproducible crystals. Even after repeated trials under different conditions, crystals could not be obtained. Upon performing SDS-PAGE analysis of the protein purified using earlier optimized conditions, it was found that the purity of the protein was insufficient for crystallization. Hence, to obtain a better quality and quantity of the protein the expression and purification protocol was re-established. The protein expression conditions, i.e., the growth media, supplements, incubation time, temperature, induction O.D., and IPTG concentration, were checked for the one with the highest protein expression. Protein expression was checked in Luria-Bertani broth and Terrific broth at temperatures of 37 °C, 30 °C, 22 °C, and 16 °C, upon which the highest expression was found in Luria-Bertani broth at 30 °C as shown in **Fig. 1.5 panel A**. The O.D. of induction was screened at 0.45-0.6, 0.6-0.8, and >1.0 O.D. for 8 hours and 16 hours of post-induction incubation time period. Best protein expression was observed for 16 hours of growth post-induction at >1.0 O.D (**Fig. 1.5 panel D**). 0.3 mM IPTG concentration was found to induce

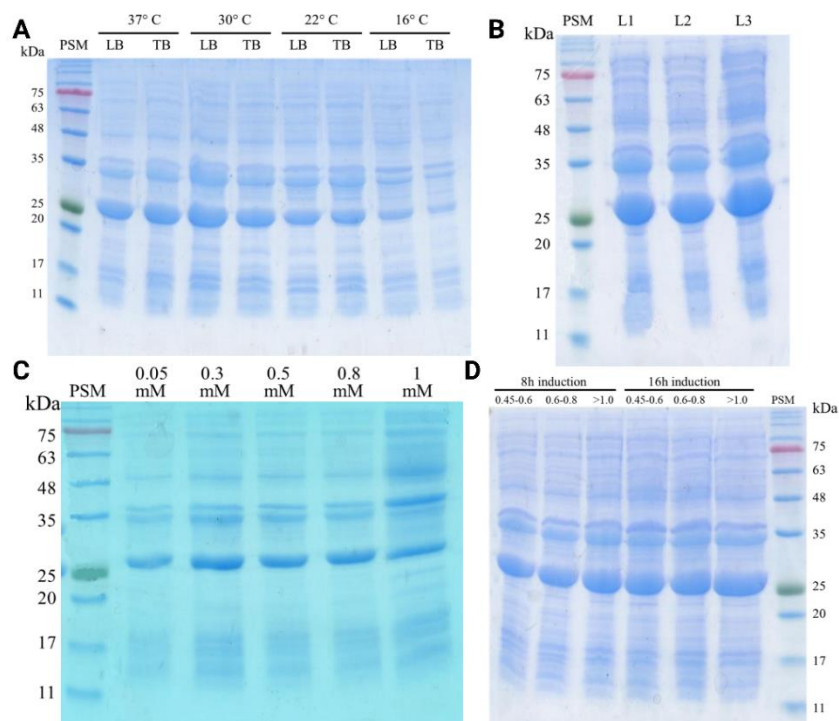


**Figure 1.5. Standardization of conditions for protein expression.** A. *E. coli* growing in Terrific Broth at 30 °C showed highest protein expression. B. Growth in presence of ferric citrate (L1) and ferric ammonium citrate (L2) does not show expression comparable to the control without any supplements (L3). C. 0.3 mM IPTG shows the best expression of both  $\alpha$  and  $\beta$  subunits. D. Induction of the secondary culture at >1.0 O.D. shows the highest expression with 16 hours of post-induction incubation.

the most protein expression (**Fig. 1.5 panel C**). Moreover, the addition of supplements like ferric ammonium citrate or ferric citrate was also attempted, as L-TTD is a Fe-S cluster protein, but they did not yield significant improvement (**Fig. 1.5 panel B**).

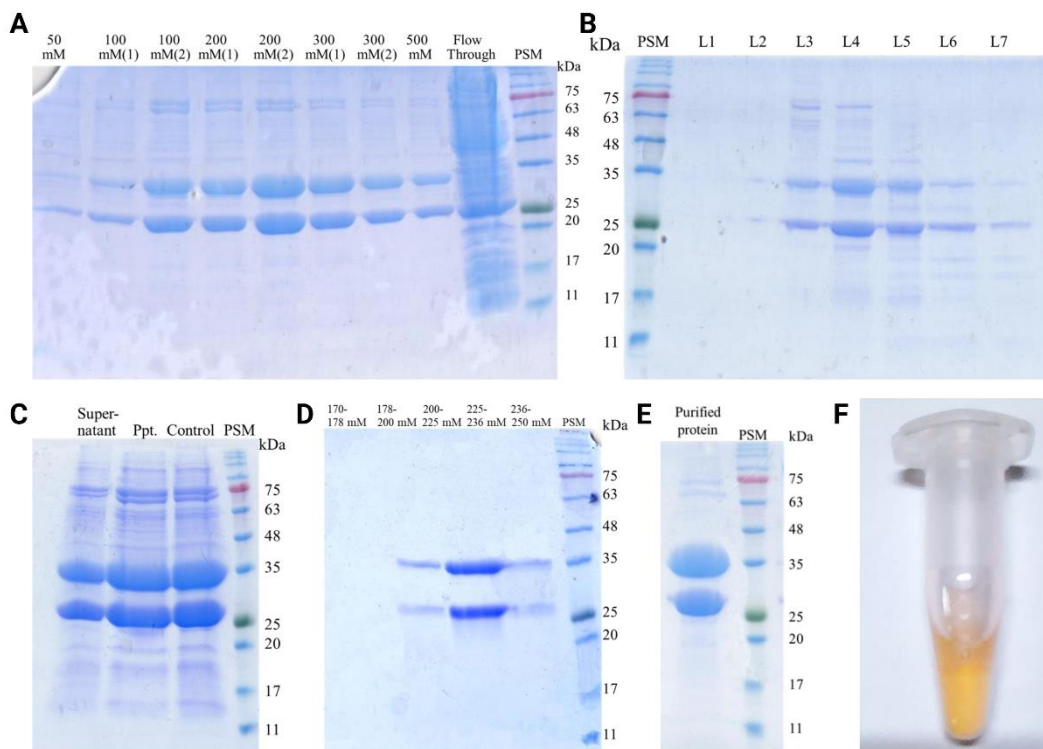


**Figure 1.6. Standardization of L-TTD purification.** A. Elution of L-TTD $\alpha\beta$  with increasing gradient of imidazole up to 500 mM with the peak at 200 mM; B. Ammonium sulfate ((NH<sub>4</sub>)<sub>2</sub>SO<sub>4</sub>) precipitation (90% cut) of L-TTD $\alpha\beta$  failed to purify the protein further as a significant proportion of the protein remains in the supernatant and does not precipitate; C. Size-exclusion chromatography fails to remove the impurities from protein as they co-elute with L-TTD; D. Ion-exchange chromatography with increasing gradient of 0-300 mM NaCl elutes the pure protein with the peak at 225-236 mM; E. L-TTD $\alpha\beta$  run on SDS-PAGE after purification and concentration; F. Purified L-TTD shows a brown coloration due to the presence of the iron-sulfur cluster in an oxidized state

Ni-NTA chromatography of the His-tagged protein helps in isolating the protein from the lysate. However, it is unable to get rid of a number of other protein impurities. Hence, an additional step of purification was added to the purification protocol. Protocols like gel filtration chromatography (using a Superdex 200 10/300 GL column) and ammonium sulphate precipitation were attempted. However, as visible in **Fig. 1.6 panel B and C** it failed to yield highly pure protein. However, ion-exchange chromatography (using a Sephadex column) and an increasing gradient of NaCl (0-300 mM NaCl) led to elution of the protein with no other contaminating proteins, as shown in **Fig. 1.6 panel D**.

### 1.3.3. Crystallisation of L-TTD $\alpha\beta$

Previous experiments in the laboratory had led to formation of crystals of unreconstituted L-TTD $\alpha\beta$  once in 1.6 M sodium citrate tri-basic dihydrate, pH 6.5, and 25% PEG 3350 and they diffracted to around 5 Å. However, these crystals were not formed reproducibly. Hence, aforesaid experiments were performed to increase the purity of the protein to increase the probability of crystallization. Crystal trays were set up with purified unreconstituted protein. Although crystals formed in many conditions, diffraction pattern indicated them to be salt crystals (**Fig. 1.7**). Attempts to obtain the apoprotein failed as the cluster remains tightly bound to the protein. Hence, the holoprotein was reconstituted and set up for crystallization inside anaerobic Coy chamber, but still no protein crystals were obtained.

Crystallizing 4Fe-4S cluster proteins comes with a lot of challenges due to several factors. The major problems include instability of the cluster, heterogeneity, sample preparation and crystal packing (Braymer & Lill, 2017; Broderick et al., 2014; Fontecilla-Camps et al., 2007; D. C. Johnson et al., 2005).

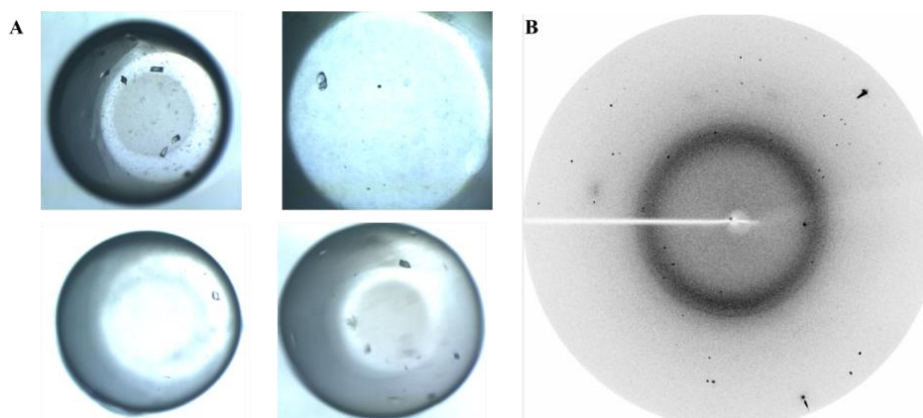


**Figure 1.7. Attempts at crystallization and structure solution of L-TTD $\alpha\beta$ .** A. Crystals obtained under the various conditions tried B. Diffraction pattern indicated that the crystals were that of salt.

Iron-sulfur cluster proteins are often sensitive to air, oxygen and changes in pH, temperature, which generally leads to denaturation of the complex and loss of activity. They can also exist in multiple states, leading to difficulty in obtaining homogenous crystals. These states can include different oxidation states of the iron-sulfur cluster or different conformations of the protein. Heterogeneity often leads to poorly packed crystals unsuitable for diffraction. Sample preparation



of pure and homogenous protein sample for crystallization is a challenge for iron-sulfur cluster proteins and even if the sample is pure and homogenous, obtaining crystals is difficult due to the inherent instability of the cluster.

### 1.3.4. Oligomeric state of L-TTD $\alpha\beta$

Analytical size- exclusion chromatography was used to determine the complex's oligomeric state. As illustrated in **Figure 1.8**, the column was calibrated using proteins of known molecular weight, and a standard curve was produced using linear regression where  $V_e$  is the protein's elution volume,  $V_o$  is the void volume, and  $Y$  is the logarithm of the protein's molecular weight. The volume at which blue dextran elutes, i.e., 7.910 ml, corresponds to the void volume.

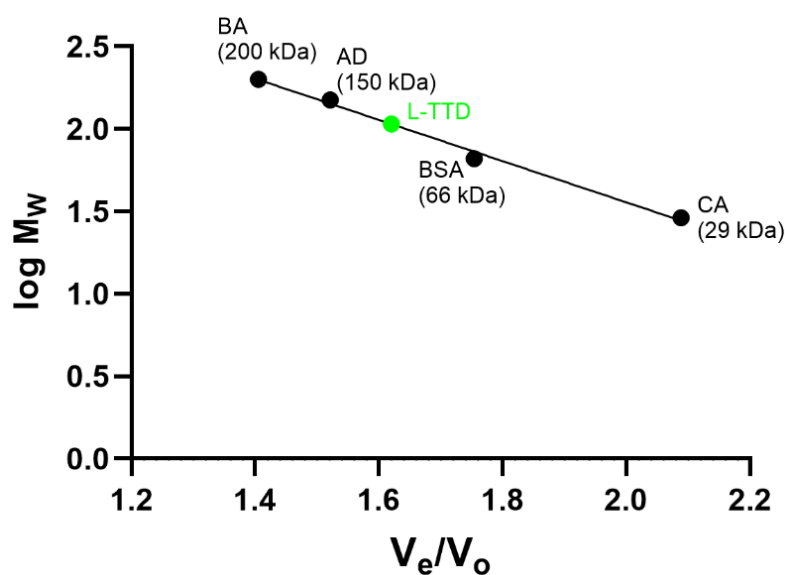


**Figure 1.8.** Analytical gel filtration to infer oligomeric status of L-TTD. 100  $\mu$ l of 10  $\mu$ M protein solution was injected into an analytical gel filtration column that had been pre-equilibrated with buffer. The flow rate was kept at 0.5 ml/min, and the column's eluate was constantly observed at a wavelength of 220 nm. Proteins of a standard molecular weight were used to calibrate the column (as seen in the inset). Elution volumes of the standard proteins (shown by black dots) were used to fit the standard curve. The standards used comprised of alcohol dehydrogenase,  $\beta$ -amylase, bovine serum albumin, and carbonic anhydrase. The protein's elution volume demonstrates that MjFH is a dimer of a heterodimer ( $2\alpha+2\beta$ ).

To determine the elution volume, 100  $\mu$ l of 10  $\mu$ M protein solution was injected. The molecular weight was calculated from the elution volume by interpolation on to the standard curve. The elution volume of the complex is close to the molecular weight of a complex containing a dimer of an  $\alpha$ + $\beta$  heterodimer as shown in **Table 1.1**. Hence, the complex contains two subunits of L-TTD $\alpha$  and two subunits of L-TTD $\beta$ .

**Table 1.1. Oligomeric state of L-TTD $\alpha$  $\beta$**

<b>Protein</b>	<b>Composition of elution buffer</b>	<b>Elution volume (ml)</b>	<b>M.W. (experimental) (kDa)</b>	<b>M.W. (theoretical tetramer) (kDa)</b>	<b>Oligomeric state</b>
<b>TTD<math>\alpha</math><math>\beta</math></b>	<b>50 mM Tris-HCl pH 8.0, 5% glycerol, 1 mM DTT</b>	<b>12.80</b>	<b>107.15</b>	<b>114.02 (<math>\alpha</math><math>\beta</math>)</b>	<b>Dimer of heterodimer</b>

### 1.3.5. Stoichiometric analysis of L-TTD by mass spectrometry

The stoichiometry of  $\alpha$  and  $\beta$  subunits in L-TTD was also examined by native mass spectrometry on the unreconstituted freshly purified  $\alpha/\beta$ -complex. The source conditions ensure that even non-covalent interactions are preserved during ionization. There was a mixture of many species observed in the spectra as shown in **Fig. 1.9**.

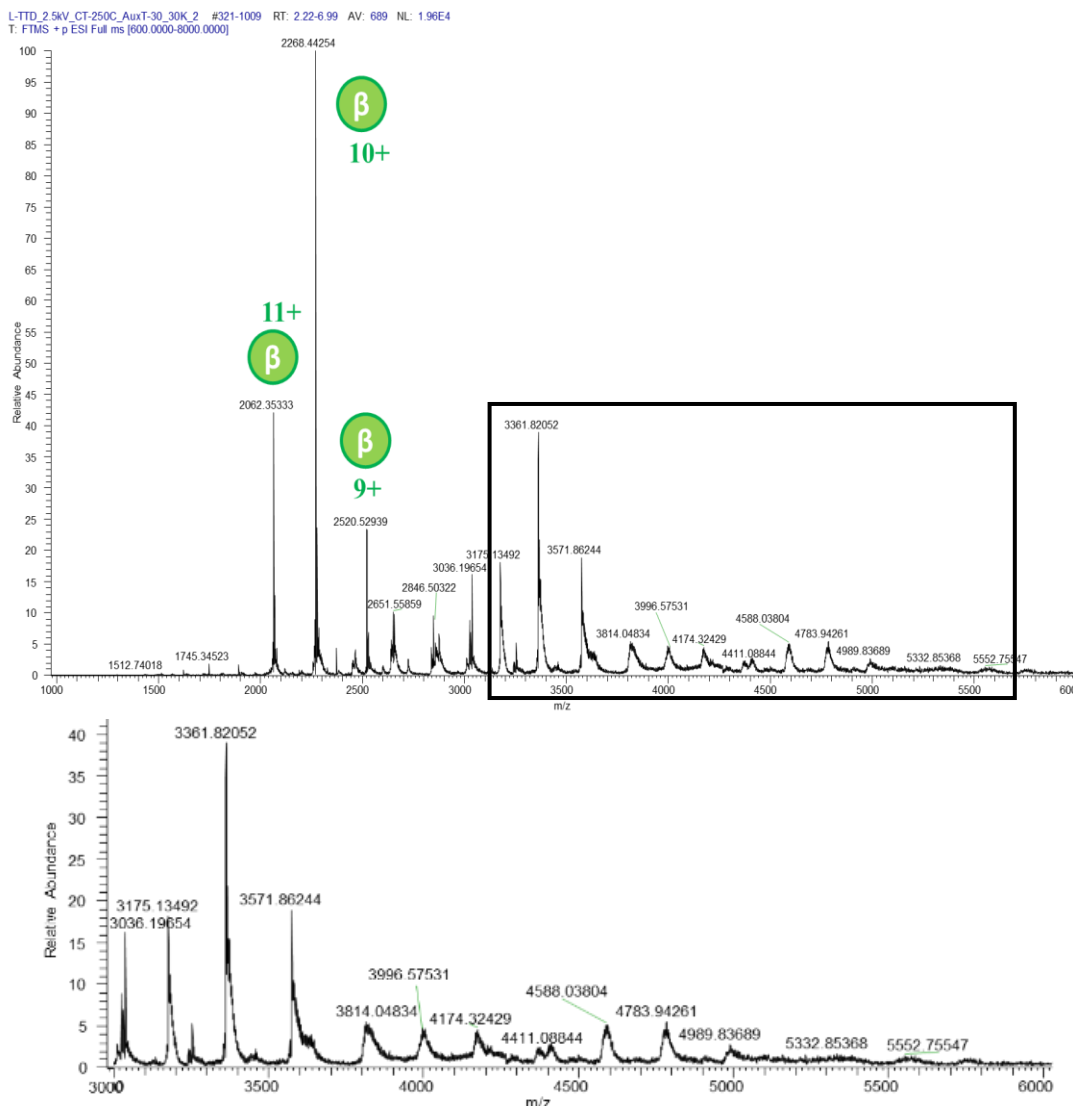


**Figure 1.9. Native mass spectrometry of L-TTD $\alpha\beta$  complex.** Purified L-TTD $\alpha\beta$  was dialyzed against 10 mM ammonium acetate and used for native mass spectrometry. The upper panel shows the complete spectrum that was obtained. The three prominent peaks in the low  $m/z$  range correspond to 11+, 10+, 9+ charge states of MjFHB $\beta$  subunit (enclosed in green circle). The charge state of these peaks was calculated from their isotope distribution obtained by running the same protein sample at a higher resolution of 120,000. The peaks in the high  $m/z$  region are highlighted by a rectangle. The lower panel shows a zoom-in of the spectrum containing peaks in the high  $m/z$  region. The masses were calculated by BioPharma Finder provided by ThermoFischer Scientific. The isotope distribution of the peaks in the higher  $m/z$  region was not resolved well-enough for unambiguous charge state assignment.

Three peaks in the lower  $m/z$  range of 2062.35, 2268.44 and 2520.52 were unambiguously assigned a charge state as calculated from its isotope distribution pattern from running the same protein sample at a higher resolution of 120,000 (Appendix I), which improves the data acquired at lower  $m/z$  range while making the data at higher  $m/z$  range noisier. The overall spectra along with zoomed in images of each of the three peaks are presented in **Appendix I, Fig. A1**. In high  $m/z$  range, the isotopic peaks were not well resolved and hence this information could not be used to calculate the charge state of the peaks. Therefore, the  $m/z$  value of these peaks (shown in **Fig. 1.9**) were compared to all theoretically possible  $m/z$  values corresponding to a charge state ranging from 1 to 40 of protein complexes containing different stoichiometries of L-TTD $\alpha$ , L-TTD $\beta$  subunits and the Fe-S cluster. From this analysis, each peak was assigned to the species that has the closest  $m/z$  value to that theoretically estimated and thus, the charge state was inferred indirectly. A particular species of protein complex was assigned to peaks for which a close match was found, and the final analysis is schematically presented in **Fig. 1.10**.

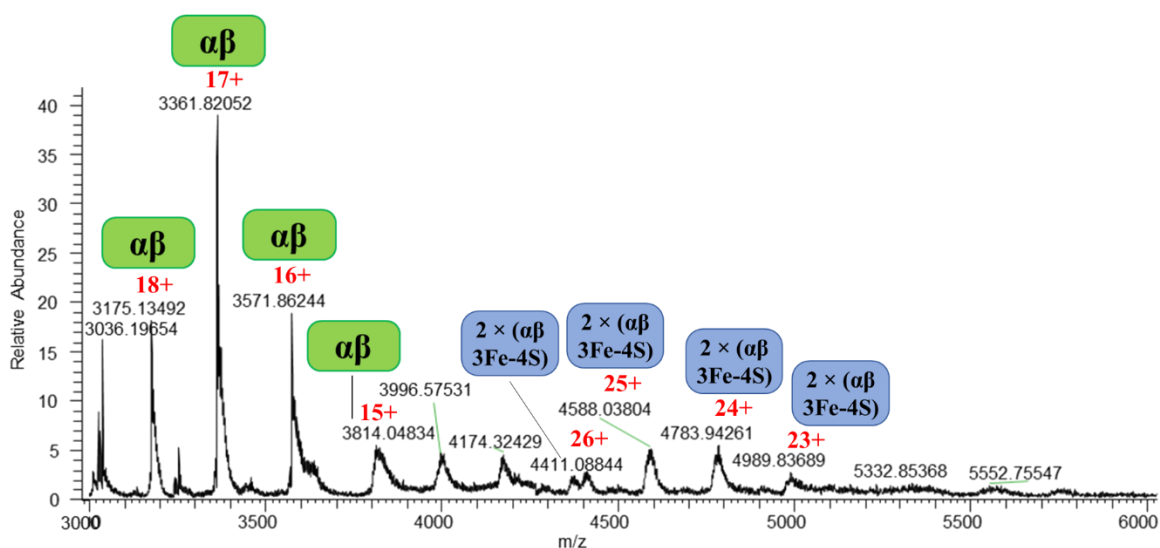


**Figure 1.10.** Assignment of different species of protein complex to the various peaks. Numbers in red are charge value of a peak for which a particular species was assigned. Numbers in black are the  $m/z$  values of the peaks.

The difference between theoretical and experimental mass is given in a tabulated form in **appendix I Table 1**. As is evident from the figure, most of the peaks belong to the dimer of L-TTD $\alpha\beta$  containing different stoichiometries of iron and sulfur. Most abundant species was L-TTD $\alpha\beta$  dimer without any 3Fe-4S cluster. The condition used at the source was gentle enough to retain the dimeric complex of L-TTD $\alpha\beta$  in the gas phase. Under the same conditions, however, very low

---

abundance of the heterotetramer  $2 \times (\text{L-TTD}\alpha + \text{L-TTD}\beta)$  population was observed. From the observed peak intensities, it can be concluded that under the conditions used, the L-TTD $\alpha$  + L-TTD $\beta$  heterodimer complex is more tightly held than the dimer of heterodimer  $2 \times (\text{L-TTD}\alpha + \text{L-TTD}\beta)$  complex. Put together, under aerobic conditions the native MS results suggest that the protein has a 3Fe-4S type iron-sulfur cluster, which is bound to the complex. This implies the presence of a 4Fe-4S cluster in the protein in anaerobic conditions which degrades with exposure to air which have been investigated in later sections.

### 1.3.5. Absorption spectra of L-TTD $\alpha\beta$

Proteins with Fe-S clusters show a characteristic ligand to metal charge transition (LMCT). The electronegativity of the ligand determines whether the absorption will be in the visible or ultraviolet region, e.g., for weakly electronegative ligands like sulfur in iron-sulfur clusters, LMCT absorption is found as an intense band in the low energy visible region (Bertini, 2007; Solomon et al., 2006). This leads to the brown coloration of the protein. The LMCT phenomenon and its role in Fe-S protein coloration are used to understand the properties of Fe-S proteins and their functions in biological processes.

In this section, all experiments were conducted using reconstituted proteins unless stated otherwise. Upon incubating the reconstituted L-TTD $\alpha\beta$  complex in an aerobic environment, we see time-dependent drop in absorbance in the 360-420 nm region (**Fig. 1.11**). However, we do not see any sharp peaks at 360 nm and 415 nm, which is characteristic 4Fe-4S clusters (Duin et al., 1997). Multiple unresolved S to Fe (II)/ (III) charge transitions lead to the broadening of the peaks (Duin et al., 1997). This is a common phenomenon previously reported in *Thermus thermophilus* NADH-quinone oxidoreductase (NDH1) (Nakamaru-Ogiso et al., 2002) and *Azotobacter vinelandii* <sup>Nif</sup>IscA (Mapolelo et al., 2012), both 4Fe-4S cluster containing enzymes. Although the peaks at 360 nm and 415 nm are not resolved, the time-dependent drop in absorbance at these wavelengths upon exposure to air, shows the gradual oxidation of the cluster.

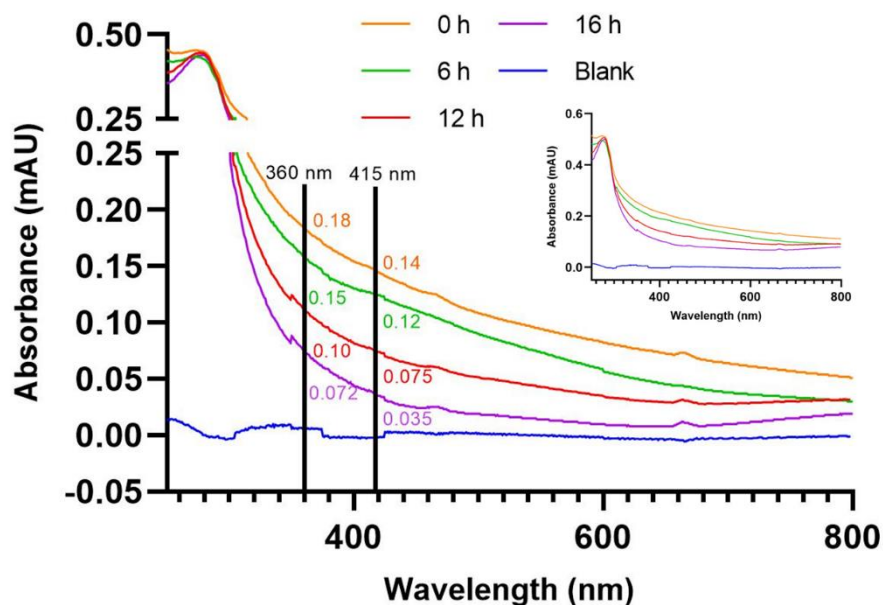


**Figure 1.11. Presence of 4Fe-4S cluster in L-TTD $\alpha$  reconstituted complex.** From the blank subtracted spectra of the reconstituted protein, it was evident that there were no evident peaks around 415 nm corresponding to the presence of 4Fe-4S cluster, which can be due to multiple unresolved transitions causing peak broadening. Furthermore, upon exposure to air, there was a time-dependent drop in absorbance around 415 nm but not that corresponding to 280 nm. This shows that the cluster, as expected, is oxygen sensitive and hence degrades with time, thereby, causing a drop in absorbance at 415 nm. 415 nm and 360 nm are marked with black lines, with absorbance values indicated for each time-point ( $n = 3$ , shown are spectra from one experiment. Similar spectra were obtained in all 3 experiments. Replicates are shown in Appendix II, Fig. A.2 and A.3) The entire spectra with continuous Y-axis are shown in the inset.

One possible way of reducing the rate of oxidation of the Fe-S cluster and the lability of the fourth Fe atom would be to include a small molecule ligand that binds to the active site and chelates the labile Fe atom. Earlier studies in the laboratory had shown that mercaptosuccinic acid (MSA) is an inhibitor of L-TTD and competes with the binding of L-tartrate and D-malate, both substrates of the enzyme. Hence, MSA was added to the reconstituted protein and the mixture was exposed to air at room temperature overnight, post which the cluster oxidation state was monitored by UV-Visible spectroscopy (**Fig. 1.12**). Upon overnight exposure to air, there is no significant decrease in the absorbance around 415 nm and we see the spectra at both of the time points (0 h and 16 h) overlap entirely. This result suggests that inclusion of MSA could yield a homogenous sample of L-TTD bound to 4Fe-4S cluster and MSA and thereby possibly increase the chances of obtaining ligand-bound protein crystals. However, it should be noted that as protein crystallization happens

over many days or even weeks, crystal trays would have to be set up in an anaerobic chamber even after inclusion of MSA.

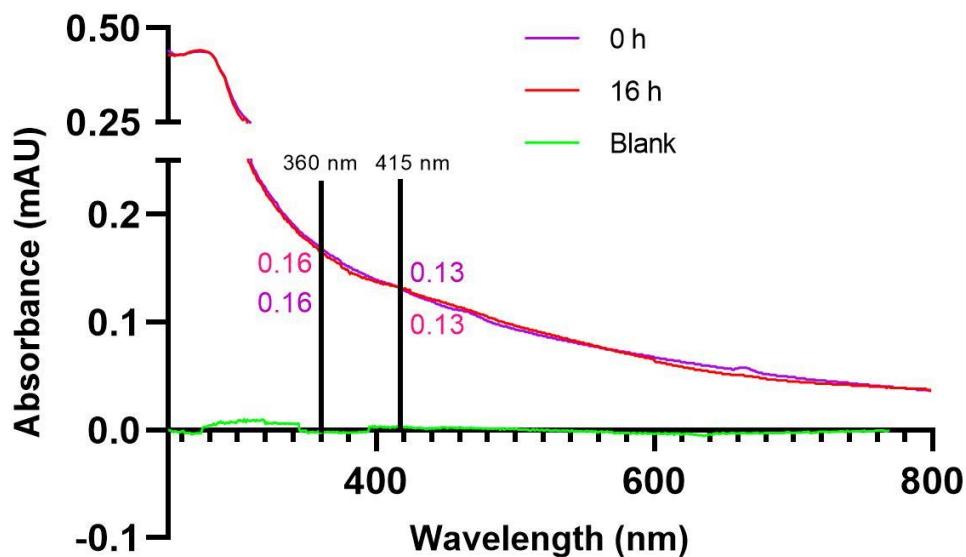


*Figure 1.12. MSA binds as an inhibitor and chelates the labile iron atom. Upon spectrophotometric examination of the reconstituted protein with bound with MSA. Overnight incubation of the reconstituted protein with 4Fe-4S cluster along with bound MSA shows very little oxidation of the cluster. ( $n = 3$ , shown are spectra from one experiment. Similar spectra were obtained in all 3 experiments. Replicates are shown in Appendix II, Fig. A.4 and A.5). 415 nm and 360 nm are marked by black lines.*

### 1.3.6. Circular dichroism spectroscopy of L-TTD

If a molecule is chiral or in a chiral environment in a protein, circular dichroism spectroscopy is used to study it. The S to Fe (II)/ (III) charge transition band shows an effect known as Cotton effect. Circular dichroism has been used extensively to probe into the biochemistry of iron-sulfur cluster proteins.

As discussed above, due to multiple unresolved S to Fe (II)/ (III) charge transitions, the UV-visible spectra show peak broadening. Hence, circular dichroism spectra were recorded to characterize the cluster. The phenomenon due to S to Fe (II)/ (III) charge transition called Cotton effect, has been studied extensively by visible CD spectroscopy for studying iron-sulfur cluster proteins (Stephens et al., 1978). It involves studying a change in the ellipticity or optical rotation with

change in the wavelength around the absorption region of the chromophore. In many cases, visible CD shows greater sensitivity to changes in the cluster environment compared to absorption spectroscopy (Stephens et al., 1978).

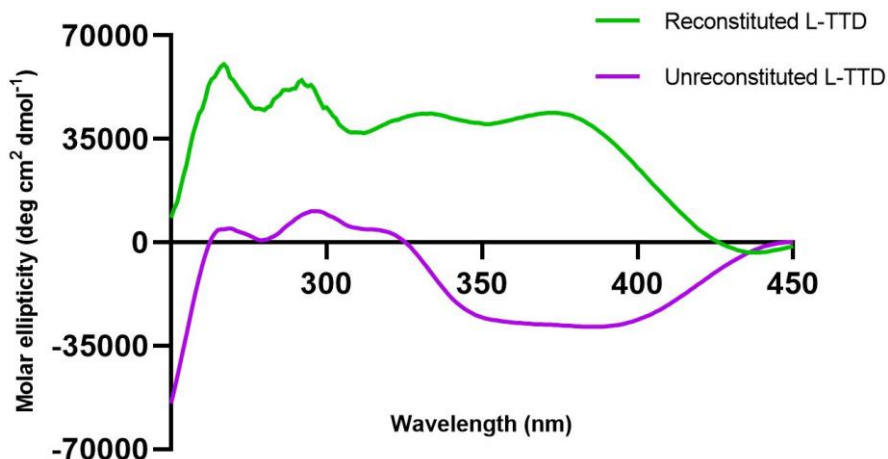


*Figure 1.13. Visible circular dichroism spectra of Fe-S reconstituted L-TTD $\alpha\beta$ . Comparison of the CD spectrum of unreconstituted and reconstituted L-TTD $\alpha\beta$ . Unlike the unreconstituted protein, the reconstituted protein exhibits a dichroic pattern. ( $n = 2$ )*

CD spectra of reconstituted L-TTD $\alpha\beta$  shows pattern characteristic for Fe-S cluster containing proteins (**Fig. 1.13**). The unreconstituted protein shows negative Cotton effect in the 320 nm- 450 nm region. The reconstituted protein, however, shows positive Cotton effect and a dichroic pattern unlike the unreconstituted protein.

### 1.3.7. Specificity of interaction between subunits of class-I FH and L-TTD

According to a prior report, the vast majority of the residues at the class-I FH interface are conserved (Feliciano et al., 2016). Only 10 of the 17 residues at the interface of  $\alpha$  and  $\beta$  subunit between class-I FH and L-TTD show sequence conservation when L-TTD and class-I FH sequences are aligned (**Fig. 1.14**).



Given that the majority of the active site residues for the two groups of enzymes are found at the interface of the  $\alpha$ - and  $\beta$ -subunit (N/C-terminal domains for class-I FH), it will be interesting to



**Figure 1.14.** Multiple sequence alignment shows the interface residues between  $\alpha$  and  $\beta$  subunits in class-I FHs and L-TTD. Conserved residues are marked with green dot while the ones that are not conserved are highlighted in red.

see how the two subunits interact when they are swapped. MjFH $\alpha$  subunit and *E. coli* FumA CTD were found to interact by a Ni-NTA pull down assay from previous experiments in the lab (Bellur, 2022). Hence, it will be intriguing to see whether L-TTD $\alpha$  interacts with FH $\beta$  or FH $\alpha$  interacts with L-TTD $\beta$  upon swapping the subunits. If there is a cross-interaction between these subunits of the two protein groups, the activity of the complex on different substrates can be checked to examine the substrate specificity of the chimeric enzymes.

Upon performing pull-down assays using His-tagged MjFH $\alpha$  and untagged L-TTD $\beta$  using Ni-NTA beads, the His-tagged subunit MjFH $\alpha$  eluted with 500 mM imidazole whereas untagged L-TTD $\beta$  came in the flowthrough. Moreover, pull-down assay was also performed with His-tagged FH $\beta$  subunit and untagged L-TTD $\alpha$  subunit in a similar manner, to study the effect of subunit

swapping. However, both of these assays failed to show any interaction between the two opposing subunits from MjFH and L-TTD (**Fig. 1.15**). This shows that subunit swapping does not lead to formation of any chimeric enzymes in the case of MjFH and L-TTD. This suggests that the dimer or tetramer of L-TTD $\alpha\beta$  is packed in a different way compared to MjFH. It can be suggested that the C-terminal tail present in L-TTD plays a critical role in subunit interaction.

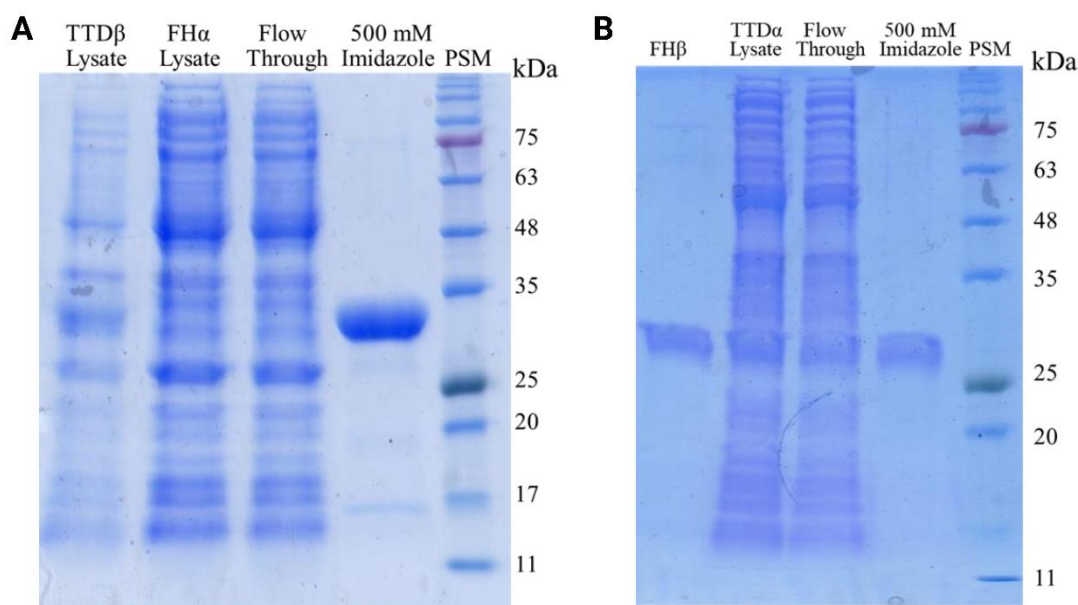


**Figure 1.15.** Ni-NTA pull down assay for interface analysis of the interacting subunits in class-I FHs and L-TTD. A. FH $\alpha$  does not bind to L-TTD $\beta$ ; B. L-TTD $\alpha$  does not bind to FH $\beta$ .

### 1.3.8. Analysis of L-TTD $\alpha$ and L-TTD $\beta$ structures predicted by AlphaFold

Due to the inability to obtain crystals and determine the 3D structure of L-TTD, AlphaFold predicted structure (Jumper et al., 2021; Varadi et al., 2022) was used to gain insights into the catalytic mechanism. The AlphaFold predicted L-TTD  $\alpha$  and  $\beta$  subunit structures superposed on to MjFH  $\alpha$  and  $\beta$  (PDB ID: 7XKY) structures with RMSD of 1.104 Å and 1.008 Å, respectively (**Fig. 1.16 panel A**). This reveals the high similarity of the predicted structure with the experimentally determined structures. Upon superposition of the L-TTD $\alpha$  and  $\beta$  subunit structures on to the LmFH structure it was observed that the three cysteine residues that bind the Fe-S cluster in LmFH i.e., Cys133, Cys252, Cys346 superpose well with Cys71, Cys190 and Cys277 in L-TTD $\alpha\beta$  (**Fig. 1.16 panel C**). Through a proteome wide analysis of *E. coli* iron-sulfur cluster

proteins by a chemoproteomics approach, these 3 cysteinyl residues in *E. coli* L-TTD have been established to bind the iron-sulfur cluster (Bak & Weerapana, 2023). This reinforces some level of confidence on the reliability of the structure predicted by AlphaFold. This structure is also similar to LmFH structure with an RMSD of 1.95 Å and 1.52 Å respectively for  $\alpha$  and  $\beta$  subunits respectively, as shown in **Fig. 1.16 panel B.**, indicating that in the absence of experimentally determined structures, the predicted models could be used for understanding the stereochemical preferences of MjFH and L-TTD. Subsequent active site analysis was done with the superposed L-TTD structures obtained from superposition with both LmFH and MjFH structures. The active site analysis reveals that except a pair of arginine residues (R33 and R82) and a lysine residue (K102), all other residues within hydrogen bonding distance of the substrate are well superposed

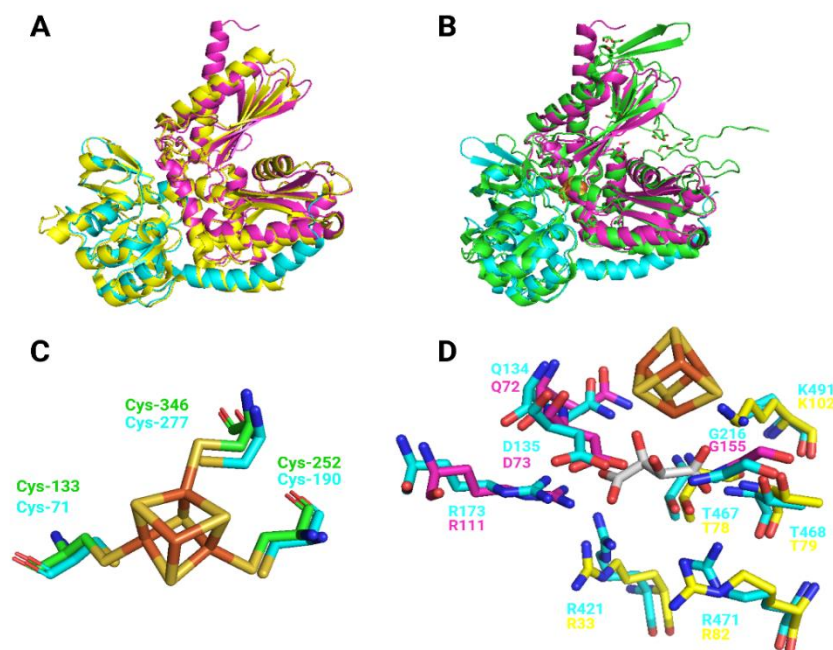


**Figure 1.16. Comparison of class-I FH structures with AlphaFold predicted structures of L-TTD $\alpha$  and L-TTD $\beta$  subunits.** A. Superposition of AlphaFold predicted L-TTD $\alpha$  (magenta) and L-TTD $\beta$  (cyan) structure over MjFH $\alpha\beta$  structure (yellow) respectively. The two structures align well with a RMSD of 1.104 and 1.008 Å. B. Superposition of AlphaFold predicted L-TTD $\alpha$  (magenta) and L-TTD $\beta$  (cyan) structure over LmFH structure (green). The two structures align well with a RMSD of 1.95 and 1.52 Å. C. Superposition of cysteine residues (C71, C190 and C277) that ligate Fe-S cluster from L-TTD predicted structure over cysteine residues (C133, C252 and C346) from LmFH structure. Fe-S cluster from LmFH structure is retained in the superposed snapshot. D. Superposition of all the active site residues that hydrogen bond with the substrate (white) from LmFH structure (cyan) with AlphaFold predicted L-TTD structure ( $\alpha$ -subunit: magenta;  $\beta$ -subunit: yellow). Sidechains from two arginine residues (R33 and R82) and a lysine (K102) residue in L-TTD are directed away from the substrate while the other residues superpose well.

with LmFH residues, thus failing to generate any data on the differences between the two proteins, as shown in **Fig. 1.16 panel D**.

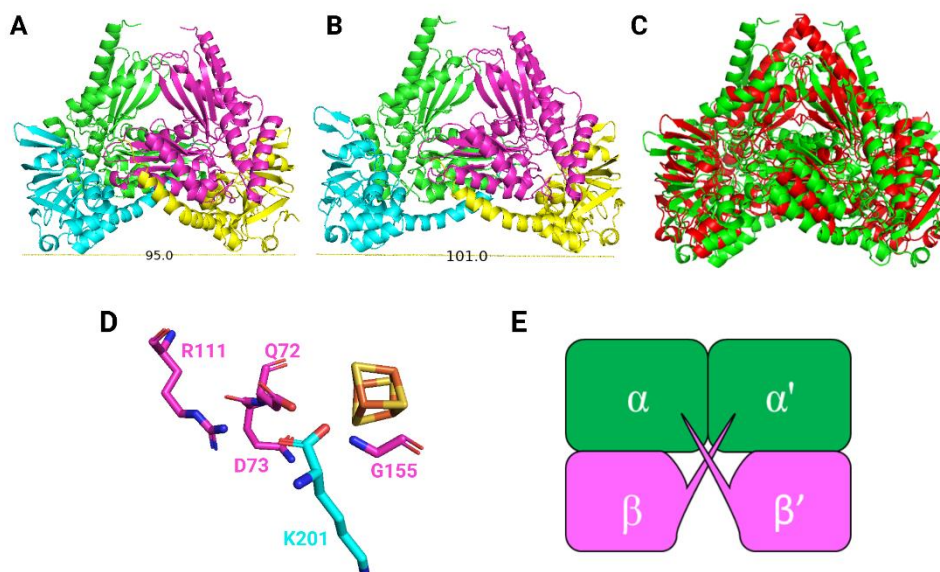


**Figure 1.17. L-TTDA $\beta$  tetramer built from superposition of AlphaFold predicted structures.** A. L-TTDA $\beta$  tetramer structure obtained from superposition of AlphaFold models on LmFH structure (PDB ID: 5L2R); B. L-TTDA $\beta$  tetramer structure obtained from superposition of AlphaFold models on MjFH structure (PDB ID: 7XKY); C. L-TTDA $\beta$  quaternary structure superposed on the tetramer structure predicted by David Baker and colleagues by sequence coevolution and homology modelling (Ovchinnikov et al., 2015). This shows that the quaternary structures obtained by superposition on Mj/Lm FH structures exhibit overall similarity in fold and subunit position to the one predicted by Ovchinnikov et al., 2015; D. The alpha carboxyl CO of the C-terminal residue K201 of the  $\beta$ -subunit of one heterodimer contacts (3.84 Å) NH of G155 of the “AGGGC” motif present at the catalytic site of the  $\alpha$  subunit of the neighbouring heterodimer. This was evident upon superposition of the AlphaFold predicted  $\alpha$  and  $\beta$  subunit structures on MjFH structure (PDB ID: 7XKY). E. Schematic diagram representing the predicted quaternary organization in L-TTD and the interaction of the C-terminus of the  $\beta$  subunit on heterodimer with the  $\alpha$ -subunit of the neighboring heterodimer.

Since L-TTD has been characterised to be a heterotetramer from analytical size exclusion chromatography, the tetramer structure was generated using superposition of the predicted structures. For generating the dimers of the TTD $\alpha\beta$  heterodimer, the heterodimers were individually aligned with LmFH dimer structure and MjFH structure with its crystallographic symmetry mate. We see that heterotetramer of L-TTD $\alpha\beta$  shows a compressed structure with (95 Å along the first inertia axis) and a relaxed structure (101 Å across) depending on the model used for generating the aligned structure i.e., LmFH and MjFH, respectively (**Fig. 1.17 panel A and B**). Thus, the quaternary structure of the heterotetramer, i.e., whether it is compressed or relaxed, depends on the quaternary structure of the model used for superposition.

David Baker and colleagues had predicted the structure of L-TTD $\alpha\beta$  tetramer by sequence coevolution and homology modelling in 2015 (Ovchinnikov et al., 2015). The heterotetramer model, obtained by superposition of AlphaFold predicted  $\alpha$  and  $\beta$  subunit structures on MjFH structure, shows an overall similarity with the structure predicted by Baker and coworkers (Ovchinnikov et al., 2015) with an RMSD of 3.880 Å (**Fig. 1.17 panel C**). One key difference in quaternary organization between the two structures is the compressed nature of subunit assembly in the L-TTD structure predicted by Baker et al. However, it is interesting to note that the quaternary organization of L-TTD predicted by Baker and coworkers (Ovchinnikov et al., 2015) was well before any FH structure was published and is highly similar to that of both Lm and Mj FH structures.

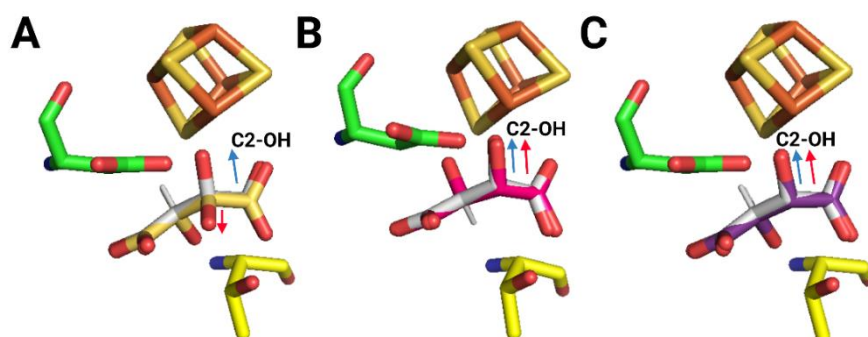


**Figure 1.18.** *L-tartrate, D-tartrate and meso-tartrate docked active site in the structure of L-TTD. A. In contrast to the bound L-malate (white), the C2-OH group of L-tartrate (yellow) faces away from the Fe-S cluster and in the opposite direction. B. The D-tartrate (pink) and bound L-malate (white) from the LmFH structure superpose nicely, with the C2-OH of both substrates coming within hydrogen bonding range of the Fe-S cluster and catalytic acid D73. C. The C2 hydroxyl group of meso-tartrate (purple) points in the same direction to the Fe-S cluster as the bound L-malate (white), while the C3-OH points in the direction of the catalytic base T79 inhibiting catalytic activity.*

The heterotetramer structure obtained from superposition with LmFH was selected for analysis of the active site residues as the cluster and the substrate L-malate are already present in the structure of the parasite enzyme. Thus, the active site of L-TTD was analysed with the superposed cluster and substrate (L-malate) from LmFH structure. This showed complete conservation and very similar organization of all the active site residues. To position the structures of L-tartrate, D-tartrate and meso-tartrate, the C2 and C3 of these dicarboxylic acids was superposed on that of L-malate. This clearly showed that the active site organization, particularly the location of the catalytic Thr79 and Asp73 as predicted by AlphaFold would be unfavorable for catalysis on the L isomer of tartrate

---

and D-isomer of malate, both substrates of L-TTD (**Fig. 1.18**). Therefore, the active site as predicted by AlphaFold failed to explain the changed substrate stereospecificity. This hints at a possible reorientation of the active site without any change in the overall fold of L-TTD from that of Lm or MjFH that results in the switch in substrate stereospecificity leading to activity on L-tartrate, not D-tartrate.

Moreover, upon closer analysis of the superposed structures, we find the C-terminal K201 of the b-subunit is at a distance of only 3.84 Å from G155 of the “AGGGC” motif in the L-TTD heterotetramer obtained by superposing on the MjFH structure (**Fig. 1.17 panel D**). This contact is between the  $\alpha$  subunit of one heterodimer in the tetramer and the  $\beta$  subunit of the other heterodimer (**Fig. 1.17 panel E**). G155 is a critical residue, and mutating its corresponding residue i.e., G147 to Ala in MjFH led to complete loss of activity (Bellur et al., 2023). Although it does not take direct part in catalysis, it is close to the catalytic acid D73 in L-TTD and plays a role in binding the substrate. Thus, the K201/G155 contact might play a critical role in orienting D73 in a manner favorable for catalysis on L-tartrate. Since the  $\beta$ -subunit C-terminal tail is absent in class-I FHs, this interaction has not yet been reported and needs experimental validation through structure determination of L-TTD. In class-I FHs, the C-terminus is located at a large distance away from the glycyl residue (G147 in MjFH and G216 in LmFH in the KGXGS motif. In the MjFH structure, the electron density for the last two amino acid residues is missing and the distance from the third last residue to that of G147 is 25.6 Å. Due to the quaternary packing in LmFH, the superposed L-TTD heterotetramer structure was more compressed as well and hence the C-terminal residues do not make such contacts; K201 lies 18.0 Å away from G155. In LmFH, the distance from carboxy-terminal residue A568 of the C-terminal domain (corresponding to the b-subunit) to G216 is 29.9 Å. These observations possibly suggest that this interface interaction between adjacent heterodimers may play a defining role in the quaternary organization and subunit interaction. Since the active site of the enzyme is at the interface of  $\alpha$  and  $\beta$  subunits, it might play a role in reorientation of the active site, which leads to the change in stereospecificity.

Moreover, since this contact is only in the structure of L-TTD obtained from superposition on MjFH structure, it can be hypothesized that a movement from compressed to relaxed structure upon 4Fe-4S cluster binding might be responsible for the proper orientation of the active site.

---

Although the entire hypothesis is based on the AlphaFold-predicted structures and the heterotetramer structure of L-TTD obtained by superposition, the presence of the C-terminal tail only in L-TTD and its location in the quaternary structure suggests a possible role for this segment in determining the unique substrate stereospecificity of L-TTD. However, this requires experimental validation.

### **1.3.8. Substrate stereospecificity in catalysis by L-TTD**

The enigma of the change of stereospecificity in L-TTD compared to class-I FHs remains unsolved due to the lack of structural information. Since the active site residues in the predicted structure superpose well with class-I FHs and do not provide much insight into the problem, it can be suggested that there is a reorientation of the residues in the catalytic pocket to enable catalysis on the L stereoisomer of tartrate.

The problem of stereospecificity in L-TTD and class-I FHs can be described as the problem of fitting a left-hand glove on one's right hand. This problem has puzzled biochemists for a long time. Stereospecific recognition of substrate by enzymes has traditionally been investigated in relation to the places in the active site to which the substrate is attached (Easson & Stedman, 1933; Ogston, 1949). According to the three-point attachment model, active site residues must anchor the substrate at each of three attachment sites in order for an enantiomer to bind at the enzyme's active site. The three-point attachment paradigm is still widely used for many substrates with a single chiral group. The three-point attachment model states that three attachment sites of the enzyme, A', B', C', must be anchored to three points on the substrate, A, B, and C, in order for a molecule with a single chiral center to be bound at the active site. For the opposite enantiomer, one of the points of contact breaks, making it impossible for correct binding or catalysis to occur. One of the sites of contact needs to be on the opposite side of the protein for the opposite enantiomer to bind at the active site. (**Fig. 1.19**).

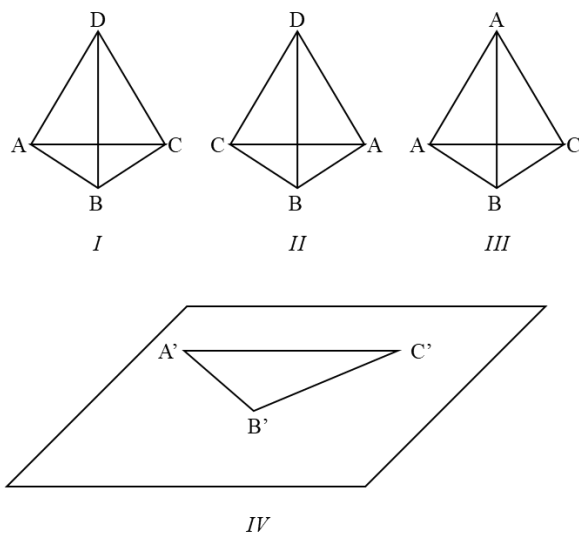


**Figure 1.19. The three-point attachment model.** Groups A, B, and C, of one enantiomer (I) of the ligand, bind to the sites A', B', and C' of the enzyme, respectively. When comparing groups, A, B, and C with A', B', and C', the other enantiomer (II) is unable to establish a similar correlation. The model is able to distinguish between two A groups that are identical and combine to make a prochiral molecule (III). The protein surface where the chiral compounds bind is visible in IV. (figure adapted from Mesecar, A., Koshland, D., 2000)

The three point attachment model does not always hold true and for such substrates, the four-location model was proposed (A. D. Mesecar & Koshland, 2000). The model is called a 'four-location' model because it is not necessary for there to be four binding sites. The four-location model is necessary to explain a protein's ability to discriminate between L- and D-isomers (A. D. Mesecar & Koshland, 2000; Andrew D. Mesecar & Koshland, 2000).

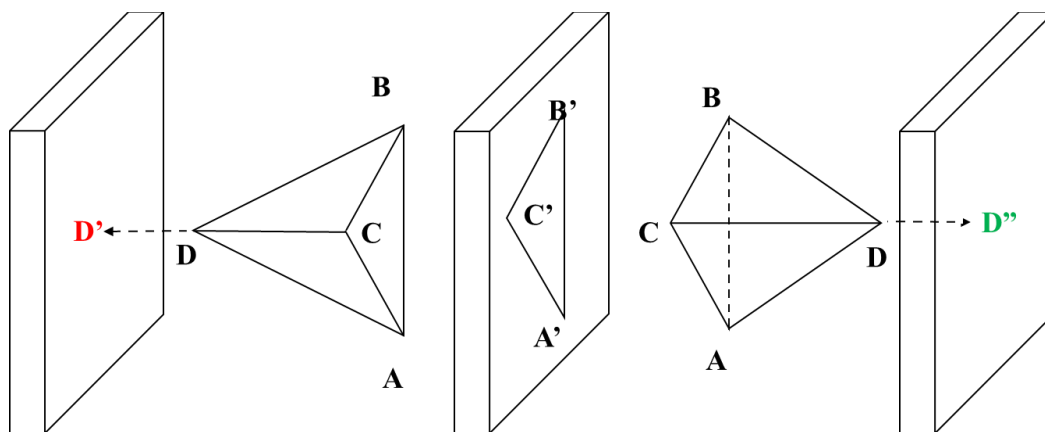


**Figure 1.20. Four-point location model for stereoselectivity of a protein.** A model representing a protein that could provide two groups (D' and D'') in either of two locations that could interact with group D on a chiral carbon atom. The protein may use D' to bind one enantiomer and it may use D'' to bind the other enantiomer. Adapted from Mesecar & Koshland, 2000.



The four locations need not necessarily be four attachment sites, it can also be three attachment sites and a direction, but a minimum of four designated locations are necessary. A rough picture of the binding of substrate to active site is shown schematically in **Fig. 1.20**. The sites or locations on the protein to which these groups attach are denoted by the letters A', B', and C'. The enzyme utilizes group D, to distinguish between the enantiomers by binding to site D' in the case of the one enantiomer and site D'' in the case of the other enantiomer. The D group, which is the key to differentiating the enantiomers, points in opposing orientations in the D- and L-isomer complexes, as shown in **Fig. 1.20**. This kind of binding has been described as “mirror-image packing” by Hanson because of the coplanar binding determinants A', B', and C' determining the pseudo-mirror plane (Hanson, 1981). However, there are two major assumptions in the four-location model proposed by Mesecar and Koshland (A. D. Mesecar & Koshland, 2000; Andrew D. Mesecar & Koshland, 2000); the first being the substrate can approach the active site from two opposing sides, which is not always true considering the strict steric constraints in active sites. The second assumption considers the binding determinants to all lie on a plane, but it has been seen from recent crystallographic data that the three binding determinants do not lie on a single plane.

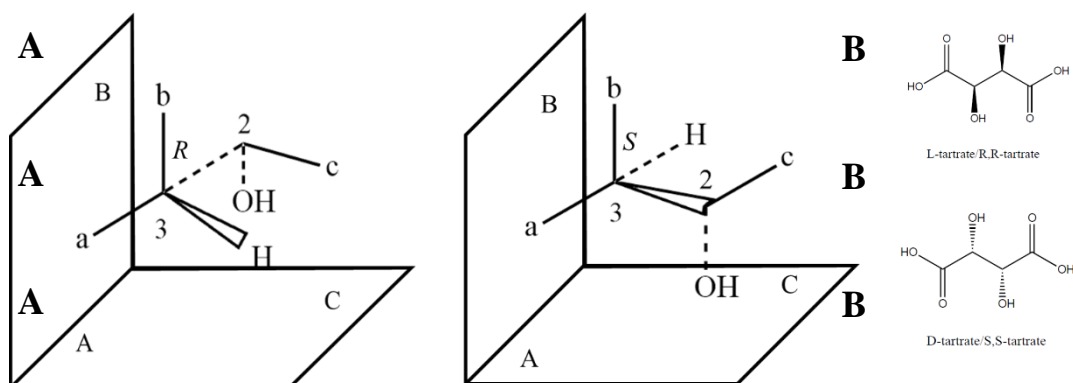


**Figure 1.21. Enantiomer superposition model describing the stereospecificity of L-TTD.** A. Using the enantiomer superposition model, 2R,3S and 2S,3R enantiomers can fit into the same site and can approach this site from the same direction. In this model, a and c are COOH and b is OH. Two necessary fourth contact points for the OH groups at C2 determine the actual binding. B. Structure of L- and D-tartrate

Bentley's enantiomer superposition model is the first model to consider the binding determinants in 3-dimensional orientation and considers substrate binding from a single side only (Bearne, 2020; Bentley, 2003). Thus, it builds on the three-point attachment model, in which out of the three binding determinants, at least one of the groups has to show a degree of flexibility for enantiomeric ligands. In this model, the two substituents on chiral carbon (A and B), and the asymmetric carbon

---

(C<sub>α</sub>) of either enantiomer may be superposed, hence giving the name ‘enantiomer superposition model’. In mirror-image packing or four location model, the enantiomers have chiral carbon atoms lying on either side of the pseudo-mirror plane facing each other but in enantiomer superposition model, they lie on the pseudo-mirror plane and may superpose, thus making the C<sub>α</sub> – D bonds orient at an angle of about 109°, instead of pointing in the complete direction as in four-location model.

In class-I FHs, the Fe-S cluster and the catalytic aspartate residue as well as the substrate carboxylate binding residues play a critical role in binding and catalysis. The binding of the substrate is the most critical step, and the substrate specificity arises out of the binding with catalytic aspartate and the Fe-S cluster which binds the C2-OH present in the substrate. However, in the L-TTD predicted structure, we do not see any significant difference in the orientation of the active site residues that can bind the C2-OH which points away from the Fe-S cluster and D73. Since in the modelled structure, the position of the cluster-binding cysteines overlap with that in Mj and Lm FH, the Fe-S cluster location will also overlap with that in FH and cannot be flipped to the opposite side to contact C2OH of L-tartrate, suggesting a possible reorientation mechanism of one or two critical residues and their side chains. The four-location model cannot explain this change in stereospecificity since it suggests substrate binding for opposing enantiomers must take place through opposing sides. However, the active site pocket is not big enough to accommodate such binding. From the enantiomer superposition model, we observe that the C2-OH group is critical in determining the specificity of the enzyme (Bearne, 2020; Bentley, 2003). It is the critical flexibility of the C2(OH)COOH group which lets L-tartrate bind to the active site. and the C2(OH) group makes proper contacts for the reaction to proceed. Hence unlike three-point attachment or four-location model, the specificity determining residue, C2-OH does not have to lie on completely opposing sides for the two enantiomers but a minor reorientation in the 3-dimensional arrangement of the binding site should suffice. This suggests a reorientation of the active site mediated by the C-terminal residues Tyr199 with Arg161 and Lys201 which makes a direct contact with Gly155, a critical glycine present in the active site as well as in the “AGGGC” motif, mutating which was found to cause inactivity in MjFH (Bellur et al., 2023). Since class-I FHs do not possess the C-terminal tail and structural information is still not available on L-TTD, this is yet to be experimentally verified. However, from the enantiomer superposition model, we find that the distinguishing group i.e., C2-OH does not have to lie on the complete opposite side, instead it is

---

the flexibility of this group which plays a determining role in the binding of the substrate. Thus, the active site aspartate residue and Fe-S cluster need to undergo only a slight reorientation for the reaction to proceed on L-tartrate in L-TTD.

## 1.4. Summary

L-TTD and class-I FHs are closely related proteins that have misannotations throughout various databases like NCBI, RCSB, and UniProt, due to the high sequence similarity. The two enzymes catalyze reactions on distinct stereoisomers despite the active site residues showing sequence conservation (Kronen et al., 2015; Lamzin et al., 1995; van Vugt-Lussenburg et al., 2009, 2013). The majority of the time, nature handles stereoisomers by creating distinct enzymes with unique active sites to catalyze reactions on opposing stereoisomers (Lamzin et al., 1995), with lipases (Cygler et al., 1994), racemases, and epimerases (Bearne, 2020) being a few exceptions. Hence, how L-TTD shows this unique stereospecificity is still an enigma which needs answer.

Previous studies in the laboratory had identified a highly conserved pattern, “KGXGS” in class-I FH and “AGGGC” in L-TTD, separating class-I FHs and L-TTD. Switching the “KGXGS” motif in MjFH to “AGGGC” motif or site-directed mutagenesis of residues around the active site failed to bring about any change in stereospecificity. The study also discovered that L-TTD and class-I FH have opposite substrate specificity despite having identical residues in their active sites, suggesting that slight variations in active site architecture must have led to the change in enzyme specificity in this class of Fe-S cluster hydrolyases.

This work aims and attempts to understand the unique stereospecificity and catalytic mechanism in L-TTD. Analytical gel filtration chromatography has showed L-TTD exists in tetrameric state, which was verified by native mass spectrometry. The protein also consists of a 4Fe-4S cluster, which gets oxidized with exposure to air, as is characteristic of iron-sulfur cluster proteins. Structure solution of the protein was attempted, but due to unstable nature of the iron-sulfur cluster, crystals could not be obtained. Hence, AlphaFold predicted structure was used to explain the change of substrate specificity in L-TTD compared to class-I FHs. It showed that the active site residues are positioned in a manner similar to class-I FHs. Aligning the C2-C3 backbone of the substrates revealed a slight reorientation of the active site residues is required for binding and catalysis of L-tartrate. However, superposition of the AlphaFold predicted structures on MjFH tetramer revealed a critical contact in L-TTD between residues near the active site i.e., G155 of the “AGGGC” motif with the carboxy-terminal K201. Since, this C-terminal extension is not found

---

in class-I FHS, it can be suggested that it plays a role in slight reorientation of the active site residues.

Upon consideration of a model more suited for enzyme specificity for enantiomers, i.e., the enantiomer superposition model, it was found out that for enantiomeric pairs, the binding at the active site is much dependent on the direction and flexibility of a particular binding constituent of the substrate which is C2-OH group in case of tartrate. This model is more suited for studying enzyme reactions involving enantiomeric pairs than previously existing models and shows us that the critical binding group i.e., C2-OH does not lie on the opposite side of the cluster and needs a slight reorientation for proper binding and catalysis. Thus, we strongly suggest a possible reorientation mechanism arising out of the quaternary organization of the protein complex which leads to altered substrate specificity.

## 1.5. Future Directions

In order to understand the stereospecificity and catalytic mechanism in L-TTD and the differences between class-I FHs and L-TTD, future directions involve solving the structure of L-TTD. The source of stereospecificity in these enzymes will be definitively solved with structural information about the active site. Additionally, directed evolution can aid in changing the substrate selectivity of these enzymes and provide fresh information that cannot be inferred straight from the structure.

### 1.5.1. Determination of L-TTD structure

AlphaFold predicted structure of L-TTD has provided insights into the enigmatic nature of this class of enzymes, however more information is needed to properly understand the catalytic mechanism. Hence, in order to solve the structure of the enzyme, crystals trays of L-TTD were set up in several conditions. Trays were set up even with the holoenzyme inside the anaerobic Coy chamber. Unfortunately, only salt crystals were found to form even after repeated trials and further standardization in the crystal tray setup along with grid screening has to be carried out to get good quality protein crystals for diffraction. Mercaptosuccinic acid has been identified as a potent ligand for obtaining crystals. It or its analogues can be screened further for crystallization.

### 1.5.2. Mutational analysis of the C-terminal tail

From bioinformatic analysis, it was found out that the  $\beta$ -subunit of one heterodimer ( $\alpha\beta$ ) makes contact with the  $\alpha$ -subunit of another heterodimer ( $\alpha'\beta'$ ) of the same tetramer. The residues involved are Tyr199 ( $\beta$ ) with Arg161 ( $\alpha'$ ) and Lys201 ( $\beta$ ) which makes a direct contact with Gly155 ( $\alpha'$ ), a critical glycine present in the active site as well as in the “AGGGC” motif. This C-terminal domain is absent in class-I FHs and hence, it would be interesting to see whether this region plays a role in the change in stereospecificity. This would require complete deletion of the C-terminal tail as well as site-directed mutagenesis studies of the involved residues in the region i.e., Y199 and K201.

**[This page is intentionally left blank]**

---

**[This page is intentionally left blank]**

---



---

## Chapter 2

# Examination of the quaternary structure of *M. jannaschii* inosine 5'-monophosphate dehydrogenase through transmission electron microscopy

---

Inosine 5'-monophosphate dehydrogenase (IMPDH) is an enzyme found across all phyla of life, as it plays a critical role in nucleotide metabolism. However, the activity of this enzyme is modulated differently in different phyla and the mode of nucleotide modulation has not been understood properly in archaeal IMPDHs. Previous work from the laboratory had shown that *Methanocaldococcus jannaschii* IMPDH (MjIMPDH) shows behaviour similar to eukaryotic IMPDHs, despite sequence similarity to prokaryotes. In addition, earlier preliminary studies showed the formation of filament-like structures mediated by ATP. However, this previously obtained result could not be reproduced. From our experiments, we see that binding of nucleotides has no effect on the quaternary organization of the protein. However, the previously assigned higher-order oligomer fraction was found to correspond to octamers in a relaxed, expanded conformation leading to a change in Stokes radius. These “relaxed octamers” have to be examined at greater structural detail in future studies.

---

---

---

## 2.1. Introduction

### 2.1.1. Regulation of nucleotide biosynthesis and IMPDH

Nucleotides form the basis of life; they are necessary for the maintenance and replication of the genome and transcription of genetic information into RNA, act as a source of energy, and participate in signal transduction (Lane & Fan, 2015). Thus, nucleotide biosynthesis pathways are highly regulated to maintain optimal cellular nucleotide levels. Owing to their tremendous importance in various cellular processes, nucleotide biosynthesis is regulated by a network of checkpoints to prevent misincorporation of dNTPs into DNA, which could result in mutations (Labesse et al., 2013).

Nucleotide biosynthesis occurs through two major pathways: *de novo* and salvage. In the *de novo* pathway simple precursors assemble to form nucleotide molecules, and in salvage pathways, the cell recycles its pre-existing nucleotide pool. Cells generally use salvage pathways to replenish degradation products and preserve their nucleotide pools. However, the flux through the *de novo* nucleotide biosynthesis pathways increases when nucleotide demand is high, such as during cell proliferation.

Purinosome formation and dynamic assembly/disassembly is a way of regulation by which living cells use subcellular localization and, the more recently discovered, supramolecular organization for optimum nucleotide biosynthesis (An et al., 2008; Narayanaswamy et al., 2009; Noree et al., 2010). The purinosome complex comprises six enzymes and produces IMP from phosphoribosyl pyrophosphate. Allosteric regulation has recently been demonstrated to have a significant function in this setting and has been regarded as a unique participant in IMP biosynthesis. While the purinosome complex ensures that IMP is generated via a substrate channeling mechanism (An et al., 2008), IMPDH is regulated at several levels, *viz.*, transcription, post-translation, and allostery as well (L Hedstrom, 2009).

IMPDH is a highly conserved enzyme, that regulates the *de novo* manufacture of guanosine nucleotides by catalyzing the first committed step in GTP biosynthesis. Its blockade results in an imbalance between adenine and guanine nucleotides, which leads to cytotoxicity (L Hedstrom, 2009; Shu & Nair, 2008). Adenine and guanine nucleotides both affect the activity of IMPDH by changing its oligomeric state, its activity, or both, through feedback regulation. The well-

---

controlled allosteric regulation of IMPDH by purine nucleotides, which in turn maintains the adenine to guanine nucleotide balance inside the cells, is closely linked to physiological activities within the cells and their proliferation. Because of this biochemical significance, IMPDH is a key target for immunosuppressive, antiviral, and cancer therapies (L Hedstrom, 2009). Differential expression patterns exist between the two IMPDH isoforms in vertebrates, which are 83% identical in sequence in humans (Collart & Huberman, 1988; Natsumeda et al., 1990). While IMPDH2 levels are increased in proliferating tissues, IMPDH1 is constitutively expressed at low levels in the majority of tissues (Carr et al., 1993; Hager et al., 1995; Jackson et al., 1975; Senda & Natsumeda, 1994). While IMPDH2 knockdown in mice causes embryonic lethality, IMPDH1 knockout causes a autosomal dominant retinal degeneration in humans, a condition known as retinitis pigmentosa or Leber congenital amaurosis (Aherne et al., 2004; Gu et al., 2000, 2003). In mice, knockout of IMPDH1 results in minor vision defects, whereas IMPDH2 knockout leads to embryonic lethality (Aherne et al., 2004; Gu et al., 2000, 2003).

### **2.1.2. Structure and catalysis in IMPDH**

Inosine 5'-monophosphate dehydrogenase (IMPDH) (EC 1.1.1.205) catalyzes the conversion of Inosine 5'-monophosphate (IMP) to xanthosine 5'-monophosphate (XMP), which in the process also reduces  $\text{NAD}^+$  to NADH. Apart from two protozoan parasites, *Giardia lamblia* and *Trichomonas vaginalis*, the IMPDH/GMPS system is found across all currently understood organisms (Carlton et al., 2007; Morrison et al., 2007). Moreover, many organisms contain more than one gene expressing IMPDH e.g., humans, etc. According to Labesse et al., 2013, IMPDHs are found in two oligomeric states, i.e., tetramers or octamers, with each monomer containing 400–500 amino acid residues, and having a core catalytic domain and a regulatory domain. The Bateman domain, also known as the CBS domain, is the regulatory domain and contains two repeating CBS motifs which were initially identified in human cystathione beta-synthase (CBS) (Bateman, 1997).

The  $(\beta/\alpha)_8$ /TIM barrel that makes up the core catalytic domain of IMPDH is further split into five important structural motifs that carry out substrate binding and catalysis. Like other TIM-barrel proteins the active site is found at C-terminal ends of the  $\beta$ -sheets. The active site cysteine is carried by the "catalytic cysteine loop," which is strictly conserved in all IMPDHs. The cysteine loop (**Fig. 2.2**) can actually move like a door on a hinge. The phosphate binding area, also known as the

---

"phosphate binding loop," is located next to the active site loop and is made up of six residues. The "finger domain", a twisted-sheet that extends from the C-terminal of TIM barrel, aids in the transmission of allosteric signals from the Bateman domain to the catalytic domain (Rubén M. Buey et al., 2015). The dynamic "mobile flap" made up of about ten residues, enters and exits the active site during catalysis, and is located at the distal end of the finger domain. The dehydrogenase reaction can take place in the open conformation, followed by hydrolysis in the closed conformation as shown in **Fig. 2.1**. The "C-terminal segment" then couples a monovalent cation to the active site. Being highly flexible, the catalytic cysteine loop, mobile flap, finger loop, and roughly 20 residues at the C-terminal end of IMPDH are absent from the X-ray crystal structures of different IMPDHs (Hedstrom, 2009; Morrow et al., 2012; Prosis & Wu, 2002.; Rao et al., 2013). The catalytic cysteine loop, phosphate binding motif, and movable flap residues make up the IMP binding site. The NAD<sup>+</sup> binding site is made up of residues from the catalytic loop and movable flap. Although IMP binding residues have been found to be highly conserved, a significant divergence has been seen in the case of the NAD<sup>+</sup> binding site (L Hedstrom, 2009).

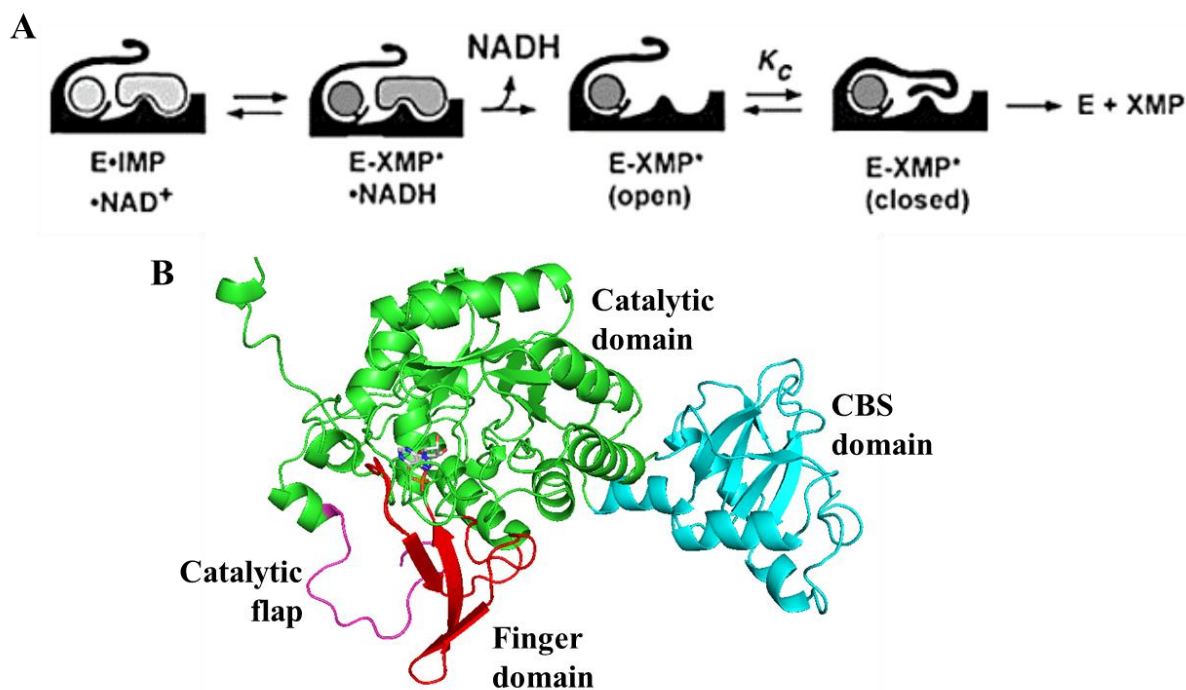


**Figure 2.1. Mechanism of IMPDH reaction and cartoon representation of IMPDH.** A. Schematic representation of IMPDH reaction mechanism (Adapted with permission from Hedstrom 2009); B. Cartoon representation of *Streptococcus pyogenes* IMPDH monomer with Bateman (cyan) and catalytic domain (green) indicated. The catalytic flap is highlighted in pink and finger domain is indicated in red (PDB 1ZFJ).

CBS domains, which are present in a variety of structurally and functionally unrelated proteins, including CIC-chloride channels, amino acid transporters and protein kinases aside from IMPDH and cystathione beta synthase (Baykov et al., 2011; Ereño-Orbea et al., 2013). It has been discovered that removing the CBS domain from IMPDH has no impact on the subunit organization or activity in vitro (Nimmegern et al., 1999; Sintchak et al., 1996). In many of the PDB-deposited structures, the CBS domain is found to be disordered, and it has been observed that getting rid of the domain makes crystallization easier (L Hedstrom, 2009).

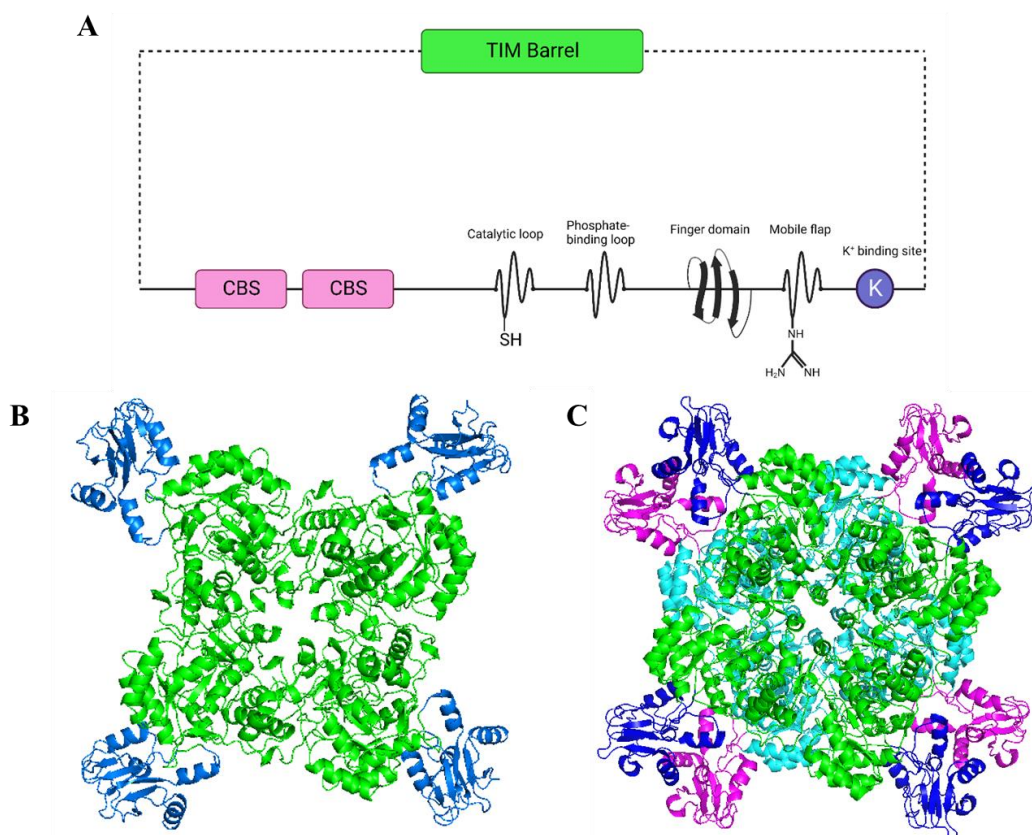


**Figure 2.2. Domain architecture and spatial arrangement of IMPDH.** **A.** Schematic bar representation of IMPDH key structural elements and CBS subdomain. **B.** Tetrameric structure of *S. pyogenes* IMPDH (1ZFJ) shown in ribbon diagram. CBS subdomain (blue) and catalytic domain (green) are highlighted in different colors. **C.** Octameric structure of human IMPDH2 (6UC2) shown in ribbon diagram. CBS subdomain and catalytic domain of one tetramer are colored in blue and green, while the opposing tetramer is highlighted in pink and cyan respectively.

All previously described IMPDHs other than MjIMPDH require a monovalent cation (ideally  $K^+$ ) for optimal activity, with about 100-fold increase in activity in the presence of the monovalent cation (Alexandre et al., 2015). The catalytic loop and the C-terminal region, which mostly do not

show densities in X-ray structures due to high disorder, make up the binding site for the monovalent cation.

IMPDH catalyzes two different chemical reactions: (i) a dehydrogenase reaction which forms the covalent intermediate E-XMP\* and NADH and (ii) a hydrolysis reaction to convert E-XMP\* into XMP. The dehydrogenase reaction involves the catalytic cysteine attacking C2 of IMP to produce the covalent thioimidate intermediate E-XMP\* while also transferring a hydride to NAD<sup>+</sup> to form NADH. After this, NADH leaves the active site, and the mobile flap moves into the vacant dinucleotide site. This brings the conserved Arg-Tyr dyad into the active site to allow the arginine to act as the catalytic base (L Hedstrom, 2009). A second hydrolyase reaction on E-XMP\* then follows, producing XMP and free enzyme.

### **2.1.3. Modulation of the activity of prokaryotic and eukaryotic IMPDHs by nucleotides**

As shown in **Fig. 2.2**, IMPDHs from both eukaryotes and prokaryotes share similar structural and functional features. However, they differ from each other in their mode of allosteric regulation (Alexandre et al., 2015). Based on allosteric control, IMPDH can be classified into two classes: class-I and class-II. Class-I IMPDHs show cooperative kinetics with IMP, activation by Mg-ATP and exist as octamers under varied conditions. Class-II IMPDHs, on the other hand, exhibit Michelis-Menten kinetics with IMP, exist as tetramers in the apo-state and shift to octamers upon Mg-ATP binding (Alexandre et al., 2015).

Prokaryotes have been found to have both class-I and class-II IMPDHs, whereas only class-II is present in eukaryotes (R M Buey & Fernández-Justel, 2017). While class-I IMPDHs show activation by Mg-ATP binding, class-II enzymes do not show any such changes in catalytic activity. Instead, they show change in structural organization. Prokaryotic and eukaryotic IMPDHs differ in many other aspects as well. Prokaryotic IMPDH shows competitive inhibition by GMP, whereas eukaryotic IMPDH shows a mixed-type inhibition by GDP and GTP. Eukaryotic IMPDHs contain a non-canonical GTP-binding site absent in prokaryotes and binding of GDP or GTP to this site causes tail-to-tail dimerization of the tetramers which leads to a more compressed shape. This compressed shape of the octamer prevents the IMP and NAD from entering the active site and thus blocks catalytic activity (R M Buey & Fernández-Justel, 2017). Upon binding of Mg-

---

ATP to the CBS or Bateman domain, the octamer is allosterically modulated to adopt a more relaxed shape and GDP/GTP falls off the non-canonical GTP-binding site.

Class-I IMPDHs show activity only in the presence of ATP, which acts as an activator. However, in the case of class-II, ATP has no effect on the catalytic activity in general. But it is the binding of GDP/GTP which controls the activation of class-II IMPDH. The binding of ATP actually leads to the alleviation of this control of GTP, thus turning on the catalytic activity. This shows that an ATP-controlled conformational switch was present in the ancestor of this two classes of enzymes, which has evolved to incorporate the control by GDP/GTP binding to the non-canonical nucleotide binding site in eukaryotic IMPDHs (R M Buey & Fernández-Justel, 2017).

#### **2.1.4. Role of cytoophidia in modulation of IMPDH activity**

IMPDH has been found to reversibly assemble into long filamentous structures called cytoophidia. This has been hypothesised to provide another level of regulation of enzyme function. Recently, several metabolic enzymes have been found to reversibly assemble together to form cytoophidia (Carcamo et al., 2011; Chang et al., 2015; Ji et al., 2006) (**Fig. 2.3**). However such filamentous structures have only been observed in eukaryotes not prokaryotes (Burrell et al., 2022). According to several studies, many non-cytoskeletal proteins reversibly assemble to form filaments under nutritional stress (Alberti et al., 2009; Aughey & Liu, 2016; Narayanaswamy et al., 2009; Noree et al., 2010; O'Connell et al., 2012, 2014; Shen et al., 2016). With time, more metabolic enzymes have been observed to show this property (O'Connell et al., 2012), thus showing that filamentation of metabolic enzymes is a way of maintaining metabolic flux (Aughey & Liu, 2016). In the studies where self-assembly of metabolic enzymes has been investigated biochemically and structurally, it has been found that the polymers are directly responsible for influencing metabolic activity by stabilizing active or inhibited conformations (Lynch et al., 2017). IMPDH has also been found to form helical polymers by stacking octamers in an ATP-dependent manner (Anthony et al., 2017; Burrell et al., 2022; M. C. Johnson & Kollman, 2020; Labesse et al., 2013). Guanine deprivation, increased intracellular IMP, presence of IMPDH inhibitors or other anti-proliferative drugs also leads to reversible assembly of IMPDH filaments (Chang et al., 2015; Ji et al., 2006; Keppeke et al., 2015, 2018).

---



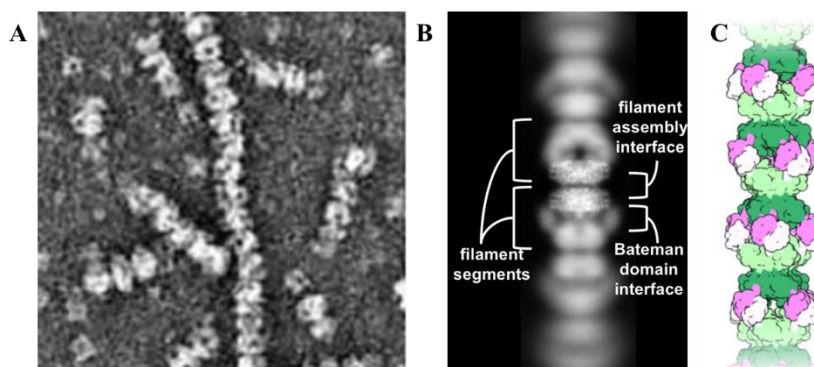


**Figure 2.3. Electron microscopy of uninhibited IMPDH2 filaments.** A. Negative stain EM of purified human IMPDH2 treated with 1 mM ATP to induce filament assembly. Scale bar 100 nm. B. Representative 2D class average of cryo-EM dataset. C. Cartoon of the filament of human IMPDH2 (Reprinted from Johnson & Kollman, 2020 under Creative Commons License (CC BY 4.0))

In some situations, IMPDH filaments colocalize with cytidine triphosphate synthase (CTPS) assemblies, an enzyme involved in pyrimidine biosynthesis, suggesting a potential coordination between purine and pyrimidine production (Keppeke et al., 2015). The role of cytophidia in IMPDH was still unknown until recently (Chang et al., 2015; Duong-Ly et al., 2018; Keppeke et al., 2018). It has been hypothesised that the assembly's function may be to maintain homeostasis by replenishing guanine nucleotide pools based on the response of IMPDH to reduced flow along the guanine nucleotide biosynthesis pathway (Anthony et al., 2017).

In a recent study on the allosteric regulation of filament formation in IMPDH2 (M. C. Johnson & Kollman, 2020), a model has been proposed that illustrates human IMPDH2 filament assembly (**Fig. 2.4**). In the absence of IMP or guanine ligands, IMPDH2 is conformationally dynamic, creating stable tetramers that freely sample both the "bowed" and "flat" tetramer conformations. Stable filaments are produced by the binding of adenine nucleotides, whereas the binding of GTP results in lattice strain and the breakdown of the filament interface. The binding of IMP stabilizes the flexible active site loops, and the compressed filaments produced by saturation with both IMP and GTP are resistant to the lattice strain caused by compression. Feedback inhibition of the enzyme is fine-tuned by the balance of these conformational dynamics, which is compatible with the states in which IMPDH filaments are seen in cells. IMPDH2 filament formation helps increase intracellular guanine nucleotide levels during the proliferative state by preventing feedback inhibition. IMP synthesis is increased in response to overall purine demand and proliferative signaling via mTOR. Because filament construction depends on IMP levels, there is a way to control assembly via recognized proliferative signaling pathways. By lowering affinity for

inhibitory downstream products, IMPDH2 filaments fine-tune the allosteric response, adding another layer of regulation to modulate flux through metabolic pathways.

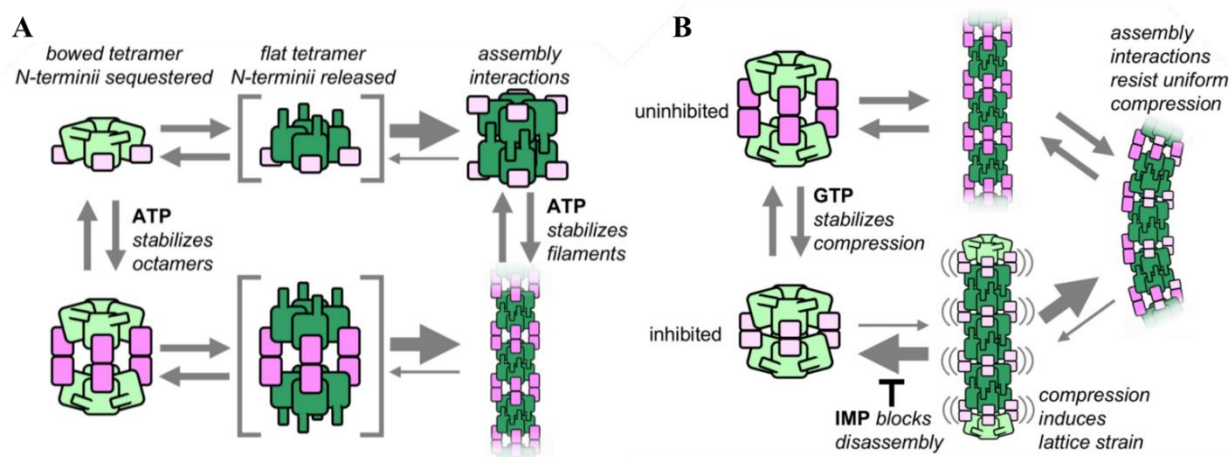


**Figure 2.4. Model of IMPDH2 assembly and the function of filaments in guanine nucleotide regulation.** A. When the catalytic tetramer (green) is flattened, the N-terminal residues are released, and the octamer contacts are stabilized by ATP binding to the regulatory domain (pink). Interactions between the filament assemblies maintain the flat shape. B. GTP binding maintains a compressed, inhibited conformation. As a result of the filament's reduced sensitivity to GTP-induced compression, octamers are kept in a population with mixed activity states. Filaments undergo strain when they are fully compressed and GTP-bound, which encourages disintegration that is prevented by substrate IMP binding. (Reprinted from Johnson & Kollman, 2020 under Creative Commons License (CC BY 4.0))

## 2.1.5. Unique regulatory features of an archaeal *Methanocaldococcus jannaschii* IMPDH

Previous studies in our group have revealed remarkable regulatory properties of an archaeal IMPDH from *Methanocaldococcus jannaschii* (MjIMPDH). All adenine and guanine nucleotides save ATP, inhibit the enzyme's activity, like eukaryotic IMPDHs. Moreover, ATP has no effect on the enzyme's catalytic activity (Prasoona, 2019). The fact that MjIMPDH is inhibited by GDP and GTP without increasing activity in the presence of ATP, in particular, demonstrates that the archaeal enzyme shares traits with eukaryotic IMPDH. It is possible that MjIMPDH also has a non-canonical nucleotide binding site based on the significant decrease in purine nucleotide inhibition brought on by deletion of the CBS domain. Moreover, MjIMPDH does not require any monovalent cation ( $K^+$ ) for its activity, unlike previously reported IMPDHs. Hence, crystallization was attempted for the holoprotein, but the inherent flexibility of the CBS domain led to formation

of crystals that either diffracted very poorly or not at all. Hence, the structure of the catalytic TIM-barrel domain of MjIMPDH was determined, as has been done with most IMPDHs in the literature. Further, preliminary investigations through negative-staining electron microscopy at in-house-facility, JNCASR (FEI Tecnai G2 transmission electron microscope; 200 kV) suggested the formation of filaments, but this required further validation.

### **2.1.6. Objectives**

Considering the unique regulatory features of archaeal MjIMPDH displays, the objective of the study was to better understand its modulatory aspects and examine the formation of filament-like structures.

## 2.2. Experimental procedures

### 2.2.1. Chemicals, strains, and molecular biology reagents

Media components for growing *E. coli* cultures were obtained from HiMedia (Mumbai, India). Akta HPLC and Q-Sepharose and Superdex resins were from GE Healthcare Life Sciences, USA.

### 2.2.2. Sequence alignment and phylogenetic tree construction

The IMPDH sequences from various organisms were obtained from the NCBI BLAST-P tool using the *Methanocaldococcus jannaschii* IMPDH (MjIMPDH) sequence as a query. Clustal Omega (Goujon et al., 2010; Sievers et al., 2011) was used for multiple sequence alignment and the output was processed using ESPRIPT (Robert & Gouet, 2014) for visualization.

### 2.2.3. Protein expression and purification

MjIMPDH-expressing clones in pET21b+ containing a fused C-terminal (His)<sub>6</sub>-tag (pET21bIMPDH) had already been generated in the laboratory. The BL21(DE3) strain of *E. coli* lacking the endogenous IMPDH enzyme  $\Delta$ guaB<sup>K</sup>, previously generated in the lab, was co-transformed with pLysS (expressing ROS tRNA) and pET21bIMPDH. The culture was grown overnight at 37 °C, and 1% inoculum was added to 800 ml of Terrific broth (TB). The cells were grown at 37 °C to an absorbance of 0.6, induced with 0.05 mM IPTG, and further grown for 12 h at 16 °C. The cells were harvested by centrifugation at 6000 g for 10 min at 4 °C and resuspended in lysis buffer containing 50 mM Tris HCl (pH 7.0), 10% glycerol, 2 mM DTT and 0.1 mM PMSF. Cell lysis was achieved using five cycles of French press (Thermo IEC Inc., USA) at 1000 psi, and the lysate was clarified by centrifugation at 30,000 × g for 30 min. The supernatant was heated at 70 °C for 30 min to precipitate bacterial proteins and clarified by centrifugation at 30,000 × g for 30 min. The supernatant was then treated with 0.01% PEI to precipitate nucleic acids and clarified by centrifugation at 30,000 g for 30 min. The clarified lysate was filtered through a 0.44 micron filter and loaded onto a Q-Sepharose anion-exchange column. The protein was eluted using a linear gradient of KCl in buffer containing 50 mM Tris HCl (pH 7.0), 10 % glycerol, and 2 mM DTT. Fractions collected at KCl concentrations above 300 mM were examined using SDS-PAGE, pooled according to purity, and precipitated using ammonium sulfate at 90% saturation. The precipitate obtained was resuspended in lysis buffer and subjected to size-exclusion

---

chromatography on a Superdex 200 column of dimension 1.6 cm x 60 cm (GE Healthcare, USA). The purified protein was analyzed by SDS-PAGE (U.K.Lammli, 1970) and protein concentration was determined by the Bradford method (Bradford, 1976) with bovine serum albumin (BSA) as standard.

#### **2.2.4. Transmission electron microscopy imaging**

Aliquots of purified MjIMPDPH protein were diluted to 2.5  $\mu$ M in buffer containing 50mM Tris HCl (pH 7.0) and 2 mM DTT and incubated with or without ATP and GTP at 1mM concentration for varying time periods at room temperature. Following incubation, aliquots were applied to glow-discharged carbon film EM grids and negatively stained using 1% uranyl acetate. The grids were imaged using a Talos L120C transmission electron microscope operating at 120 kV and a Ceta camera (CMOS detector).

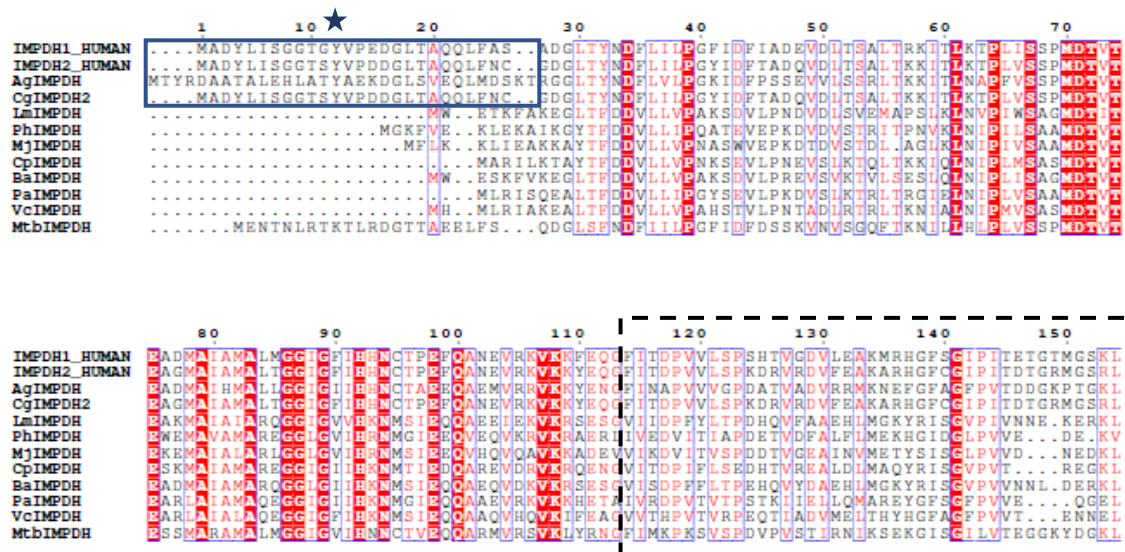
#### **2.2.5. Image Analysis**

Image analysis was performed using EMAN2 (Tang et al., 2007). Image analysis involved interactive particle picking with a box size of 180 and particle size of 120, followed by reference-free 2D classification, to determine the class averages.

## 2.3. Results & Discussion

### 2.3.1. Sequence analysis

Preliminary experiments done earlier in the group showed that MjIMPDH forms filamentous structures in the presence of ATP. Such structures have previously been reported in IMPDHs of eukaryotic origin only and have been shown to form through the stacking of octamers mediated by interaction between the TIM-barrel domains and N-terminal extensions of adjacent octamers (M. C. Johnson & Kollman, 2020). This N-terminal extension (~30 amino acids) plays a critical role in forming the filament assembly interface. It is this N-terminal tail which innervates the catalytic domain of the opposing octamer. A key tyrosine residue (Y12 in human IMPDH2) forms the key contact with an arginine residue (R356) of the adjacent octamer. Mutation of these key residues does not impair catalytic activity but abrogates octamer assembly and filament formation. A multiple sequence alignment of biochemically characterized IMPDH sequences from prokaryotes, eukaryotes and archaea shows that this N-terminal domain is found in eukaryotes only, not in prokaryotes and archaea. However, *Mycobacterium tuberculosis* (MtbIMPDH) was found to have a N-terminal tail longer than the ones present in eukaryotes. Upon performing a BLAST search with the N-terminal in MtbIMPDH, we found that the N-terminal tail is a characteristic feature of IMPDHs from the *mycobacteriaceae* family. However, this region does not contain the key residues which have previously been found to form the filament assembly interface and no previous literature were also found to show any evidence of filament formation in MtbIMPDH.



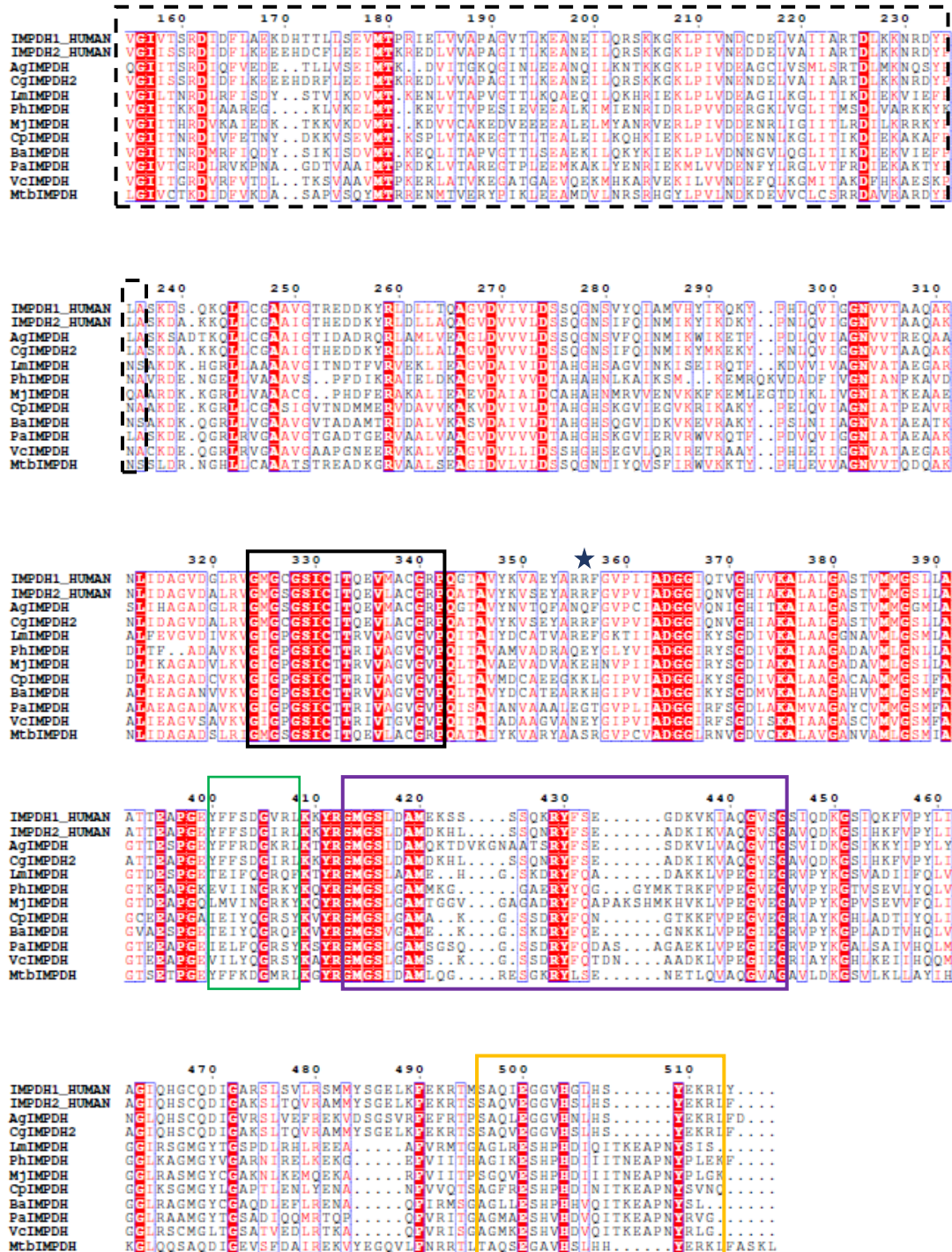


**Figure 2.5. Multiple sequence alignment of IMPDH sequences from various organisms.** Sequences of IMPDHs from prokaryotes, eukaryotes and archaea were aligned using Clustal Omega (Sievers et al, 2011) and rendered using ESPrpt 3.0 (Robert & Gouet, 2014). The sequences show high conservation (>70% consensus). The N-terminal tail has been highlighted in blue box with the critical residues marked with blue stars. Residues from the catalytic cysteine loop are marked with a black box, phosphate-binding loop in a black dashed box, finger loop in a green box, mobile flap loop in a purple box and C-terminal loop in a yellow box.

### 2.3.2. Transmission electron microscopy of IMPDH

Previous experiments in the laboratory had demonstrated that MjIMPDH shows behaviour similar to its eukaryotic counterparts despite high sequence similarity to prokaryotic IMPDHs (Prasoon, 2019). Most prokaryotic IMPDHs exist as tetramers, whereas MjIMPDH was found to form an octamer (Prasoon, 2019). In addition, very preliminary experiments carried out using a FEI Tecnai G2 microscope, at 120 kV suggested the possibility of assembly into filaments in the presence of Mg-ATP (Bellur, 2022). To evaluate the reproducibility and conditions that mediate filament formation, I undertook fresh studies using JEOL JEM 2100 Plus (200 kV) available in the in-house imaging facility. The octamer fraction was examined in the presence and absence of ATP and GTP. Grid preparation involved spotting samples on carbon-coated 200-mesh copper grids, that were not glow-discharged. Following this, the sample was dried overnight in a desiccator and imaged the next day. Despite multiple trials, all images acquired were of poor quality. Problems encountered were beam-induced damage of the sample on the grid leaving very few fields yielding good quality images. 6-7 attempts were made to acquire images on JEOL JEM 2100 Plus (200 kV) but we failed to obtain good quality images. Thereafter, we acquired images on ThermoFischer Talos L120C transmission electron microscope at the Electron Microscope Facility, Division of Biological Sciences, Indian Institute of Science.

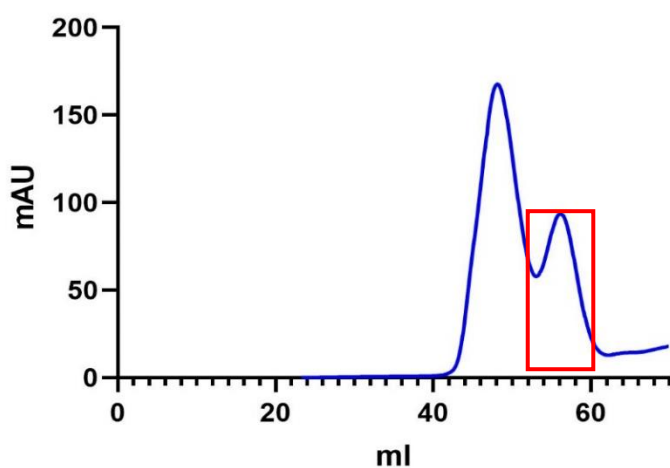
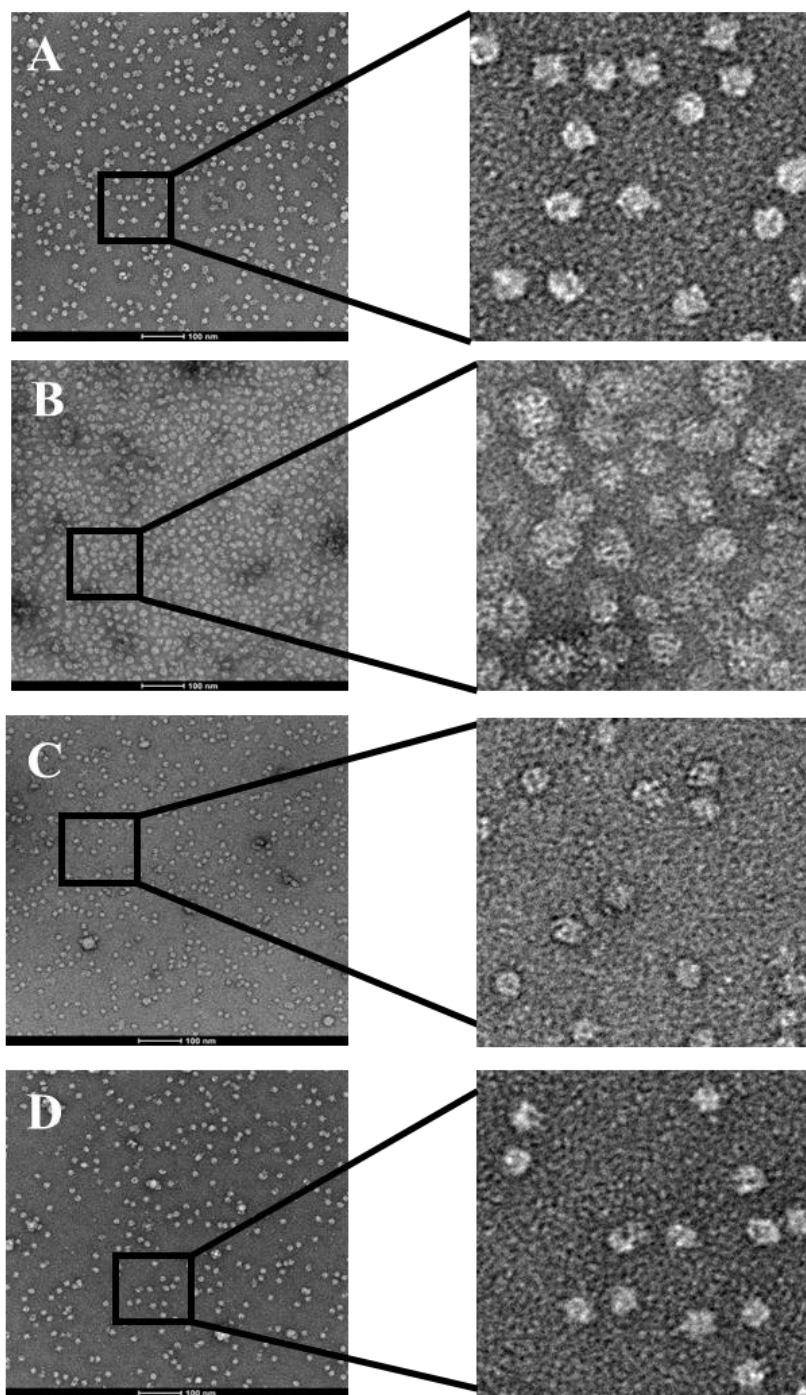


*Figure 2.6. Gel filtration profile of MjIMPDH. The chromatogram shows a major peak which was assigned to be higher order oligomers and a smaller fraction which corresponded to octamers (highlighted in red box).*

Previous experiments in the group had shown that MjIMPDH elutes out of a size-exclusion column as two separate peaks as shown in **Fig. 2.6**. Both of the peaks show similar catalytic activity,



however only one of them, the smaller peak, could be assigned the stoichiometry of an octamer (Prasootna, 2019). It was with this fraction only, that crystallization was attempted as well (Bellur, 2022). Since the larger fraction could not be stoichiometrically characterized, it was assigned as higher order oligomers (HOO) (Prasootna, 2019). All the TEM imaging has been done with the octameric fraction only unless mentioned otherwise.



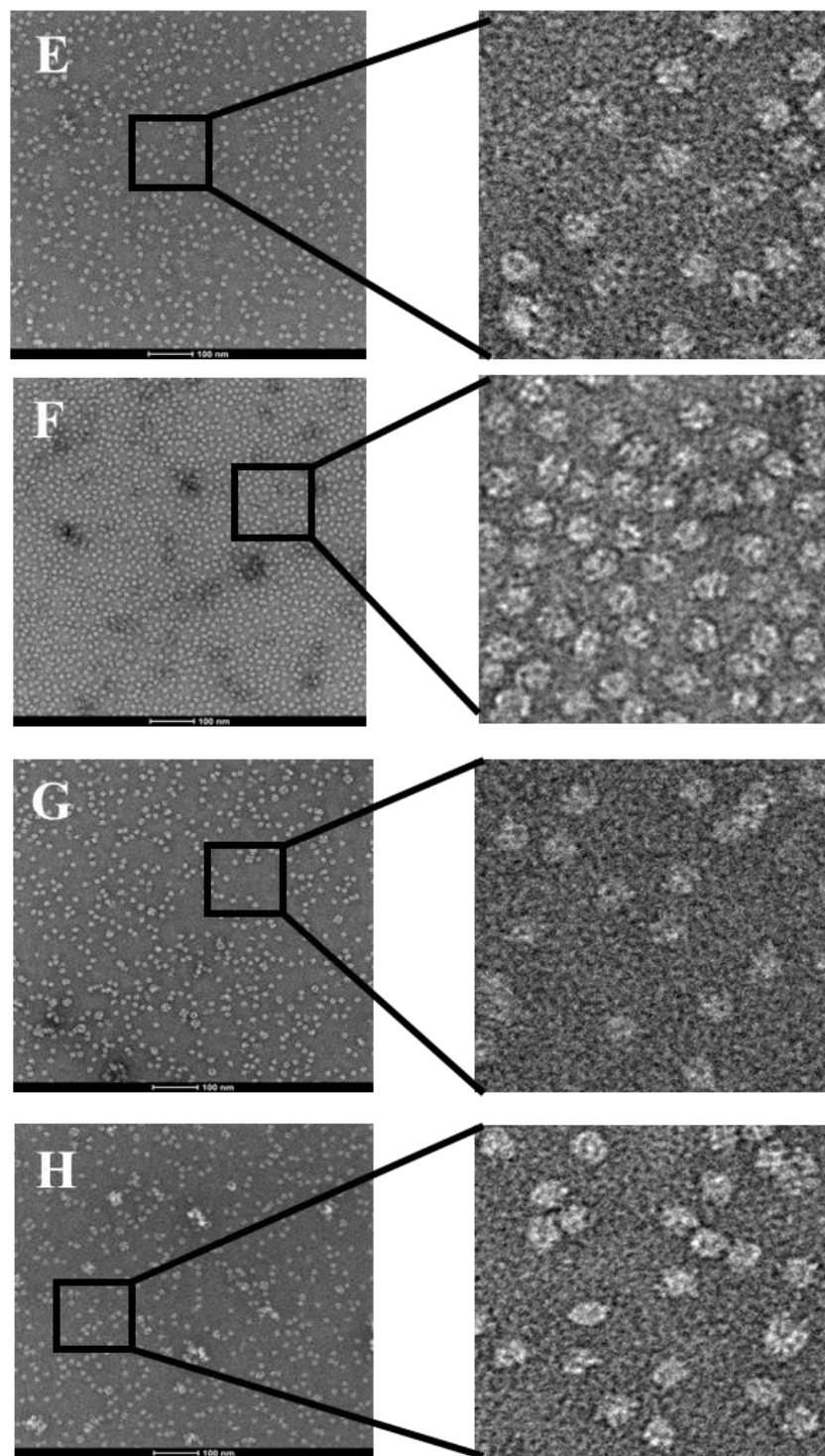


**Figure 2.7.** *Negative-staining transmission electron micrographs of IMPDH under various conditions. A. Octamer; B. Stoichiometrically undefined higher order oligomer fraction; C. Octamer + 1 mM Mg-ATP; D. Octamer + 2 mM Mg-ATP; E. Octamer + 1 mM GTP; F. Octamer + 1mM NAD + 1mM IMP + 1mM Mg-ATP; G. Octamer + 1mM Mg-ATP + 1mM KCl; H. Octamer + 1 mM Na-ATP + 1 mM MgCl<sub>2</sub>; Scale bar 100 nm.*

Upon performing transmission electron microscopy using ThermoFischer Talos L120C transmission electron microscope with samples being air-dried for a brief time period after spotting on glow-discharged grids, we could easily identify numerous distinct particles of uniform size in all fields. However, upon addition of ATP, we do not see the octamers coming together to form filamentous structures. Various conditions were tried (**Table 2.1**) to reproduce the previous preliminary observation of filaments; however, none were observed (**Fig. 2.6**). Interestingly, upon imaging the “higher order oligomer” fraction, no aggregate formation was noticed, instead well-separated particles were observed to be distributed throughout the field. Moreover, the particles seemed to have a different kind of shape and morphology than the octamers.

**Table 2.1. List of conditions screened for negative-staining EM of MjIMPDH.**

<b>Sample No.</b>	<b>Conditions</b>	<b>Time period of incubation (min.)</b>
<b>1</b>	Octamer	0
<b>2</b>	Octamer + 1 mM Mg-ATP	30
<b>3</b>	Octamer + 2 mM Mg-ATP	30
<b>4</b>	Octamer + 1 mM GTP	30
<b>5</b>	Octamer + 1mM NAD + 1mM IMP + 1mM Mg-ATP	30
<b>6</b>	Octamer + 1mM Mg-ATP + 1mM KCl	30
<b>7</b>	Octamer + 1 mM Na-ATP + 1 mM MgCl <sub>2</sub>	30
<b>8</b>	Stoichiometrically undefined fraction	0

### **2.3.3. Image processing by reference free 2D classification**

Negative-staining electron microscopy (EM) is a widely used technique in biological research to obtain 2D images of macromolecules. However, this technique has certain limitations; in the process of enhancing the contrast of the particles, it results in the loss of high-resolution information. Nonetheless, information about the organization of the macromolecules can still be obtained through clustering of similar particle images i.e., 2D average calculation. In this study, a

reference-free 2D image classification algorithm was used to generate representative average images for the dataset.

The data from the different ligand bound conditions were not taken for further analysis as they did not show any significant differences in their morphology. Since, the “higher order oligomers” appeared as distinct single similar-sized particles in the images, they were taken further for image analysis and 2D classification with the aim of distinguishing the features of the octamers and HOOs. Upon performing reference free 2D classification, we selected the best 25 classes for octamers and 30 classes for the higher-order oligomers. Here we see a stark difference between the two fractions as shown in **Fig. 2.7**. The overall shape and dimensions of the octamers varies significantly from that of the higher-order oligomer fraction. The latter appear to have adapted a more relaxed conformation with individual domains visible in some of the class averages, whereas octamers show a compressed state. This shows that the previous assignment of “higher order oligomers” to the fraction eluting first on size-exclusion chromatography was incorrect. The class averages show them to be octamers in a relaxed state. This suggest that the difference in retention times between the two fractions in a size exclusion column is not due to a change in their molecular weight arising from the number of associating subunits , but rather due a change in the hydrodynamic radius or Stokes radius of the octamer. Such phenomena have been previously found to happen in Ca-binding calmodulins (Papish et al., 2002), cyclic nucleotide dependent protein kinases (Francis et al., 1998), muscle pyruvate kinase (Heyduk et al., 1992), etc. Thus, our previous annotation of the first SEC fraction as higher order oligomers needs amendment and henceforth referred to as relaxed octamers. The two different states of the octamer may arise from the binding of a metabolite whose identity is yet to be established. We have not yet examined filament formation by the relaxed octamer upon binding nucleotides. Determining the structures of the compressed and relaxed octamers by single particle cryo-EM would throw light on the structural transitions that lead to the two conformational states.

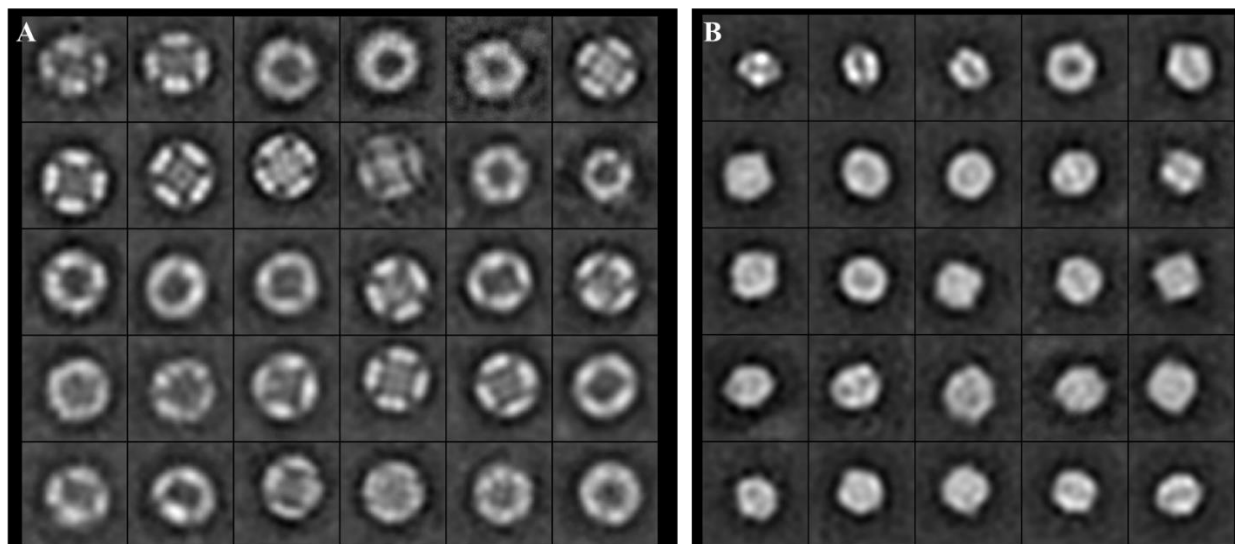


*Figure 2.8. Class averages of (A) stoichiometrically undetermined higher-order oligomer fraction, and (B) octamer fraction.*

## 2.4. Summary

Despite a plethora of work on IMPDHs from different organisms, no archaeal IMPDH has been biochemically and structurally characterized till date. Previous work from our group had showed critical biochemical features of MjIMPDH and also determined the crystal structure of the catalytic domain. However, since the modulatory aspect of the enzyme is mostly due to the flexible CBS domain, it is important to understand its role in allosteric regulation of the enzyme. Previous work in the laboratory had found preliminary evidence of MjIMPDH forming filament like structures, as seen in IMPDHs of eukaryotic origin. However, upon further detailed investigation, we found that under the various conditions tried with the octamer fraction, filament formation could not be observed. This could be due to the absence of the N-terminal extension that has been shown to play a role in filament assembly in IMPDHs of eukaryotic origin. MjIMPDH lacks the N-terminal extension and hence possibly the inability to form filaments. However, we found out that the fraction previously designated “higher order oligomer” fraction is composed of only octamers but with a very different overall shape and morphology. The fast eluting oligomers were found to exist in a relaxed state compared to slow eluting octamers, Hence, it can be proposed that MjIMPDH adapts two completely different states which have different hydrodynamic or Stokes radii. This leads to the difference in migration in a gel filtration column, which shows up as two peaks on the chromatogram. Our hypothesis needs structural validation using single particle cryo-EM.

## 2.5. Future directions

The question of how MjIMPDPH shows high similarity to its eukaryotic counterparts instead of prokaryotic IMPDHS despite high sequence similarity still remains an enigma. To understand this unique nucleotide-mediated regulation of the enzyme, it has to be studied in a far greater detail. The number of nucleotide binding sites in the CBS domain and the presence or absence of a non-canonical nucleotide binding site have to be investigated. Moreover, the relaxed octamers have not been studied as extensively as the octamers in the laboratory till now. Their characterization can also help in understanding this unique phenomenon. The major goal for the project now will be the structural characterization of the enzyme through cryo-electron microscopy. Determination of the structure of the enzyme will help us elucidate some of the questions posed by kinetic studies, X-ray crystallography and TEM imaging.

# Appendix I

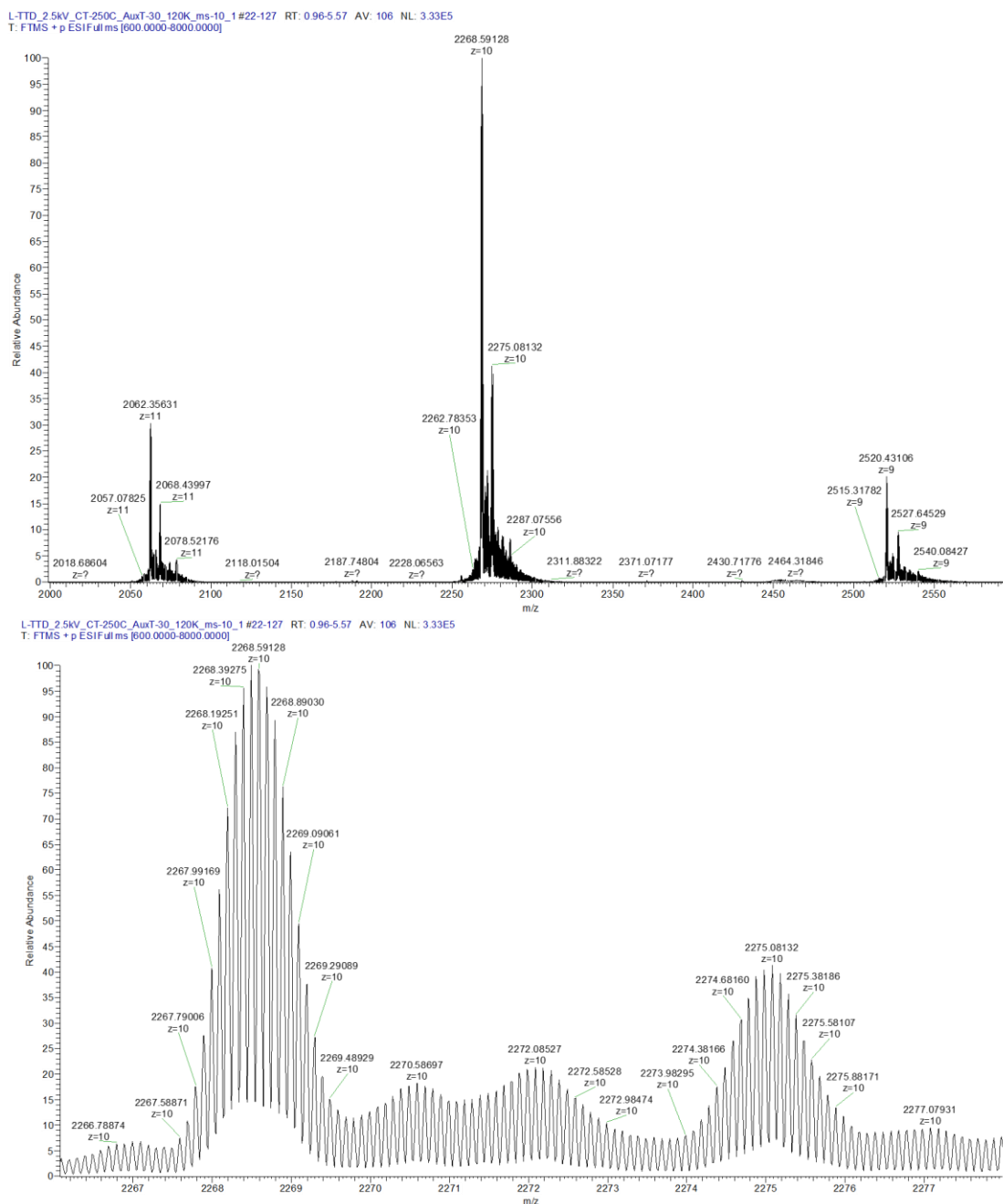


**Figure A.1.** Isotopic distribution of peaks of L-TTD $\beta$  at high resolution (120,000) under native conditions. A. The three peaks (highlighted by arrows) of L-TTD $\beta$  with charges assigned from isotopic distribution. B. Isotopic distribution in the central peak

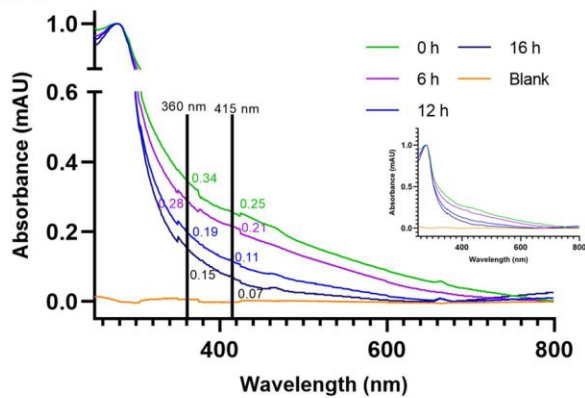


**Table A1. Mass difference in peaks with no isotopic distribution.**

<b>m/z</b>	<b>Charge state</b>	<b>Experimental mass (Da) (<math>M_E</math>)</b>	<b>Theoretical mass (Da) (<math>M_T</math>)</b>	<b>Mass difference (Da) <math>\Delta M = M_E - M_T</math></b>	<b>Assigned species</b>
3175.13492	18	57152.43	57063.29 (L-TTD $\alpha\beta$ )	89.13856	L-TTD $\alpha\beta$
3361.82052	17	57150.95	57063.29 (L-TTD $\alpha\beta$ )	87.65884	L-TTD $\alpha\beta$
3571.86244	16	57149.8	57063.29 (L-TTD $\alpha\beta$ )	86.50904	L-TTD $\alpha\beta$
3814.04834	15	57210.73	57063.29 (L-TTD $\alpha\beta$ )	147.4351	L-TTD $\alpha\beta$
4411.08844	26	114688.3	114716.7 2 × (L-TTD $\alpha\beta$ + 3Fe-4S)	-28.3806	2 × (L-TTD $\alpha\beta$ + 3Fe-4S)
4588.03804	25	114701	114716.7 2 × (L-TTD $\alpha\beta$ + 3Fe-4S)	-15.729	2 × (L-TTD $\alpha\beta$ + 3Fe-4S)
4783.94261	24	114814.6	114716.7 2 × (L-TTD $\alpha\beta$ + 3Fe-4S)	97.94264	2 × (L-TTD $\alpha\beta$ + 3Fe-4S)
4989.83689	23	114766.2	114716.7 2 × (L-TTD $\alpha\beta$ + 3Fe-4S)	49.56847	2 × (L-TTD $\alpha\beta$ + 3Fe-4S)

## Appendix II

A.2.



A.3.

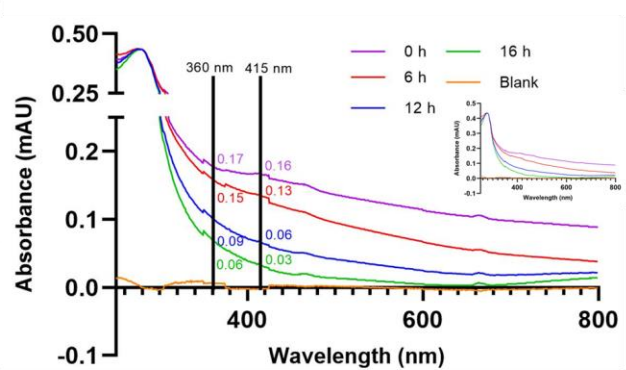
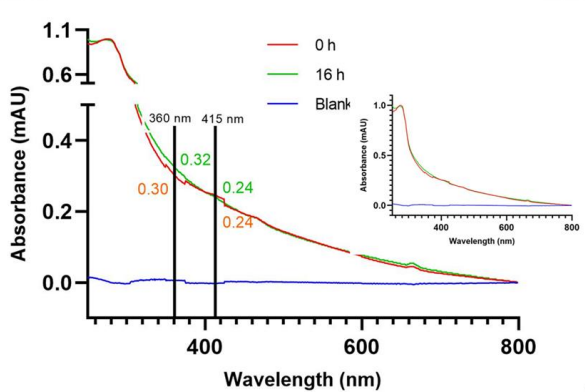


Figure A.2. & A.3. Replicates of incubation of reconstituted L-TTD in air as shown in Fig. 1.11

A.4.



A.5.

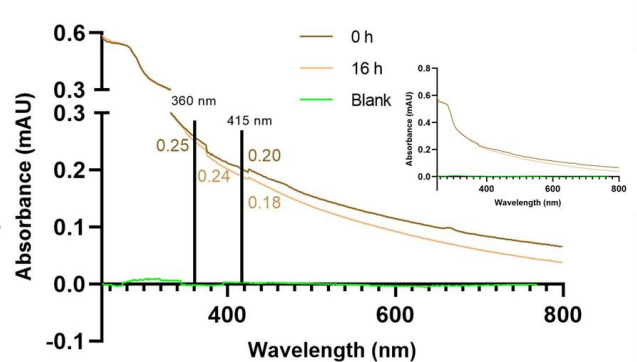


Figure A.4. & A.5. Replicates of incubation of reconstituted L-TTD in air in presence of MSA as shown in Fig. 1.12

# Rights and Permissions

4/21/23, 12:56 AM

Rightslink® by Copyright Clearance Center



RightsLink



Home



Help ▾



Live Chat



Sign in



Create Account



## Revisiting the Burden Borne by Fumarase: Enzymatic Hydration of an Olefin

Author: Asutosh Bellur, Soumik Das, Vijay Jayaraman, et al

Publication: Biochemistry

Publisher: American Chemical Society

Date: Jan 1, 2023

*Copyright © 2023, American Chemical Society*

### PERMISSION/LICENSE IS GRANTED FOR YOUR ORDER AT NO CHARGE

This type of permission/license, instead of the standard Terms and Conditions, is sent to you because no fee is being charged for your order. Please note the following:

- Permission is granted for your request in both print and electronic formats, and translations.
- If figures and/or tables were requested, they may be adapted or used in part.
- Please print this page for your records and send a copy of it to your publisher/graduate school.
- Appropriate credit for the requested material should be given as follows: "Reprinted (adapted) with permission from {COMPLETE REFERENCE CITATION}. Copyright {YEAR} American Chemical Society." Insert appropriate information in place of the capitalized words.
- One-time permission is granted only for the use specified in your RightsLink request. No additional uses are granted (such as derivative works or other editions). For any uses, please submit a new request.

If credit is given to another source for the material you requested from RightsLink, permission must be obtained from that source.

[BACK](#)[CLOSE WINDOW](#)

© 2023 Copyright - All Rights Reserved | [Copyright Clearance Center, Inc.](#) | [Privacy statement](#) | [Data Security and Privacy](#)  
| [For California Residents](#) | [Terms and Conditions](#) Comments? We would like to hear from you. E-mail us at [customer-care@copyright.com](mailto:customer-care@copyright.com)

<https://s100.copyright.com/AppDispatchServlet#formTop>

1/1

4/18/23, 11:19 AM

Rightslink® by Copyright Clearance Center



RightsLink



Home



Help ▾



Live Chat



Sign in



Create Account

### Iron–Sulfur Proteins with Nonredox Functions

**Author:** Dennis H. Flint, Ronda M. Allen**Publication:** Chemical Reviews**Publisher:** American Chemical Society**Date:** Jan 1, 1996*Copyright © 1996, American Chemical Society*

#### PERMISSION/LICENSE IS GRANTED FOR YOUR ORDER AT NO CHARGE

This type of permission/license, instead of the standard Terms and Conditions, is sent to you because no fee is being charged for your order. Please note the following:

- Permission is granted for your request in both print and electronic formats, and translations.
- If figures and/or tables were requested, they may be adapted or used in part.
- Please print this page for your records and send a copy of it to your publisher/graduate school.
- Appropriate credit for the requested material should be given as follows: "Reprinted (adapted) with permission from {COMPLETE REFERENCE CITATION}. Copyright {YEAR} American Chemical Society." Insert appropriate information in place of the capitalized words.
- One-time permission is granted only for the use specified in your RightsLink request. No additional uses are granted (such as derivative works or other editions). For any uses, please submit a new request.

If credit is given to another source for the material you requested from RightsLink, permission must be obtained from that source.

[BACK](#)[CLOSE WINDOW](#)

© 2023 Copyright - All Rights Reserved | [Copyright Clearance Center, Inc.](#) | [Privacy statement](#) | [Data Security and Privacy](#)  
| [For California Residents](#) | [Terms and Conditions](#) Comments? We would like to hear from you. E-mail us at [customercare@copyright.com](mailto:customercare@copyright.com)

4/28/23, 4:26 AM

Rightslink® by Copyright Clearance Center



RightsLink



Home



Help ▾



Live Chat



Sign in



Create Account

### IMP Dehydrogenase: Structure, Mechanism, and Inhibition



Author: Lizbeth Hedstrom

Publication: Chemical Reviews

Publisher: American Chemical Society

Date: Jul 1, 2009

*Copyright © 2009, American Chemical Society*

#### PERMISSION/LICENSE IS GRANTED FOR YOUR ORDER AT NO CHARGE

This type of permission/license, instead of the standard Terms and Conditions, is sent to you because no fee is being charged for your order. Please note the following:

- Permission is granted for your request in both print and electronic formats, and translations.
- If figures and/or tables were requested, they may be adapted or used in part.
- Please print this page for your records and send a copy of it to your publisher/graduate school.
- Appropriate credit for the requested material should be given as follows: "Reprinted (adapted) with permission from {COMPLETE REFERENCE CITATION}. Copyright {YEAR} American Chemical Society." Insert appropriate information in place of the capitalized words.
- One-time permission is granted only for the use specified in your RightsLink request. No additional uses are granted (such as derivative works or other editions). For any uses, please submit a new request.

If credit is given to another source for the material you requested from RightsLink, permission must be obtained from that source.

[BACK](#)[CLOSE WINDOW](#)

© 2023 Copyright - All Rights Reserved | [Copyright Clearance Center, Inc.](#) | [Privacy statement](#) | [Data Security and Privacy](#)  
| [For California Residents](#) | [Terms and Conditions](#) Comments? We would like to hear from you. E-mail us at [customer@copyright.com](mailto:customer@copyright.com)

---

## References

1. Aherne, A., Kennan, A., Kenna, P. F., McNally, N., Lloyd, D. G., Alberts, I. L., Kiang, A. S., Humphries, M. M., Ayuso, C., Engel, P. C., Gu, J. J., Mitchell, B. S., Farrar, G. J., & Humphries, P. (2004). On the molecular pathology of neurodegeneration in IMPDH1-based retinitis pigmentosa. *Human Molecular Genetics*, *13*(6), 641–650. <https://doi.org/10.1093/hmg/ddh061>
  2. Alberti, S., Halfmann, R., King, O., Kapila, A., & Lindquist, S. (2009). A Systematic Survey Identifies Prions and Illuminates Sequence Features of Prionogenic Proteins. *Cell*, *137*(1), 146–158. <https://doi.org/10.1016/j.cell.2009.02.044>
  3. Alexandre, T., Raynal, B., & Munier-Lehmann, H. (2015). Correction: Two Classes of Bacterial IMPDHs according to Their Quaternary Structures and Catalytic Properties. *PLOS ONE*, *10*(4), e0125884. <https://doi.org/10.1371/journal.pone.0125884>
  4. An, S., Kumar, R., Sheets, E. D., & Benkovic, S. J. (2008). Reversible compartmentalization of de novo purine biosynthetic complexes in living cells. *Science*, *320*(5872), 103–106. <https://doi.org/10.1126/science.1152241>
  5. Anthony, S. A., Burrell, A. L., Johnson, M. C., Duong-Ly, K. C., Kuo, Y. M., Simonet, J. C., Michener, P., Andrews, A., Kollman, J. M., & Peterson, J. R. (2017). Reconstituted IMPDH polymers accommodate both catalytically active and inactive conformations. *Molecular Biology of the Cell*, *28*(20), 2600–2608. <https://doi.org/10.1091/mbc.E17-04-0263>
  6. Aughey, G. N., & Liu, J. L. (2016). Metabolic regulation via enzyme filamentation. *Critical Reviews in Biochemistry and Molecular Biology*, *51*(4), 282–293. <https://doi.org/10.3109/10409238.2016.1172555>
  7. Bak, D. W., & Weerapana, E. (2023). Monitoring Fe–S cluster occupancy across the E. coli proteome using chemoproteomics. *Nature Chemical Biology*, *19*(3), 356–366. <https://doi.org/10.1038/s41589-022-01227-9>
  8. Bateman, A. (1997). The structure of a domain common to archaeobacteria and the homocystinuria disease protein. *Trends in Biochemical Sciences*, *22*(1), 12–13. [https://doi.org/10.1016/S0968-0004\(96\)30046-7](https://doi.org/10.1016/S0968-0004(96)30046-7)
  9. Baykov, A. A., Tuominen, H. K., & Lahti, R. (2011). The CBS domain: A protein module with an emerging prominent role in regulation. *ACS Chemical Biology*, *6*(11), 1156–1163.
-

- 
- <https://doi.org/10.1021/cb200231c>
10. Bearne, S. L. (2020). Through the Looking Glass: Chiral Recognition of Substrates and Products at the Active Sites of Racemases and Epimerases. *Chemistry - A European Journal*, 26(46), 10367–10390. <https://doi.org/10.1002/chem.201905826>
  11. Bearne, S. L., & Wolfenden, R. (1995). Enzymatic Hydration of an Olefin: The Burden Borne by Fumarase. *Journal of the American Chemical Society*, 117(37), 9588–9589. <https://doi.org/10.1021/ja00142a037>
  12. Beinert, H., Kennedy, M. C., & Stout, C. D. (1996). Aconitase as iron-sulfur protein, enzyme, and iron-regulatory protein. *Chemical Reviews*, 96(7), 2335–2373. <https://doi.org/10.1021/cr950040z>
  13. Bellur, A. (2022). *Catalytic mechanism and stereospecificity in class-I fumarate hydratase and L-tartrate dehydratase, and structural characterization of an archaeal IMP dehydrogenase*. <http://lib.jncasr.ac.in:8080/jspui/handle/123456789/3283>
  14. Bellur, A., Das, S., Jayaraman, V., Behera, S., Suryavanshi, A., Balasubramanian, S., Balaram, P., Jindal, G., & Balaram, H. (2023). Revisiting the Burden Borne by Fumarase: Enzymatic Hydration of an Olefin. *Biochemistry*, 62(2), 476–493. <https://doi.org/10.1021/acs.biochem.2c00541>
  15. Bentley, R. (2003). Diastereoisomerism, contact points, and chiral selectivity: A four-site saga. *Archives of Biochemistry and Biophysics*, 414(1), 1–12. [https://doi.org/10.1016/S0003-9861\(03\)00169-3](https://doi.org/10.1016/S0003-9861(03)00169-3)
  16. Bertini, I. (2007). *Biological Inorganic Chemistry: Structure and Reactivity*. University Science Books. <https://books.google.co.in/books?id=a52CE0vWRXQC>
  17. Bradford, M. M. (1976). A rapid and sensitive method for the quantitation of microgram quantities of protein utilizing the principle of protein-dye binding. *Analytical Biochemistry*, 72(1–2), 248–254. [https://doi.org/10.1016/0003-2697\(76\)90527-3](https://doi.org/10.1016/0003-2697(76)90527-3)
  18. Braymer, J. J., & Lill, R. (2017). Iron-sulfur cluster biogenesis and trafficking in mitochondria. *Journal of Biological Chemistry*, 292(31), 12754–12763. <https://doi.org/10.1074/jbc.R117.787101>
  19. Broderick, J. B., Duffus, B. R., Duschene, K. S., & Shepard, E. M. (2014). Radical S-Adenosylmethionine Enzymes. *Chemical Reviews*, 114(8), 4229–4317. <https://doi.org/10.1021/cr4004709>
-

- 
20. Buey, R M, & Fernández-Justel, D. (2017). Marcos-Alcalde, Í., Winter, G., Gómez-Puertas, P., De Pereda, J. M., & Luis Revuelta, J. A *Nucleotide-Controlled Conformational Switch Modulates the Activity of Eukaryotic IMP Dehydrogenases*. *Scientific Reports*, 7(1), 1–12.
  21. Buey, Rubén M., Ledesma-Amaro, R., Velázquez-Campoy, A., Balsera, M., Chagoyen, M., De Pereda, J. M., & Revuelta, J. L. (2015). Guanine nucleotide binding to the Bateman domain mediates the allosteric inhibition of eukaryotic IMP dehydrogenases. *Nature Communications*, 6, 8923. <https://doi.org/10.1038/ncomms9923>
  22. Burrell, A. L., Nie, C., Said, M., Simonet, J. C., Fernández-Justel, D., Johnson, M. C., Quispe, J., Buey, R. M., Peterson, J. R., & Kollman, J. M. (2022). IMPDH1 retinal variants control filament architecture to tune allosteric regulation. *Nature Structural and Molecular Biology*, 29(1), 47–58. <https://doi.org/10.1038/s41594-021-00706-2>
  23. Carcamo, W. C., Satoh, M., Kasahara, H., Terada, N., Hamazaki, T., Chan, J. Y. F., Yao, B., Tamayo, S., Covini, G., von Mühlen, C. A., & Chan, E. K. L. (2011). Induction of cytoplasmic rods and rings structures by inhibition of the CTP and GTP synthetic pathway in mammalian cells. *PLoS ONE*, 6(12), 29690. <https://doi.org/10.1371/journal.pone.0029690>
  24. Carlton, J. M., Hirt, R. P., Silva, J. C., Delcher, A. L., Schatz, M., Zhao, Q., Wortman, J. R., Bidwell, S. L., Alsmark, U. C. M., Besteiro, S., Sicheritz-Ponten, T., Noel, C. J., Dacks, J. B., Foster, P. G., Simillion, C., Van De Peer, Y., Miranda-Saavedra, D., Barton, G. J., Westrop, G. D., ... Johnson, P. J. (2007). Draft genome sequence of the sexually transmitted pathogen *Trichomonas vaginalis*. *Science*, 315(5809), 207–212. <https://doi.org/10.1126/science.1132894>
  25. Carr, S. F., Papp, E., Wu, J. C., & Natsumeda, Y. (1993). Characterization of human type I and type II IMP dehydrogenases. *Journal of Biological Chemistry*, 268(36), 27286–27290. [https://doi.org/10.1016/s0021-9258\(19\)74247-1](https://doi.org/10.1016/s0021-9258(19)74247-1)
  26. Chan, H. C. S., Pan, L., Li, Y., & Yuan, S. (2019). Rationalization of stereoselectivity in enzyme reactions. *Wiley Interdisciplinary Reviews: Computational Molecular Science*, 9(4), 1403. <https://doi.org/10.1002/wcms.1403>
  27. Chan, H. C. S., Wang, J., Palczewski, K., Filipek, S., Vogel, H., Liu, Z. J., & Yuan, S. (2018). Exploring a new ligand binding site of G protein-coupled receptors. *Chemical Science*, 9(31), 6480–6489. <https://doi.org/10.1039/c8sc01680a>
  28. Chang, C. C., Lin, W. C., Pai, L. M., Lee, H. S., Wu, S. C., Ding, S. T., Liu, J. L., & Sung, L.
-



- 
- Y. (2015). Cytoophidium assembly reflects upregulation of IMPDH activity. *Journal of Cell Science*, 128(19), 3550–3555. <https://doi.org/10.1242/jcs.175265>
29. Collart, F. R., & Huberman, E. (1988). Cloning and sequence analysis of the human and Chinese hamster inosine-5'-monophosphate dehydrogenase cDNAs. *Journal of Biological Chemistry*, 263(30), 15769–15772. [https://doi.org/10.1016/s0021-9258\(19\)37654-9](https://doi.org/10.1016/s0021-9258(19)37654-9)
30. Cygler, M., Grochulski, P., Kazlauskas, R. J., Schrag, J. D., Bouthillier, F., Rubin, B., Serreqi, A. N., & Gupta, A. K. (1994). A Structural Basis for the Chiral Preferences of Lipases. *Journal of the American Chemical Society*, 116(8), 3180–3186. <https://doi.org/10.1021/ja00087a002>
31. de Pádua, R. A. P., Kia, A. M., Costa-Filho, A. J., Wilkinson, S. R., & Nonato, M. C. (2017). Characterisation of the fumarate hydratase repertoire in *Trypanosoma cruzi*. *International Journal of Biological Macromolecules*, 102, 42–51. <https://doi.org/10.1016/j.ijbiomac.2017.03.099>
32. Dennis, D., & Kaplan, N. O. (1960). d- and l-Lactic Acid Dehydrogenases in *Lactobacillus plantarum*. *Journal of Biological Chemistry*, 235(3), 810–818. [https://doi.org/https://doi.org/10.1016/S0021-9258\(19\)67943-3](https://doi.org/https://doi.org/10.1016/S0021-9258(19)67943-3)
33. Duin, E. C., Lafferty, M. E., Crouse, B. R., Allen, R. M., Sanyal, I., Flint, D. H., & Johnson, M. K. (1997). [2Fe-2S] to [4Fe-4S] Cluster Conversion in *Escherichia coli* Biotin Synthase. *Biochemistry*, 36(39), 11811–11820. <https://doi.org/10.1021/bi9706430>
34. Duong-Ly, K. C., Kuo, Y. M., Johnson, M. C., Cote, J. M., Kollman, J. M., Soboloff, J., Rall, G. F., Andrews, A. J., & Peterson, J. R. (2018). T cell activation triggers reversible inosine-5'-monophosphate dehydrogenase assembly. *Journal of Cell Science*, 131(17), 17. <https://doi.org/10.1242/jcs.223289>
35. Easson, L. H., & Stedman, E. (1933). Studies on the relationship between chemical constitution and physiological action. *Biochemical Journal*, 27(4), 1257–1266. <https://doi.org/10.1042/bj0271257>
36. Ereño-Orbea, J., Oyenarte, I., & Martínez-Cruz, L. A. (2013). CBS domains: Ligand binding sites and conformational variability. *Archives of Biochemistry and Biophysics*, 540(1–2), 70–81. <https://doi.org/10.1016/j.abb.2013.10.008>
37. Feliciano, Patricia R., & Drennan, C. L. (2019). Structural and Biochemical Investigations of the [4Fe-4S] Cluster-Containing Fumarate Hydratase from *Leishmania major*. *Biochemistry*, 58(49), 5011–5021. <https://doi.org/10.1021/acs.biochem.9b00923>
-

- 
38. Feliciano, Patricia R., Drennan, C. L., & Nonato, M. C. (2016). Crystal structure of an Fe-S cluster-containing fumarate hydratase enzyme from *Leishmania major* reveals a unique protein fold. *Proceedings of the National Academy of Sciences*, *113*(35), 9804–9809. <https://doi.org/10.1073/pnas.1605031113>
  39. Feliciano, Patrícia R., Gupta, S., Dyszy, F., Dias-Baruffi, M., Costa-Filho, A. J., Michels, P. A. M., & Nonato, M. C. (2012). Fumarate hydratase isoforms of *Leishmania major*: Subcellular localization, structural and kinetic properties. *International Journal of Biological Macromolecules*, *51*(1–2), 25–31. <https://doi.org/10.1016/j.ijbiomac.2012.04.025>
  40. Fernandez, P., Cañada, F. J., Jiménez-Barbero, J., & Martín-Lomas, M. (1995). Substrate specificity of small-intestinal lactase: study of the steric effects and hydrogen bonds involved in enzyme-substrate interaction. *Carbohydrate Research*, *271*(1), 31–42. [https://doi.org/10.1016/0008-6215\(95\)00034-q](https://doi.org/10.1016/0008-6215(95)00034-q)
  41. Fersht, A. R., Blow, D. M., & Fastrez, J. (1973). Leaving group specificity in the chymotrypsin-catalyzed hydrolysis of peptides. Stereochemical interpretation. *Biochemistry*, *12*(11), 2035–2041. <https://doi.org/10.1021/bi00735a002>
  42. Fishbein, W. N. (1969). Urease Catalysis: III. Stoichiometry, Kinetics, and Inhibitory Properties of a Third Substrate: Dihydroxyurea. *Journal of Biological Chemistry*, *244*(5), 1188–1193. [https://doi.org/10.1016/S0021-9258\(18\)91828-4](https://doi.org/10.1016/S0021-9258(18)91828-4)
  43. Flint, D. H. (1994). Initial kinetic and mechanistic characterization of *Escherichia coli* fumarase A. *Archives of Biochemistry and Biophysics*, *311*(2), 509–516. <https://doi.org/10.1006/abbi.1994.1269>
  44. Flint, D. H., & Allen, R. M. (1996). Iron–Sulfur Proteins with Nonredox Functions. *Chemical Reviews*, *96*(7), 2315–2334. <https://doi.org/10.1021/cr950041r>
  45. Fontecilla-Camps, J. C., Volbeda, A., Cavazza, C., & Nicolet, Y. (2007). Structure/Function Relationships of [NiFe]- and [FeFe]-Hydrogenases. *Chemical Reviews*, *107*(10), 4273–4303. <https://doi.org/10.1021/cr050195z>
  46. Francis, S. H., Chu, D. M., Thomas, M. K., Beasley, A., Grimes, K., Busch, J. L., Turko, I. V., Haik, T. L., & Corbin, J. D. (1998). Ligand-induced conformational changes in cyclic nucleotide phosphodiesterases and cyclic nucleotide-dependent protein kinases. *Methods (San Diego, Calif.)*, *14*(1), 81–92. <https://doi.org/10.1006/meth.1997.0567>
  47. Genheden, S., & Ryde, U. (2015). The MM/PBSA and MM/GBSA methods to estimate ligand-
-

- 
- binding affinities. *Expert Opinion on Drug Discovery*, 10(5), 449.
48. Goujon, M., McWilliam, H., Li, W., Valentin, F., Squizzato, S., Paern, J., & Lopez, R. (2010). A new bioinformatics analysis tools framework at EMBL-EBI. *Nucleic Acids Research*, 38(SUPPL. 2), W695–W699. <https://doi.org/10.1093/nar/gkq313>
49. Gu, J. J., Stegmann, S., Gathy, K., Murray, R., Laliberte, J., Ayscue, L., & Mitchell, B. S. (2000). Inhibition of T lymphocyte activation in mice heterozygous for loss of the IMPDH II gene. *Journal of Clinical Investigation*, 106(4), 599–606. <https://doi.org/10.1172/JCI8669>
50. Gu, J. J., Tolin, A. K., Jain, J., Huang, H., Santiago, L., & Mitchell, B. S. (2003). Targeted Disruption of the Inosine 5'-Monophosphate Dehydrogenase Type I Gene in Mice. *Molecular and Cellular Biology*, 23(18), 6702–6712. <https://doi.org/10.1128/mcb.23.18.6702-6712.2003>
51. Hager, P. W., Collart, F. R., Huberman, E., & Mitchell, B. S. (1995). Recombinant human inosine monophosphate dehydrogenase type I and type II proteins. *Biochemical Pharmacology*, 49(9), 1323–1329. [https://doi.org/10.1016/0006-2952\(95\)00026-V](https://doi.org/10.1016/0006-2952(95)00026-V)
52. Hammer, S. C., Knight, A. M., & Arnold, F. H. (2017). Design and evolution of enzymes for non-natural chemistry. *Current Opinion in Green and Sustainable Chemistry*, 7, 23–30. <https://doi.org/10.1016/j.cogsc.2017.06.002>
53. Hanson, K. R. (1981). Phenylalanine ammonia-lyase: Mirror-image packing of d- and l-phenylalanine and d- and l-transition state analogs into the active site. *Archives of Biochemistry and Biophysics*, 211(2), 575–588. [https://doi.org/10.1016/0003-9861\(81\)90492-6](https://doi.org/10.1016/0003-9861(81)90492-6)
54. Hedstrom, L. (2009). IMP Dehydrogenase: Structure, Mechanism, and Inhibition. *Chemical Reviews*, 109(7), 2903–2928.
55. Hedstrom, Lizbeth. (2001). Enzyme Specificity and Selectivity. In *eLS*. Wiley. <https://doi.org/10.1038/npg.els.0000716>
56. Heyduk, E., Heyduk, T., & Lee, J. C. (1992). Global conformational changes in allosteric proteins. A study of Escherichia coli cAMP receptor protein and muscle pyruvate kinase. *Journal of Biological Chemistry*, 267(5), 3200–3204. [https://doi.org/10.1016/S0021-9258\(19\)50716-5](https://doi.org/10.1016/S0021-9258(19)50716-5)
57. Jackson, R. C., Weber, G., & Morris, H. P. (1975). IMP dehydrogenase, an enzyme linked with proliferation and malignancy. *Nature*, 256(5515), 331–333. <https://doi.org/10.1038/256331a0>
58. Jayaraman, V., Suryavanshi, A., Kalale, P., Kunala, J., & Balaram, H. (2018). Biochemical characterization and essentiality of Plasmodium fumarate hydratase. *Journal of Biological*
-

- 
- Chemistry*, 293(16), 5878–5894. <https://doi.org/10.1074/jbc.M117.816298>
59. Ji, Y. S., Gu, J. J., Makhov, A. M., Griffith, J. D., & Mitchell, B. S. (2006). Regulation of the interaction of inosine monophosphate dehydrogenase with mycophenolic acid by GTP. *Journal of Biological Chemistry*, 281(1), 206–212. <https://doi.org/10.1074/jbc.M507056200>
60. Johnson, D. C., Dean, D. R., Smith, A. D., & Johnson, M. K. (2005). STRUCTURE, FUNCTION, AND FORMATION OF BIOLOGICAL IRON-SULFUR CLUSTERS. *Annual Review of Biochemistry*, 74(1), 247–281. <https://doi.org/10.1146/annurev.biochem.74.082803.133518>
61. Johnson, M. C., & Kollman, J. M. (2020). Cryo-EM structures demonstrate human IMPDH2 filament assembly tunes allosteric regulation. *ELife*, 9, 53243. <https://doi.org/10.7554/eLife.53243>
62. Jorgensen, W. L., & Thomas, L. L. (2008). Perspective on free-energy perturbation calculations for chemical equilibria. *Journal of Chemical Theory and Computation*, 4(6), 869–876. <https://doi.org/10.1021/ct800011m>
63. Jumper, J., Evans, R., Pritzel, A., Green, T., Figurnov, M., Ronneberger, O., Tunyasuvunakool, K., Bates, R., Židek, A., Potapenko, A., Bridgland, A., Meyer, C., Kohl, S. A. A., Ballard, A. J., Cowie, A., Romera-Paredes, B., Nikolov, S., Jain, R., Adler, J., ... Hassabis, D. (2021). Highly accurate protein structure prediction with AlphaFold. *Nature*, 596(7873), 583–589. <https://doi.org/10.1038/s41586-021-03819-2>
64. Kelly, J. M., & Scopes, R. K. (1986). L-(+)-Tartrate dehydratase from *Pseudomonas putida* is an iron-sulphur enzyme. *FEBS Letters*, 202(2), 274–276. [https://doi.org/10.1016/0014-5793\(86\)80700-1](https://doi.org/10.1016/0014-5793(86)80700-1)
65. Keppeke, G. D., Calise, S. J., Chan, E. K. L., & Andrade, L. E. C. (2015). Assembly of IMPDH2-Based, CTPS-Based, and Mixed Rod/Ring Structures Is Dependent on Cell Type and Conditions of Induction. *Journal of Genetics and Genomics*, 42(6), 287–299. <https://doi.org/10.1016/j.jgg.2015.04.002>
66. Keppeke, G. D., Chang, C. C., Peng, M., Chen, L. Y., Lin, W. C., Pai, L. M., Andrade, L. E. C., Sung, L. Y., & Liu, J. L. (2018). IMP/GTP balance modulates cytoophidium assembly and IMPDH activity. *Cell Division*, 13(1), 1–18. <https://doi.org/10.1186/s13008-018-0038-0>
67. Koshland, D. E. (1958). Application of a Theory of Enzyme Specificity to Protein Synthesis\*. *Proceedings of the National Academy of Sciences*, 44(2), 98–104.
-

- 
- <https://doi.org/10.1073/pnas.44.2.98>
68. Kronen, M., Sasikaran, J., & Berg, I. A. (2015). Mesaconase activity of class I fumarase contributes to mesaconate utilization by *Burkholderia xenovorans*. *Applied and Environmental Microbiology*, *81*(16), 5632–5638. <https://doi.org/10.1128/AEM.00822-15>
69. Labesse, G., Alexandre, T., Vaupré, L., Salard-Arnaud, I., Him, J. L. K., Raynal, B., Bron, P., & Munier-Lehmann, H. (2013). MgATP regulates allostery and fiber formation in IMPDHs. *Structure*, *21*(6), 975–985. <https://doi.org/10.1016/j.str.2013.03.011>
70. Lamzin, V. S., Dauter, Z., & Wilson, K. S. (1994). Dehydrogenation through the looking-glass. *Nature Structural Biology*, *1*(5), 281–282. <https://doi.org/10.1038/nsb0594-281>
71. Lamzin, V. S., Dauter, Z., & Wilson, K. S. (1995). How nature deals with stereoisomers. *Current Opinion in Structural Biology*, *5*(6), 830–836. [https://doi.org/10.1016/0959-440X\(95\)80018-2](https://doi.org/10.1016/0959-440X(95)80018-2)
72. Lane, A. N., & Fan, T. W. M. (2015). Regulation of mammalian nucleotide metabolism and biosynthesis. *Nucleic Acids Research*, *43*(4), 2466–2485. <https://doi.org/10.1093/nar/gkv047>
73. Li, G., & Reetz, M. T. (2016). Learning lessons from directed evolution of stereoselective enzymes. *Organic Chemistry Frontiers*, *3*(10), 1350–1358. <https://doi.org/10.1039/c6qo00210b>
74. Lynch, E. M., Hicks, D. R., Shepherd, M., Endrizzi, J. A., Maker, A., Hansen, J. M., Barry, R. M., Gitai, Z., Baldwin, E. P., & Kollman, J. M. (2017). Human CTP synthase filament structure reveals the active enzyme conformation. *Nature Structural and Molecular Biology*, *24*(6), 507–514. <https://doi.org/10.1038/nsmb.3407>
75. Mapolelo, D. T., Zhang, B., Naik, S. G., Huynh, B. H., & Johnson, M. K. (2012). Spectroscopic and Functional Characterization of Iron–Sulfur Cluster-Bound Forms of *Azotobacter vinelandii* NifIscA. *Biochemistry*, *51*(41), 8071–8084. <https://doi.org/10.1021/bi3006658>
76. McCarter, J. D., & Stephen Withers, G. (1994). Mechanisms of enzymatic glycoside hydrolysis. *Current Opinion in Structural Biology*, *4*(6), 885–892. [https://doi.org/10.1016/0959-440X\(94\)90271-2](https://doi.org/10.1016/0959-440X(94)90271-2)
77. Mesecar, A. D., & Koshland, J. (2000). Erratum: A new model for protein stereospecificity (Nature (2000) 403 (614-615)). *Nature*, *408*(6813), 668. <https://doi.org/10.1038/35047170>
78. Mesecar, Andrew D., & Koshland, D. E. (2000). Sites of binding and orientation in a four-location model for protein stereospecificity. *IUBMB Life*, *49*(5), 457–466.
-

---

<https://doi.org/10.1080/152165400410326>

79. Morrison, H. G., McArthur, A. G., Gillin, F. D., Aley, S. B., Adam, R. D., Olsen, G. J., Best, A. A., Cande, W. Z., Chen, F., Cipriano, M. J., Davids, B. J., Dawson, S. C., Elmendorf, H. G., Hehl, A. B., Holder, M. E., Huse, S. M., Kim, U. U., Lasek-Nesselquist, E., Manning, G., ... Sogin, M. L. (2007). Genomic minimalism in the early diverging intestinal parasite *Giardia lamblia*. *Science*, *317*(5846), 1921–1926. <https://doi.org/10.1126/science.1143837>
  80. Morrow, C. A., Valkov, E., Stamp, A., Chow, E. W. L., Lee, I. R., Wronski, A., Williams, S. J., Hill, J. M., Djordjevic, J. T., Kappler, U., Kobe, B., & Fraser, J. A. (2012). De novo GTP Biosynthesis Is Critical for Virulence of the Fungal Pathogen *Cryptococcus neoformans*. *PLoS Pathogens*, *8*(10), 1002957. <https://doi.org/10.1371/journal.ppat.1002957>
  81. Mu, R., Wang, Z., Wamsley, M. C., Duke, C. N., Lii, P. H., Epley, S. E., Todd, L. C., & Roberts, P. J. (2020). Application of enzymes in regioselective and stereoselective organic reactions. *Catalysts*, *10*(8), 832. <https://doi.org/10.3390/catal10080832>
  82. Nagashima, F., Tanase, S., & Morino, Y. (1986). Inactivation of cytosolic aspartate aminotransferase accompanying modification of Trp 48 by N-bromosuccinimide. *FEBS Letters*, *197*(1–2), 129–133. [https://doi.org/10.1016/0014-5793\(86\)80312-X](https://doi.org/10.1016/0014-5793(86)80312-X)
  83. Nakamaru-Ogiso, E., Yano, T., Ohnishi, T., & Yagi, T. (2002). Characterization of the Iron-Sulfur Cluster Coordinated by a Cysteine Cluster Motif (CXXCXXXCX27C) in the Nqo3 Subunit in the Proton-translocating NADH-Quinone Oxidoreductase (NDH-1) of *Thermus thermophilus* HB-8. *Journal of Biological Chemistry*, *277*(3), 1680–1688. <https://doi.org/10.1074/jbc.M108796200>
  84. Narayanaswamy, R., Levy, M., Tsechansky, M., Stovall, G. M., O'Connell, J. D., Mirrieles, J., Ellington, A. D., & Marcotte, E. M. (2009). Widespread reorganization of metabolic enzymes into reversible assemblies upon nutrient starvation. *Proceedings of the National Academy of Sciences of the United States of America*, *106*(25), 10147–10152. <https://doi.org/10.1073/pnas.0812771106>
  85. Natsumeda, Y., Ohno, S., Kawasaki, H., Konno, Y., Weber, G., & Suzuki, K. (1990). Two distinct cDNAs for human IMP dehydrogenase. *Journal of Biological Chemistry*, *265*(9), 5292–5295. [https://doi.org/10.1016/s0021-9258\(19\)34120-1](https://doi.org/10.1016/s0021-9258(19)34120-1)
  86. Nimmesgern, E., Black, J., Futer, O., Fulghum, J. R., Chambers, S. P., Brummel, C. L., Raybuck, S. A., & Sintchak, M. D. (1999). Biochemical analysis of the modular enzyme
-

- 
- inosine 5'-monophosphate dehydrogenase. *Protein Expression and Purification*, 17(2), 282–289. <https://doi.org/10.1006/prev.1999.1136>
87. Noree, C., Sato, B. K., Broyer, R. M., & Wilhelm, J. E. (2010). Identification of novel filament-forming proteins in *Saccharomyces cerevisiae* and *Drosophila melanogaster*. *Journal of Cell Biology*, 190(4), 541–551. <https://doi.org/10.1083/jcb.201003001>
88. O'Connell, J. D., Tsechansky, M., Royall, A., Boutz, D. R., Ellington, A. D., & Marcotte, E. M. (2014). A proteomic survey of widespread protein aggregation in yeast. *Molecular BioSystems*, 10(4), 851–861. <https://doi.org/10.1039/c3mb70508k>
89. O'Connell, J. D., Zhao, A., Ellington, A. D., & Marcotte, E. M. (2012). Dynamic reorganization of metabolic enzymes into intracellular bodies. *Annual Review of Cell and Developmental Biology*, 28, 89–111. <https://doi.org/10.1146/annurev-cellbio-101011-155841>
90. Ogston, A. G. (1949). Interpretation of experiments on metabolic processes, using isotopic tracer elements [9]. *Nature*, 163(4131), 963.
91. Ohno, H., Takeda, K., Niwa, S., Tsujinaka, T., Hanazono, Y., Hirano, Y., & Miki, K. (2017). Crystallographic characterization of the high-potential iron-sulfur protein in the oxidized state at 0.8 Å resolution. *PLOS ONE*, 12(5), e0178183. <https://doi.org/10.1371/journal.pone.0178183>
92. Ovchinnikov, S., Kinch, L., Park, H., Liao, Y., Pei, J., Kim, D. E., Kamisetty, H., Grishin, N. V., & Baker, D. (2015). Large-scale determination of previously unsolved protein structures using evolutionary information. *ELife*, 4(September), 1–25. <https://doi.org/10.7554/eLife.09248>
93. Papish, A. L., Tari, L. W., & Vogel, H. J. (2002). Dynamic light scattering study of calmodulin-target peptide complexes. *Biophysical Journal*, 83(3), 1455–1464. [https://doi.org/10.1016/S0006-3495\(02\)73916-7](https://doi.org/10.1016/S0006-3495(02)73916-7)
94. Pasteur, L. (1858). Mémoiresur la fermentation de l'acide tantriqu. *COMPTEs RENDUS DES SÉANCES DE L'ACADÉMIE DES SCIENCES.*, 46, 615–618.
95. Prasoona, T. L. (2019). *Biochemical studies on inosine 5'-monophosphate dehydrogenase from the mesophilic protozoan plasmodium falciparum and hyperthermophilic archaeon methanocaldococcus jannaschii*. <http://lib.jncasr.ac.in:8080/jspui/handle/123456789/3209>
96. Prosise, G. L., & Wu, Z. (n.d.). J., & Luecke, H. (2002). *Crystal Structure of Tritrichomonas Foetus Inosine Monophosphate Dehydrogenase in Complex with the Inhibitor Ribavirin*
-

- 
- Monophosphate Reveals a Catalysis-Dependent Ion-Binding Site*, 277(52), 50654–50659.
97. Rao, V. A., Shepherd, S. M., Owen, R., & Hunter, W. N. (2013). Structure of *Pseudomonas aeruginosa* inosine 5'-monophosphate dehydrogenase. *Acta Crystallographica Section F: Structural Biology and Crystallization Communications*, 69(3), 243–247. <https://doi.org/10.1107/S1744309113002352>
98. Reaney, S. K., Begg, C., Bungard, S. J., & Guest, J. R. (1993). Identification of the L-tartrate dehydratase genes (ttdA and ttdB) of *Escherichia coli* and evolutionary relationship with the Class I fumarase genes. *Journal of General Microbiology*, 139(7), 1523–1530. <https://doi.org/10.1099/00221287-139-7-1523>
99. Reetz, M. T. (2011). Laboratory evolution of stereoselective enzymes: A prolific source of catalysts for asymmetric reactions. *Angewandte Chemie - International Edition*, 50(1), 138–174. <https://doi.org/10.1002/anie.201000826>
100. Robert, X., & Gouet, P. (2014). Deciphering key features in protein structures with the new ENDscript server. *Nucleic Acids Research*, 42(W1), 320–324. <https://doi.org/10.1093/nar/gku316>
101. Robertson, D. W., Krushinski, J., Fuller, R. W., & David Leander, J. (1988). Absolute Configurations and Pharmacological Activities of the Optical Isomers of Fluoxetine, a Selective Serotonin-Uptake Inhibitor. *Journal of Medicinal Chemistry*, 31(7), 1412–1417. <https://doi.org/10.1021/jm00402a027>
102. Rüter, A. De, & Oostenbrink, C. (2016). Extended Thermodynamic Integration: Efficient Prediction of Lambda Derivatives at Nonsimulated Points. *Journal of Chemical Theory and Computation*, 12(9), 4476–4486. <https://doi.org/10.1021/acs.jctc.6b00458>
103. Schink, B. (1984). Fermentation of tartrate enantiomers by anaerobic bacteria, and description of two new species of strict anaerobes, *Ruminococcus pasteurii* and *Ilyobacter tartaricus*. *Archives of Microbiology*, 139(4), 409–414. <https://doi.org/10.1007/BF00408388>
104. Senda, M., & Natsumeda, Y. (1994). Tissue-differential expression of two distinct genes for human IMP dehydrogenase (E.C.1.1.1.205). *Life Sciences*, 54(24), 1917–1926. [https://doi.org/10.1016/0024-3205\(94\)90150-3](https://doi.org/10.1016/0024-3205(94)90150-3)
105. Shen, Z., Lv, C., & Zeng, S. (2016). Significance and challenges of stereoselectivity assessing methods in drug metabolism. *Journal of Pharmaceutical Analysis*, 6(1), 1–10. <https://doi.org/10.1016/j.jpha.2015.12.004>
-



- 
106. Shibata, H., Gardiner, W. E., & Schwartzbach, S. D. (1985). Purification, characterization, and immunological properties of fumarase from *Euglena gracilis* var. *bacillaris*. *Journal of Bacteriology*, *164*(2), 762–768. <https://doi.org/10.1128/jb.164.2.762-768.1985>
107. Shimoyama, T., Rajashekhara, E., Ohmori, D., Kosaka, T., & Watanabe, K. (2007). MmcBC in *Pelotomaculum thermopropionicum* represents a novel group of prokaryotic fumarases. *FEMS Microbiology Letters*, *270*(2), 207–213. <https://doi.org/10.1111/j.1574-6968.2007.00665.x>
108. Shu, Q., & Nair, V. (2008). Inosine monophosphate dehydrogenase (IMPDH) as a target in drug discovery. *Medicinal Research Reviews*, *28*(2), 219–232. <https://doi.org/10.1002/med.20104>
109. Siegel, J. B., Zanghellini, A., Lovick, H. M., Kiss, G., Lambert, A. R., St.Clair, J. L., Gallaher, J. L., Hilvert, D., Gelb, M. H., Stoddard, B. L., Houk, K. N., Michael, F. E., & Baker, D. (2010). Computational design of an enzyme catalyst for a stereoselective bimolecular diels-alder reaction. *Science*, *329*(5989), 309–313. <https://doi.org/10.1126/science.1190239>
110. Sievers, F., Wilm, A., Dineen, D., Gibson, T. J., Karplus, K., Li, W., Lopez, R., McWilliam, H., Remmert, M., Söding, J., Thompson, J. D., & Higgins, D. G. (2011). Fast, scalable generation of high-quality protein multiple sequence alignments using Clustal Omega. *Molecular Systems Biology*, *7*(1), 539. <https://doi.org/10.1038/msb.2011.75>
111. Sintchak, M. D., Fleming, M. A., Futer, O., Raybuck, S. A., Chambers, S. P., Caron, P. R., Murcko, M. A., & Wilson, K. P. (1996). Structure and mechanism of inosine monophosphate dehydrogenase in complex with the immunosuppressant mycophenolic acid. *Cell*, *85*(6), 921–930. [https://doi.org/10.1016/S0092-8674\(00\)81275-1](https://doi.org/10.1016/S0092-8674(00)81275-1)
112. Solomon, E. I., Gorelsky, S. I., & Dey, A. (2006). Metal–thiolate bonds in bioinorganic chemistry. *Journal of Computational Chemistry*, *27*(12), 1415–1428. <https://doi.org/https://doi.org/10.1002/jcc.20451>
113. Stephens, P. J., Thomson, A. J., Dunn, J. B., Keiderling, T. A., Rawlings, J., Rao, K. K., & Hall, D. O. (1978). Circular dichroism and magnetic circular dichroism of iron-sulfur proteins. *Biochemistry*, *17*(22), 4770–4778. <https://doi.org/10.1021/bi00615a026>
114. Tang, G., Peng, L., Baldwin, P. R., Mann, D. S., Jiang, W., Rees, I., & Ludtke, S. J. (2007). EMAN2: an extensible image processing suite for electron microscopy. *Journal of Structural Biology*, *157*(1), 38–46. <https://doi.org/10.1016/j.jsb.2006.05.009>
-

- 
115. U.K. Lammler. (1970). Cleavage of Structural Proteins during the Assembly of the Head of Bacteriophage T4. *Nature*, 227(15), 680–685.
116. Van Kuijk, B. L. M., & Stams, A. J. M. (1996). Purification and characterization of malate dehydrogenase from the syntrophic propionate-oxidizing bacterium strain MPOB. *FEMS Microbiology Letters*, 144(2–3), 141–144. [https://doi.org/10.1016/0378-1097\(96\)00349-7](https://doi.org/10.1016/0378-1097(96)00349-7)
117. van Vugt-Lussenburg, B. M. A., van der Weel, L., Hagen, W. R., & Hagedoorn, P. L. (2009). Identification of two [4Fe-4S]-cluster-containing hydro-lyases from *Pyrococcus furiosus*. *Microbiology*, 155(9), 3015–3020. <https://doi.org/10.1099/mic.0.030320-0>
118. van Vugt-Lussenburg, B. M. A., van der Weel, L., Hagen, W. R., & Hagedoorn, P. L. (2013). Biochemical Similarities and Differences between the Catalytic [4Fe-4S] Cluster Containing Fumarases FumA and FumB from *Escherichia coli*. *PLoS ONE*, 8(2), 1–7. <https://doi.org/10.1371/journal.pone.0055549>
119. Varadi, M., Anyango, S., Deshpande, M., Nair, S., Natassia, C., Yordanova, G., Yuan, D., Stroe, O., Wood, G., Laydon, A., Zidek, A., Green, T., Tunyasuvunakool, K., Petersen, S., Jumper, J., Clancy, E., Green, R., Vora, A., Lutfi, M., ... Velankar, S. (2022). AlphaFold Protein Structure Database: Massively expanding the structural coverage of protein-sequence space with high-accuracy models. *Nucleic Acids Research*, 50(D1), D439–D444. <https://doi.org/10.1093/nar/gkab1061>
120. Wombacher, R., Keiper, S., Suhm, S., Serganov, A., Patel, D. J., & Jäschke, A. (2006). Control of stereoselectivity in an enzymatic reaction by backdoor access. *Angewandte Chemie - International Edition*, 45(15), 2469–2472. <https://doi.org/10.1002/anie.200503280>
121. Xu, J., Cen, Y., Singh, W., Fan, J., Wu, L., Lin, X., Zhou, J., Huang, M., Reetz, M. T., & Wu, Q. (2019). Stereodivergent Protein Engineering of a Lipase to Access All Possible Stereoisomers of Chiral Esters with Two Stereocenters. *Journal of the American Chemical Society*, 141(19), 7934–7945. <https://doi.org/10.1021/jacs.9b02709>
122. Yano, T., Sled, V. D., Ohnishi, T., & Yagi, T. (1996). Expression and characterization of the flavoprotein subcomplex composed of 50-kDa (NQO1) and 25-kDa (NQO2) subunits of the proton-translocating NADH-quinone oxidoreductase of *Paracoccus denitrificans*. *Journal of Biological Chemistry*, 271(10), 5907–5913. <https://doi.org/10.1074/jbc.271.10.5907>
123. Zheng, L., Kennedy, M. C., Beinert, H., & Zalkin, H. (1992). Mutational analysis of active site residues in pig heart aconitase. *Journal of Biological Chemistry*, 267(11), 7895–7903.
-

[https://doi.org/10.1016/s0021-9258\(18\)42597-5](https://doi.org/10.1016/s0021-9258(18)42597-5)